Department MTM Metallurgy and
Materials Engineering
Faculty of Engineering

Departamento de Ciencia e Ingeniería de
Materiales e Ingeniería Química

PROYECTO FIN DE CARRERA

SURFACE ROUGHNESS MODIFICATION OF BONE TISSUE ENGINEERING SCAFFOLDS BY ELECTROCHEMICAL ETCHING: OPTIMIZATION AND QUANTITATIVE CHARACTERIZATION

(Modificación de la rugosidad superficial de *scaffolds* metálicos para la ingeniería de tejidos por ataque electrolítico: optimización y caracterización cuantitativa)

Autor: Enrique Velasco Martín

BÉLGICA

Promotors: Prof. dr. ir. M. Wevers
Prof. dr. ir. J. Schrooten
Assesors: Prof. dr. ir. S. V. Lomov
Prof. dr. ir. M. Seefeldt
Counsellor: Dr. ing. G. Kerckhofs

ESPAÑA

Tutor: María Elisa Ruiz Navas

Fecha de presentación (Bélgica): junio 2010

Fecha de entrega (España): octubre 2011

Preface

To my family, to my mother, my father, Marta and my grandparents, especially to Consuelo. To my friends, the ones I met in Leuven and those who I left behind in Spain. Especially thanks to Alex, Ana, João, Jorge, Juan, Miguel, Miquel, Teresa and Quique, and also to Andrés, Carlitos, Chavo, Elisa, Ferpelos, Gonzalo, Iván, Javo, Jesuli, Jorge, José Manuel, Marisa, Maru, Paquito, Remi, Rodri and Toni. To Laura. You all inspired me to keep on going during this long-distance race.

Thanks to MTM staff, their welcome was unbeatable. Especially thanks to Martine, Jan, Simon and, overall, to Huberte, Gregory and Greet, your patience was my everyday calm.

Thanks to Ellen, you introduced me your culture, but not the Belgian timetable at all.

Thanks, Leuven.

Summary

Since surface roughness is known as an important property that determines and controls cell attachment and proliferation on the surfaces of porous TE scaffolds, a more controlled and homogeneous surface is required. In this study, two surface roughness modification procedures were proposed for Ti6Al4V scaffolds in order to achieve this aim: chemical etching followed by electrochemical polishing. This study dealt with the in depth characterization of the effect of the surface roughness modification on the morphological and mechanical properties of the porous Ti6Al4V scaffolds and on their roughness. In this way, feedback could be provided for optimization or fine-tuning of the surface roughness modification procedures. During electrochemical polishing, the current was maintained constant, thus depending on the scaffold design a different current density was applied. The role of the current density was found to be important for the changes in morphological, mechanical and roughness properties. Therefore, controlling this parameter, and hence also the reduction in morphological, mechanical and roughness properties, the surface roughness modification procedures will be more controlled and designing and producing customized porous Ti6Al4V scaffolds will be feasible. Additionally, in this study, initial characterization of the morphological and mechanical properties of two designs of porous PCL scaffolds was carried out and the effect of two different surface roughness modification procedures was qualitatively assessed, namely immersion for 96 hours in NaOH or in KOH.

List of Symbols

2D	Two Dimensional
3D	Three Dimensional
3D-P	Three Dimensional Printing
hPDCs	Human Periosteum Derived (osteogenic) Cells
r	Radius [μm]
CAD	Computer Aided Design
CH	Chemical Etching
CT	Computed Tomography
CVD	Chemical Vapour Deposition
DNA	Deoxyribonucleic acid
E	Young's modulus [MPa]
EDM	Electrical Discharge Machining
EP	Electrochemical Polishing
FDM	Fused Deposition Modeling
FEA	Finite Element Analysis
FEM	Finite Element Method
G	Buoyancy [g]
PCL	Polycaprolactone
R_p	The highest point in surface roughness calculations [μm]
R_v	The lowest point in the evaluated length in surface roughness calculations [μm]
RMS	Root Mean Square
RP	Rapid Prototyping
SBF	Simulated Body Fluid
SEBM	Selective Electron Beam Melting
SEM	Scanning Electron Microscopy
SFF	Solid Freeform Fabrication
SLM	Selective Laser Melting
SLS	Selective Laser Sintering
TE	Tissue Engineering
V	Volume [cm^3]
W	Mass [g]
WD	Working Distance [μm]
μCT	Micro Computed Tomography
ρ	Density [g/cm^3]
Ø	Diameter [μm]

List of Figures

List of Tables

Table of Contents

1. Introduction

Porous scaffolds have an extensive use in the engineering world nowadays, going from the chemical industry (as filters) to thermal insulation, packaging, as structural materials or floating ones. Good mechanical properties, a wide variety of possible designs and easy production are three reasons why porous materials are so common in everyday life. One of the most recent fields of application of porous materials is tissue engineering (TE). Porous materials with cells attached on them are used as implants for example for the healing of large bone defects. For this kind of porous materials, known as scaffolds, a perfect balance between mechanical properties and biological cell behaviour is required. There are different material types that could be used to fulfill these requirements. The present project will deal with Ti6Al4V and polycrapolactone (PCL) TE porous scaffolds. Since the morphological surface properties of the TE scaffolds also play a crucial role on cell proliferation, the control and improvement of these properties is the main aim of the work carried out in this master thesis.

Chapter 2 of this master thesis will discuss, as was found in literature, the most important characteristics porous materials to be used as TE scaffolds should have, the different possible production techniques, different characterization techniques for porous structures and will look at different surface roughness modification procedures. This chapter will introduce the initial experiments performed at the start of this master thesis and the aims of this master thesis.

Chapter 3 describes thoroughly the two material types studied as porous TE scaffolds in this master thesis, namely Ti6Al4V and PCL, and also their production techniques, SLM and FDM respectively. This chapter will also deal with the different characterization techniques used, such as the Archimedes test, micro-CT, SEM, high resolution micro-CT and mechanical testing. Finally, the surface roughness modification procedures carried out on both the Ti6Al4V and the PCL scaffolds will be explained in detail.

In chapter 4, the initial experiments on the Ti6Al4V porous TE scaffolds are described, which have been performed in order to compare the biological cell behaviour of as-produced and surface roughness modified scaffold. It was found that not only the surface roughness, but also the available surface plays an important role in the cell behavior. As a conclusion of this chapter, it was found that in order to only assess the effect of the surface roughness on the cell behaviour, a more controlled surface roughness modification procedure is required, and hence it is also the main aim of this master thesis to optimize surface roughness modification procedure according to the required morphological and mechanical properties and the required roughness, and make the procedure more robust. The crucial role of the current density during electrochemical polishing related with the effect on surface properties was here also suggested and therefore, this initial study formed the basis of all the experiments performed in this master thesis.

Chapter 5 presents a summary of the problem statement and aims and connects the initial experiments on the Ti6Al4V scaffolds with the main body of the master thesis. Additionally, the importance of the characterization and surface roughness modification of the biodegradable PCL scaffolds will be pointed out.

The following two chapters, 6, and 7 will present the in depth characterization of the effect of surface roughness modification of the Ti6Al4V

porous TE scaffolds on the morphological and mechanical properties, and on the roughness carried out. Three batches of scaffolds with different designed structure thickness were used. This part will be focused on the structure thickness modifications measured with micro-CT device, the mechanical properties and roughness heterogeneities observed along the scaffolds, after each surface roughness modification. The effects of the surface roughness modifications will be related to the current density values obtained due to a constant current applied during electrochemical polishing. Two roughness measurement techniques were implemented and their differences, pros and cons will be observed in chapter 7.

Chapter 8 will talk about the characterization of the as-produced PCL scaffolds, and the effect of two surface roughness modification procedures applied on them will be compared qualitatively using SEM images.

Finally, chapter 9 summarizes the most important conclusions of the master thesis and will indicate suggestions for future work.

2. Literature review

2.1. Porous structure

Porous materials exist in a wide variety of engineering applications, mainly because of their good mechanical properties, flexibility of design and high productivity. They can be found for example in chemical industry as filter materials, in buildings as insulation or heat exchangers, or even in the human body as trabecular bone or porous scaffolds for tissue engineering (TE). They can be described as a dense matrix containing voids or pores.

The macroscopic properties of porous materials depend apart from the material type (metals, polymers, ceramics or their composites) on various geometrical and morphological features of their structure, such as the pore connectivity, the shape of the pores' struts or walls, and at a larger scale the geometrical arrangement of the pores. The major physical properties (mechanical, thermal and electrical) of porous materials are related to their relative density and architecture. By modifying the morphological characteristics of the porous structure, the strength-to-weight ratio and other mechanical properties can be optimized [1]. Pore connectivity also plays a major role in the barrier properties of the materials. Open pores are known for high absorption capacity of water and moisture, high permeability, and efficient noise absorption. In contrast, closed pores impart thermal and electrical insulating properties in direct relation with the nature of the gas, imprisoned in the cells. Of course, totally open or entirely closed pores are extreme cases. Intermediate situations are available depending on the material formulation and processing [2, 3].

A very important field of study with regard to porous structures and the field of application focused on in this master thesis work is tissue engineering (TE). TE is a field of knowledge that tries to understand the biological mechanisms that are behind the development of a specific tissue of the human body. It is an interdisciplinary field that applies the principles of engineering and life science for the development of biological substitutes that restore, maintain or improve tissue function [4, 5]. One of the main purposes of TE is to get cells to grow in a porous material, which should preferably be made of a biodegradable material, also called a porous TE scaffolds. These cell-seeded scaffolds are then implanted replacing the damaged tissue. Over time the body preferably should absorb the scaffold and the cells should produce their own natural extra cellular matrix. Tissues currently being studied for regeneration include skin, cartilage, bone, nerve and liver [6]. Figure 2.1 shows a typical schematic overview of the process [4].

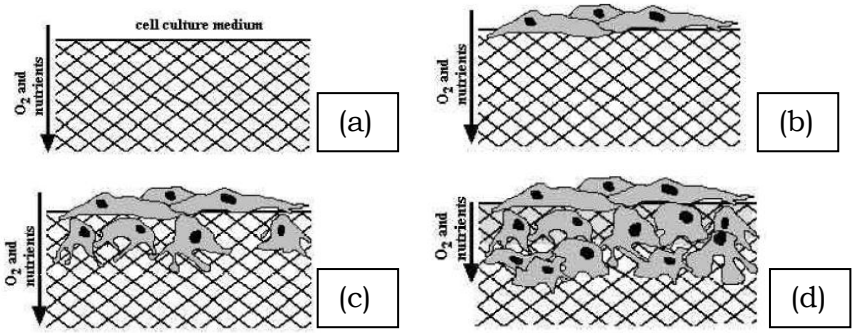

Fig.2.1. Schematic overview of the TE process: a) Oxygen and nutrients are supplied from the liquid cell culture medium. b) Cell seeding on scaffold. c) Cells start to proliferate and migrate into the pores of the scaffold. d) The cells fully colonize the pores and start to lay down their own extracellular matrix.[2]

In this master thesis work, the main field of application for the TE scaffolds is to heal damaged or defect bones (= bone TE). A schematic overview of the principle of bone TE can be found in figure 2.2, showing that the combination of porous TE scaffolds with osteogenic cells can, after a process of cell seeding and bioreactor culture, be implanted in large bone defects for healing. Because the scaffolds will be a part of the body structure starting from the moment of implantation, they are designed for both mechanical loading and mass transport. Furthermore, they preferably should have the following important characteristics [5]:

- An open-pore geometry with a highly porous structure that enables cell ingrowth.
- An optimal pore size employed to encourage tissue regeneration and to avoid pore occlusion.
- A suitable macrostructure to promote cell proliferation and cell-specific matrix production.
- Being made from a material with a known rate of degradation or from a bio-inert material.
- Adequate mechanical properties.
- A suitable surface morphology and physiochemical properties to favour intracellular signaling and recruitment of cells.

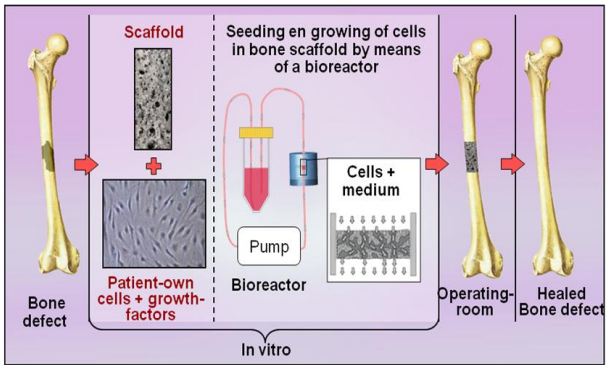

Fig.2.2. Schematic overview of the principle of TE, showing that the combination of scaffolds with osteogenic cells can, after a process of cell seeding and bioreactor culture, be implanted in large bone defects for healing [courtesy of Saartje Impens].

Different materials are currently being used to build porous TE scaffolds with these specific characteristics. For example, porous ceramics and polymers have been studied widely, but mostly these materials do not have the mechanical properties required for the demanding load [4, 7]. Metals on the other hand became, from the mechanical point of view, the most suitable ones where ceramics and polymers fail [7]. For example, titanium alloy scaffolds have been used frequently due to their excellent strength-to-weight ratio, toughness, corrosion resistance, and surface oxide biocompatibility [7], which makes them especially suitable for orthopaedic uses. However, some polymers such as polycaprolactone (PCL), have been extensively investigated due to their biodegradability and because of their soft- and hard-tissue compatibility, and easy processing [6, 8]. For these reasons, in the present work both titanium alloy, and more specific Ti6Al4V scaffolds, and PCL scaffolds will be investigated.

2.2. Production of porous materials

There are many ways to produce porous structures. Most of the production techniques have the common objective to maintain high levels of well-controlled macro- (e.g., spatial form, mechanical strength, density, porosity) and micro-structural (e.g., pore size, pore distribution, pore interconnectivity) properties. Regarding the production of porous TE scaffolds, there are a lot of conventional scaffold fabrication techniques available, such as solving casting and particulate leaching, emulsion freeze drying, phase separation, melt molding, gas foaming, solution casting and freeze drying, fibre meshes and fibre bonding. However, most of them cannot guarantee a high control of the different pore properties such as size, density and geometry, as well as of the formation of the internal channels within the scaffold through which the cells, nutrients and oxygen need to be transported. Indeed, the following factors have to be kept in mind when a processing technique is to be used to make a porous TE scaffold: processing conditions, process accuracy, robustness, consistency and repeatability [9].

Solid free-form fabrication technique (SFF), also commonly known as rapid prototyping (RP), provides a solution. The main advantage of this family of techniques is the possibility to obtain the desirable scaffold geometry both internal and external, controlling the pore properties and also the most important macro-scale structural properties. With RP techniques, three-dimensional (3D) objects are fabricated layer-by-layer using a computer system and CAD programs. In order to clarify the work sequence, a typical SFF process chain is shown in figure 2.3. Starting from the bottom and building layers up, each newly formed layer adheres to the previous. Each layer corresponds to a cross-sectional division [4].

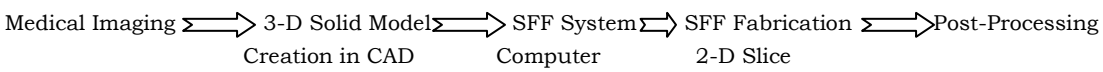

Fig.2.3. Typical SFF process chain, for biomedical application [9].

The most important and often used RP techniques are the following [9]:

- Three-dimensional printing (3D-P): this technique employs ink jet printing and works with polymeric, metallic and ceramic powders. A liquid binder is fabricated onto thin layers of powder by a printer head, following the model generated by a computer program. The final object is embedded inside a cake of unprocessed powders at the end of the process. 3D-P is perhaps one of the most widely investigated SFF techniques for scaffold fabrication.
- Fused deposition modeling (FDM): using the concept of melt extrusion a material layer is formed by the deposit of parallel series of material rods. For each material layer, the direction of material deposition can be changed. In this way, it is easy to get highly compacted structures and controllable pore morphology and interconnectivity.
- Selective laser melting (SLM) or sintering (SLS): these techniques form material layers by selectively melt or sinter polymeric, ceramic or metallic powders with the help of a CO_2 laser beam. The fusion of material layers that are stacked on top of one another conclude in the final object's height. Surrounding unprocessed powder is used during the whole process to support and embed the object. With SLS and SLM, porous materials with a controlled porosity and morphology can be produced.

In table 2.1, the pros and cons of the different production techniques are reflected [9].

Table 2.1. The pros and cons of the different production techniques [9].

Technique	PROS
Three-dimensional painting (3D-P)	- Structures with controlled anisotrophy - Complex scaffold designs allowed - Wide range of biomaterials
Fused deposition modelling (FDM)	- Really good mechanical properties and structural integrity of the scaffolds
Selective laser melting (SLM) and sintering (SLS)	- Highly consistent microstructural properties of the scaffolds - Irregularly shaped scaffolds allowed - Secondary binder system not required

Technique	CONS
Three-dimensional painting (3D-P)	- Not well-controlled pore size - Not so good mechanical properties and accuracy - Not well-controlled surface properties
Fused deposition modelling (FDM)	- Not consistent pore openings in the whole sample - Complex scaffold designs not allowed - Conversion the scaffolding materials into filament forms obligatory - Not well-controlled surface properties
Selective laser melting (SLM) and sintering (SLS)	- Not well-controlled surface properties

Another interesting RP production technique to be considered for titanium alloys for TE applications is selective electron beam melting (SEBM). As opposed to SLM, where a laser is used to melt the powder, SEBM consists in building structures layer-by-layer by selectively melting powder material by an electron beam under vacuum. Currently, two designs can be achieved with this technique: the diamond structure and the hatched structure [10]. The differences between them correspond to the manufacturing method, the porosity and the cell structure. Using SEBM for implant applications, the scaffold will have mechanical properties similar to those of human bones so stress-shielding effects after implantation might be avoided due to a reduced stiffness mismatch between implant and bone. Tissue ingrowth and vascularisation are favoured, also the fixation of the implant in the surrounding bone [10].

Still some challenges exist regarding RP: the limited range of materials, the optimal design and the bioactivity of the scaffold, and the issues of cell seeding and vascularisation. These limitations could be reduced or eliminated through slight modifications of the hard- and software that is used in order to eliminate or reduce the differences between the idealized CAD models and the manufactured scaffolds, and also looking for other types of processing procedures and material stocks [9].

In figure 2.4, typical SEM images of a Ti6Al4V scaffold and PCL scaffolds are shown after RP production, which are the materials that will be investigated in this master thesis. The Ti6Al4V scaffolds (fig. 2.4a) have been produced using SLM and the PCL scaffolds (fig. 2.4b and 2.4c) using FDM. It can be seen that for the SLM produced Ti6Al4V scaffolds a significant amount of non-melted powder grains is still present on the strut's surfaces and thus a high control of the surface properties is difficult. For the PCL scaffolds, a very smooth surface is noticed, which might also not be ideal for the cell attachment. Thus, although RP techniques allow a high control of the morphology of porous structures, still a lack of control of the surface properties is present.

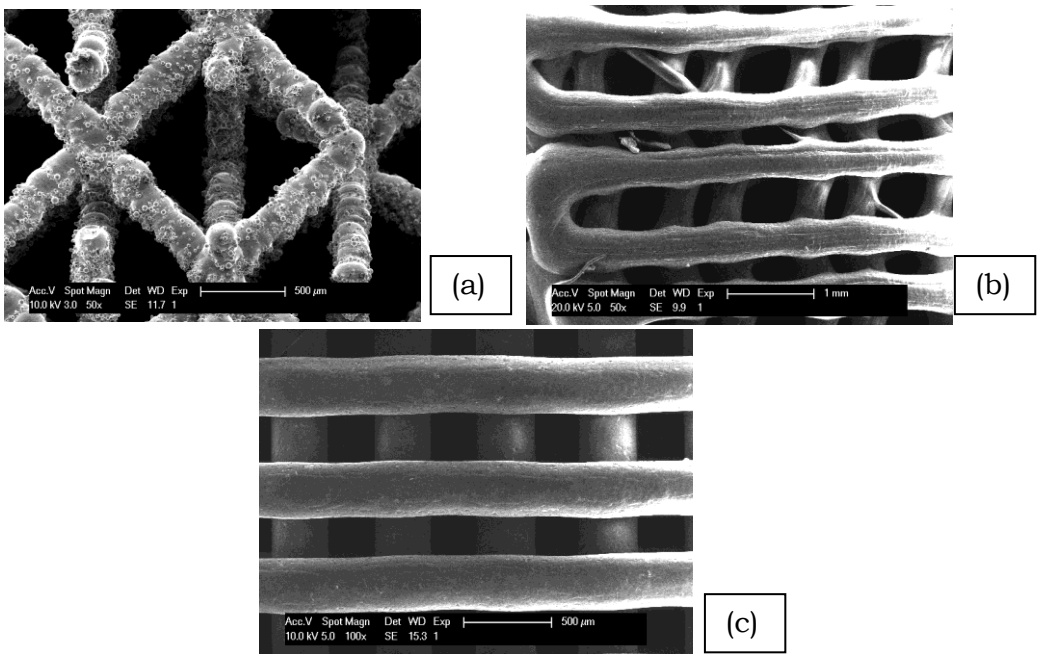

Fig.2.4. Typical SEM images of (a) an SLM produced Ti6Al4V scaffold, (b) an FDM produced PCL scaffold fabricated by De Nayer Institute (DNI) Mechelen and (c) an FDM produced PCL scaffold fabricated by the Hogeschool Gent.

2.3. Surface roughness modification of porous materials

As was mentioned, a lack of control of the surface properties is present when producing porous TE scaffolds using RP techniques. Since one of the requisites a TE scaffold has to fulfill is to have a suitable and controlled surface morphology and physiochemical properties to favour intracellular signaling and recruitment of cells, one of the main goals of this master thesis is to analyze how surface roughness modifications will affect the characteristics of the TE scaffolds, both morphologically and mechanically.

Some studies for example have modified the surfaces of titanium alloys to enhance their bioactivity. It has been demonstrated that alkali-heat treatment is an efficient method to deposit a hydroxyapatite layer on the surface of that materials. The pre-treated porous titanium alloy therefore has the potential to be bioactive implant material. In these studies, the porous samples were firstly polished to remove undesirable material, secondly cleaned and dried and thirdly soaked in an aqueous solution of NaOH (alkali treatment). Finally, soaking again the sample into simulated body fluid (SBF) was carried out to study the bioactivity of the pre-treated titanium alloy sample. In this way, the mechanical properties of the porous material could be tailored to come close to those of human bone [11].

According to the work of Gao et al. [12], not only for improvement of the biocompatibility and bioactivity of titanium alloys, but also for obtaining a sufficiently low elastic modulus which minimize the stress shielding phenomenon between bone and implant (elastic modulus of titanium alloys is greater than that of bone), anodic oxidation has been carried out on Ti-24Nb-4Zr-7.9Sn (TNZS). TNZS is a family of β-Ti alloys, which has the lowest elastic modulus. During the anodic oxidation, Ca ions were incorporated into the oxide layer. Cell viability on the surfaces of the porous samples was improved and also the pull-out forces increased [12].

For the Ti6Al4V TE scaffolds assessed in this master thesis, currently a chemical etching process is applied in order to eliminate undesirable powder grains after production (ref. figure 2.4a). Next, electrochemical polishing is performed to obtain a smoother and more homogenous surface. Finally, a second chemical etching step is carried out for improving and fine-tuning the surface to control cell behaviour on the samples. In this way, micro- or nano-pits and holes are obtained on the surface structure; they will improve cell attachment. Figure 2.5 shows this surface roughness modification steps on SLM produced Ti6Al4V TE scaffolds. Although this protocol has been used previously, an optimization of the electrochemical polishing needs to be performed and will be the main topic of this master thesis. This optimization will have to be carried out based on a thorough characterization of the effect of the surface roughness modification settings on the mechanical and morphological properties.

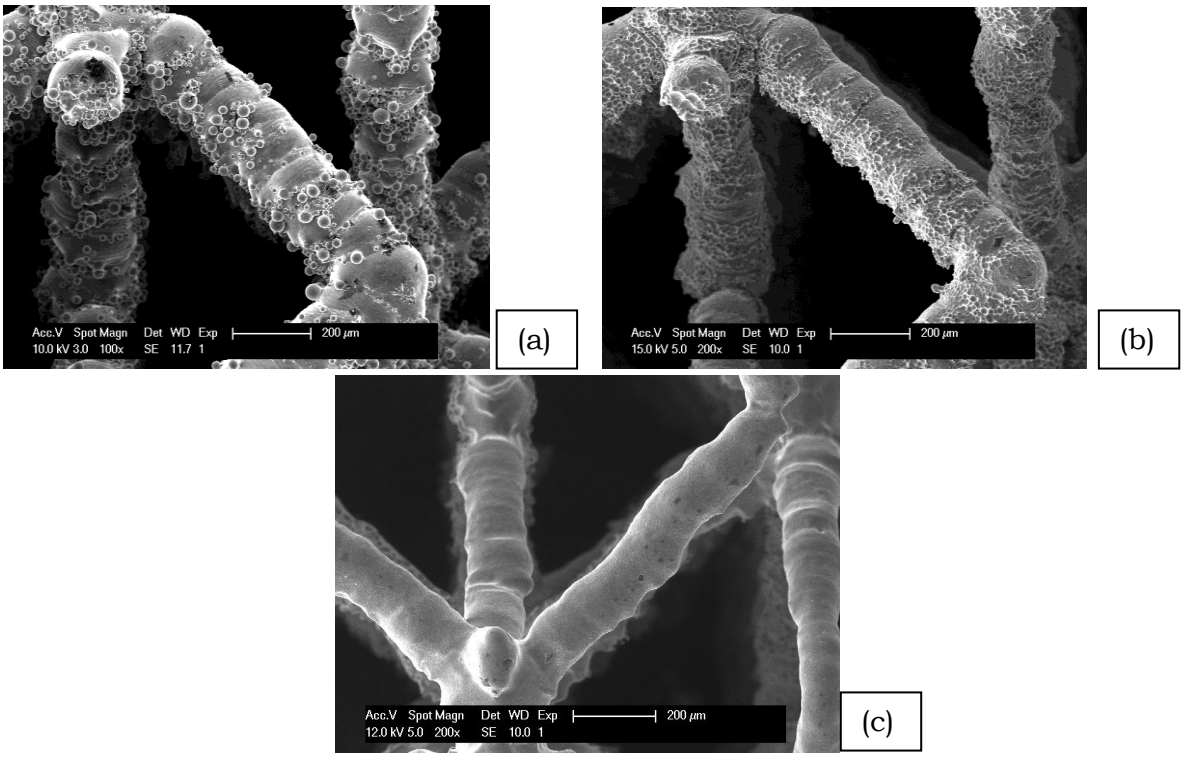

Fig.2.5. Typical SEM images of an SLM produced Ti6Al4V scaffold (a) after production, (b) after chemical etching and (c) after electrochemical polishing.

Concerning PCL scaffolds, the main problems found in literature can be summarized into the following ones: (i) absence of cell recognition sites on the surface of the scaffolds; (ii) hydrophobicity; (iii) acidic degradation products generated from hydrolysis of PCL [8]. Results indicate that blending these samples with other synthetic or natural polymers like chitosan is a good solution to improve their properties: acceleration of the degradation of the PCL components and buffering the acidic degradation products of some others PCL components [8]. Mechanical properties such as compressive characteristics and dimension stability are maintained or even improved working with both materials blended. Well-controlled pore parameters PCL/chitosan scaffolds

have been developed using a particle-leaching technique and salt particles as porogen [8].

Another option to enhance the surface of PCL scaffolds is to apply surface coatings. In contrast with high energy radiation such as plasma, laser, and ion beam which can be only applied to 2D films or very thin 3D scaffolds, CVD (Chemical Vapour Deposition) has the ability of getting absolute conformance to substrate topology and penetrate into complex geometries porous structures for coating them totally [13]. The mechanism foundation is the deposition of poly ((4-amino-p-xylylene)-co-(p-xylylene)) (PPX-NH2) on inert PCL surface in order to build a reactive amine layer on the substrate surfaces. Results demonstrate high cells survival rates and also a continuously proliferation of them on that CVD treated PCL surfaces [13].

In order to enhance osteoblasts adhesion and proliferation, alkaline treatment is found as a straightforward way on improving the surface hydrophilicity of scaffolds by increasing the hydrophilic terminal groups (carboxyl and hydroxyl groups) on the rods surface [14]. The strategy is to modify the PCL scaffolds by sodium hydroxide (NaOH) pretreatment with the intention of altering the surface characteristics of the scaffolds rods. Results suggest that an increase of surface roughness on the scaffolds rods largely influence the extent early new bone formation. In some studies, vascular endothelial and smooth muscle cells demonstrated also better adhesion and enhanced proliferation when NaOH was utilized to modify PCL films [14]. There were no reports of any complications detected; it suggests that the additional series of rinsing and sterilization following NaOH treatment of the PCL scaffolds assisted in promoting a conducive in vivo environment for healing to take place [14].

In this master thesis, first and in depth characterization of the as-produced PCL scaffolds needs to be performed. Then, a 96 hours 3M NaOH and also KOH immersion was carried out in different groups of samples in order to get the appropriate surface morphology for further biological and mechanical specifications into the scaffolds, according to the procedure found in the literature.

2.4. Characterization of porous material

One of the main goals of this master thesis is to analyze how surface roughness modifications will affect the characteristics of the TE scaffolds, both morphologically and mechanically and both on a global and a local scale. To morphologically characterize a porous structure like TE scaffolds, the most important architectural and structural characteristics that are necessary to have in mind are: porosity, surface area and volume ratio, interconnectivity, pore size, and strut/wall thickness. All of them are necessary in order to adjust the scaffold design with the functional specifications that it will have during its lifetime and to fine-tune the surface roughness modification protocol. Additionally a thorough mechanical characterization is necessary.

The following methods and techniques have been frequently used to characterize porous structures [7, 15, 16, 17]:

(1) Finite Element Method (FEM) for mechanical characterization: finite element models can be created using tomographic techniques to account for the architecture in the modeling of porous materials. The tomographic images describe perfectly the complexity of the architecture of porous materials in three dimensions, and FEM is

the most appropriate tool to interpret these results [15]. Using Finite Element Analysis (FEA), it is possible to determine the difference in mechanical properties between the idealized CAD models and the physical scaffolds. In the study of Garrett Ryan et al. [7], FEA simulations of randomly selected repeating unit-cells were performed and compared with both the macroscale FEA models and experimental data. This technique has an enormous potential to describe the properties of the scaffolds as a whole using unit-cell models.

(2) X-ray Microfocus Computed Tomography (micro-CT) [17]: Micro-CT provides precise quantitative and qualitative information on the 3D morphology of the specimen. Even the interior of the specimen can be studied without any damage or destruction of it. In micro CT scanning, the specimen, which is in between the X-ray source and the detector, is divided into a series of 2D slices which are irradiated with X-rays. Upon travelling through the sample, the X-rays are attenuated because of the different absorption coefficients of the sample. These are depending on: the density, the atomic number of the constituent and the energy of the X-ray beam. The emergent X-rays with reduced intensities are captured by the detector. Once the X-ray source is working, the data acquisition system reads the signal from each individual detector element and converts it into numeric values and transfers the data to a computer to be processed. Figure 6 shows this process [16]. The system creates a 2D pixel map from the computations and each pixel is denoted by a threshold value which corresponds to the attenuation coefficient measured at a similar location with the specimen. The results are 2D maps showing the material phases within the specimen. 3D image processing and analysis programs are required to visualize and analyze in a more complete way the internal structure of the material [17]. One important practical advantage of this method is that its non-destructive character allows large deformation on the piece to be imaged so it is possible to visualize phenomena like buckling, bending or fracture [15].

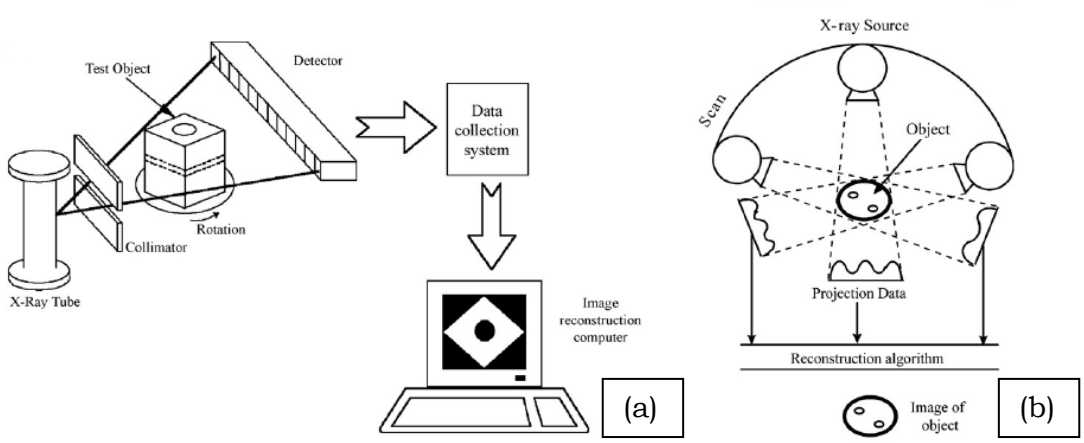

Fig.2.6. (a) A schematic presentation of a micro-CT scanning system and (b) a schematic presentation of CT image reconstruction with its algorithm.

(3) Scanning electron microscopy (SEM): the surface properties can also be examined using SEM images. The main difference with micro-CT and the big disadvantage too is the need of physical sectioning to examine the scaffold interior. The problem is that this would introduce unnecessary compression and edge effects into the scaffold architecture, thereby compromising the results and damaging the sample so that is no longer possible to perform other tests, like compression or tensile tests [17].

Other methods used to measure the main properties of porous structures like scaffolds are: theoretical calculation, mercury porosimetry, gas pycnometry, flow porosimetry and gas adsorption [17]. For mechanical characterization of porous structures, compression tests can be carried out with a universal testing machine. In this way, the elastic modulus, the compressive yield strength, etc. can be obtained. To be able to correlate the mechanical properties directly to the morphology of porous structures, in situ loading tests inside a micro-CT system can be carried out in order to examine and evaluate the behaviour of the samples for their future application requirements: load resistance, deformation, break or crack presence, etc. [7, 18, 19]. E-modulus and maximum permissible deformation and load can be obtained with the help of stress-strain curves. Micro-CT is very useful for analyzing the structural changes during the loading process [18, 19].

2.5. Conclusion

Porous materials are present and are used in a lot of different applications. The field of application of the porous structures that have been examined in this master thesis are biodegradable or bio-inert porous materials for tissue engineering (TE), and more specific titanium alloy (Ti6Al4V) and PCL (polycaprolactone) scaffolds. An important goal when these structures are built is provide them with mechanical properties comparable to the ones of bone, but also a robust and controlled morphology and surface properties. Rapid prototyping (RP) represent the most advanced method to build porous structures because they allow obtaining a desirable scaffold geometry both

internal and external, controlling the pore factors and also the most important properties. However, they do not allow a high control of the surface properties.

Since also the available surface and the surface roughness of scaffolds are known as two important factors that will allow the scaffold to be cell-friendly, a robust control of them is desired. In order to obtain this purpose, several surface roughness modification procedures of porous scaffolds have been developed. Nowadays, chemical etching and electrochemical polishing are two of the most important techniques applied. Elimination of unmelted powder grains and other impurities on the surface and getting more homogeneous and controlled surface properties are the effects expected after these surface treatments.

The parameters for the surface roughness modification however, also need to be controlled and when the effect of the surface roughness modification on the morphological and mechanical properties, and on the surface roughness, are characterized, a feed back to the surface roughness modification protocol can be provided in order to obtain, after surface roughness modification, porous scaffolds with the required morphological, mechanical and roughness properties. If the surface roughness modification can be performed in a controlled and robust way, even a correlation with the production and design parameters can be made, so the relation between the designed scaffolds and surface modified ones is well-known. It is therefore the purpose of this master thesis to perform an in depth characterization of the effect of surface roughness modification on the morphological and mechanical properties, and on the surface roughness, so that in this way, the surface roughness modification procedure can be optimized and be made more controlled and robust.

3. Materials & Methods

3.1. Materials

In this master thesis, two different material types have been used to produce porous TE scaffolds: a titanium-alloy (Ti6Al4V) and polycaprolactone (PCL). The main powder characteristics of these two material types can be found in Table 3.1 and Table 3.2.

Table 3.1. Specifications of the Ti6Al4V powder.

	Ti6Al4V
Density (g/cm³)	4,42
Max. Tensile Strength (MPa)	1000
Tensile Strength at 0,2% deformation (MPa)	920
Max. Strain (%)	12
E modulus (GPa)	110
Melting point (ºC)	1649
Average Grain Size (μm)	25

Table 3.2. Specifications of the PCL powder.

	PCL
Average Molecular Weight	50000
Particle size (μm)	<600 (98%)
Melting point (ºC)	59
Water content (%)	<1
Solubility parameter (cal/cm³)	9,38

3.1.1. Ti6Al4V porous TE scaffolds

The Ti6Al4V porous TE scaffolds were produced using selective laser melting (SLM), a rapid prototyping technique (RP). Fig. 3.1 shows schematically the SLM process. With SLM, the actual part is generated by a repeating process of applying new material layers by moving the built cylinder down in the Z-direction, flattening the new powder layer with a roll and transferring the area and contour information of each layer into the material using a laser beam. The structures are mostly built on top of a plate that acts as a support from which they are removed by wire electrical discharge machining (wire EDM). Building layer by layer by selectively melting of the titanium alloy powders with the help of a CO_2 laser beam, this method allows producing porous structures with a controlled porosity and morphology. The technical details of the SLM machine used for this master thesis are presented in Table 3.3.

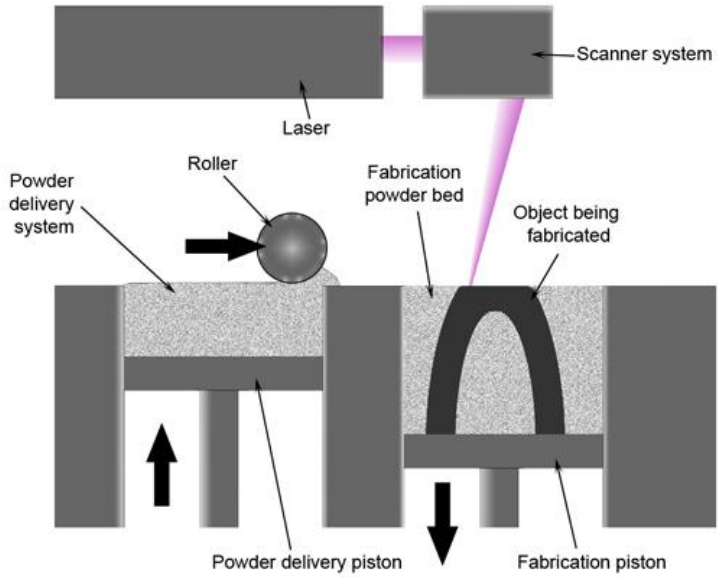

Fig.3.1. Schematic overview of the SLM production process: a repeating process of applying new material powder layers by moving the built cylinder down in the Z-direction, flattening the new powder layer with a roll and transferring the area and contour information of each layer into the material using a laser beam.

Table 3.3. Technical details of the SLM machine.

Laser	Yb: YAG
Mode	continuous
Wavelength (nm)	1085
Spot size (mm)	80
Scan speed (mm/s)	260
Power (W)	42

Concerning the design of the Ti6Al4V porous TE scaffolds used in this master thesis, figure 3.2a shows a typical 3D Computer Aided Design (CAD) model of the design. It is based on a parametric unit cell (fig. 3.2b), which consists entirely of identical beams with constant circular cross-section that meet in the nodes and is defined by three parameters: the beam diameter, the beam length and the pore diameter (fig. 3.2c).

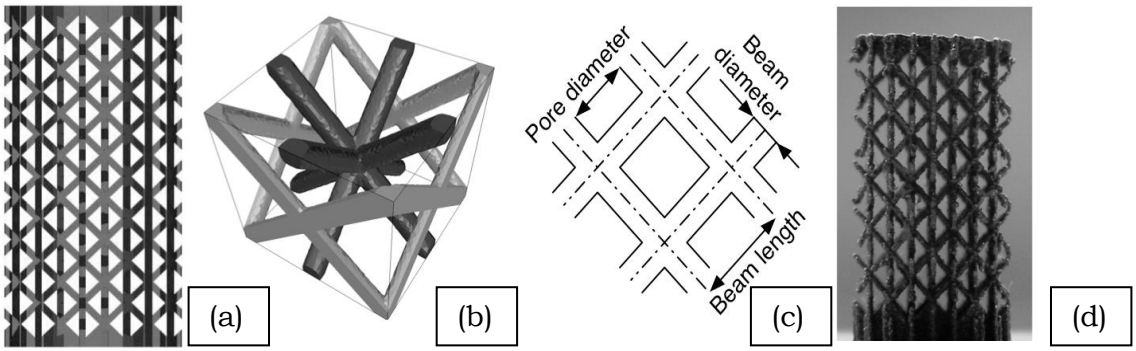

Fig.3.2. A typical (a) 3D CAD-model, (b) unit cell of the designed porous structures, (c) cross-section of the unit cell showing the beam diameter, the beam length and the pore diameter and (d) SLM fabricated open porous Ti6Al4V structure including the horizontal supports.

Note that the unit cell, as shown in figure 3.2b, consists of two identical (apart from a translation) but disconnected components. Nesting both components requires that both components are joined at the bottom and/or top of the structure using horizontal supports, as shown in figure 3.2d, which represents an SLM fabricated open porous structure.

Three different design variations have been assessed in this master thesis, having the same unit cell, but different designed beam diamater, namely 100 µm (beam 100), 140 µm (beam 140), 180 µm (beam 180) respectively. Table 3.4 summarizes the design characteristics for these porous scaffolds, and table 3.5 shows the diameter and height of all the porous scaffolds.

Table 3.4. All types of scaffolds used.

Material	Sample name	Number of samples	Designed strut thickness (µm)
Ti6Al4V	Beam 100	15	100
	Beam 140	10	140
	Beam 180	10	180

Table 3.5. Diameter and height of the Ti6Al4V porous scaffolds.

Material	Sample name	Diameter (mm)	Height (mm)
Ti6Al4V	Beam 100	5,98 ± 0,02	11,79 ± 0,06
	Beam 140	6,15 ± 0,09	11,82 ± 0,04
	Beam 180	6,39 ± 0,09	11,83 ± 0,06

Although SLM allows producing porous structures with a well-controlled morphology, the surface roughness can currently not be controlled in a robust manner. Fig. 3.3 shows a typical strut of a porous Ti6Al4V scaffold after production, where a significant amount of unmelted powder grains can be noticed on the surface of the struts, resulting in a high and uncontrolled surface roughness. Therefore, the aim of this master thesis is to develop and

optimize a proper surface roughness modification procedure and a profound characterization protocol for the quantification of the effect of the surface roughness on the morphological and mechanical properties.

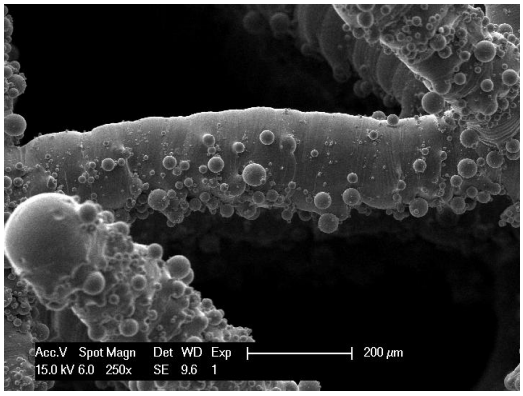

Fig.3.3. A typical scanning electron microscopic (SEM) image of a single strut of a porous Ti6Al4V scaffold after production, where a significant amount of unmelted powder grains can be noticed on the surface of the struts.

3.1.2. PCL porous TE scaffolds

For the PCL porous TE scaffolds, another RP technique was applied, namely fused deposition modeling (FDM). By depositing parallel series of material rods by melt extrusion and changing the direction of material deposition, a different design can be obtained. Fig. 3.4 shows a schematic representation of the FDM production process. The device used for the production was the 'Bioscaffolder' of Sys+eng (www.syseng.be)

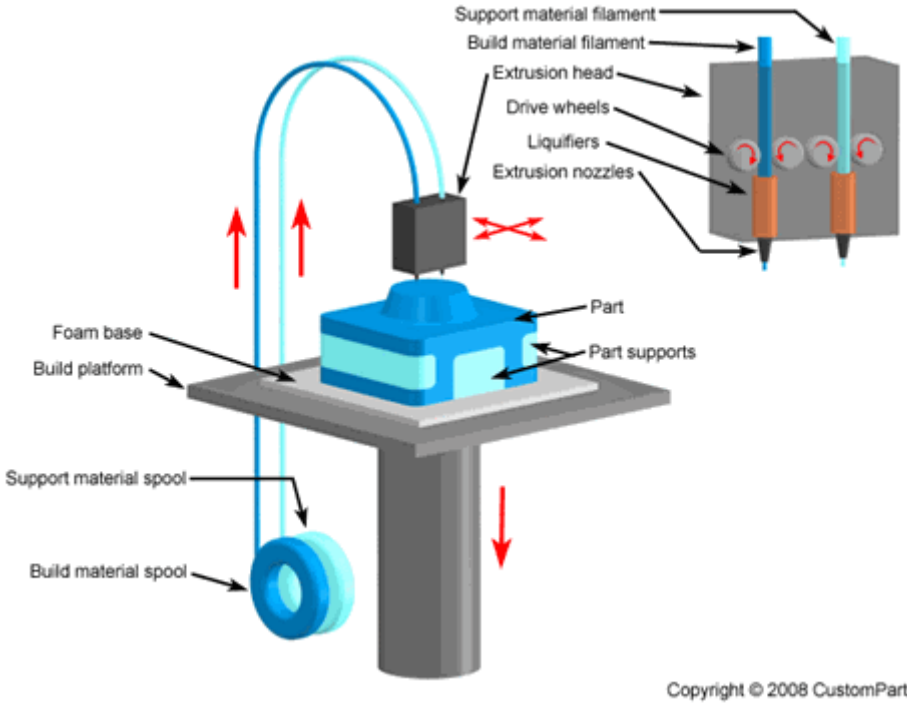

Fig.3.4. Schematic overview of the FDM production process: deposition of parallel series of material rods by melt extrusion and changing the direction of material deposition for changing the design.

Two types of design have been applied for the PCL scaffolds, namely the (i) 0-45-90-45´ lay-up design (beam A) and the 0-90 lay-up design (beam B).

Table 3.6 summarizes the different types of PCL scaffolds. The longitudinal micro-CT images of Fig. 3.5 clarify the difference between the two designs. The diameter and the height of all the PCL scaffolds are given in Table 3.7.

Table 3.6. The different types of PCL scaffolds.

Material	Group name	Number of samples	Designed strut thickness (μm)	Strut design
PCL	Beam A	6	300	0-45-90-45´
	Beam B	5	300	0-90

Table 3.7. Diameter and height of the PCL scaffolds.

Material	Group name	Diameter (mm)	Height (mm)
PCL	Beam A	5,36 ± 0,10	11,97 ± 0,06
	Beam B	5,44 ± 0,14	12,01 ± 0,06

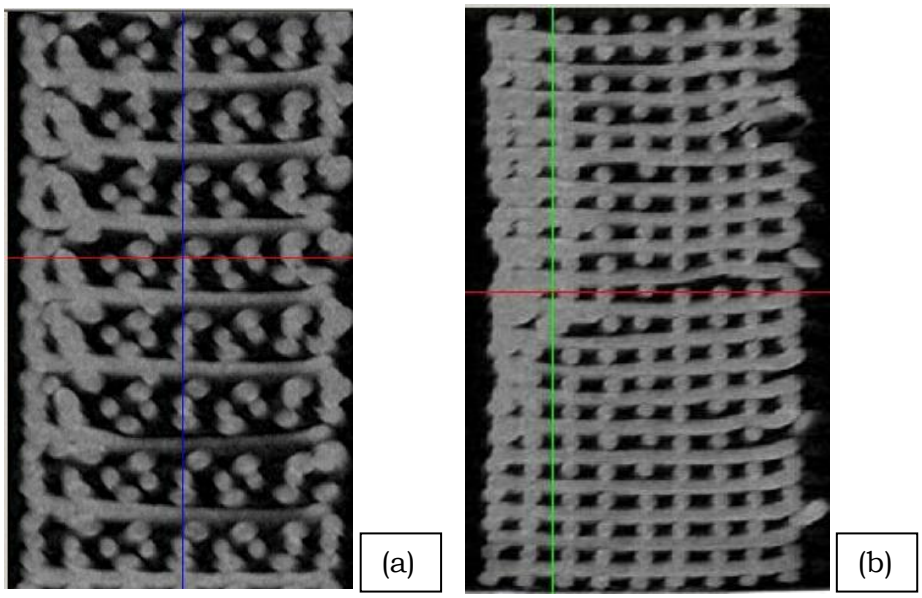

Fig.3.5. Typical longitudinal micro-CT slices through a PCL scaffold with (a) 0-45-90-45´ lay-up design (beam A) and (b) 0-90 lay-up design (beam B).

FDM, as it is also a RP technique, allows producing porous structures with a well-controlled morphology. FDM produced PCL scaffold also have a quite well-controlled surface roughness, as shown in Fig. 3.6 where a typical strut of a porous PCL scaffold after production can be seen. The surface of the PCL scaffolds is very smooth, containing some porosities, thus the cells will have difficulties to attach to the surfaces Therefore, also for the PCL scaffolds, the aim of this master thesis is to look for a proper surface roughness modification procedure.

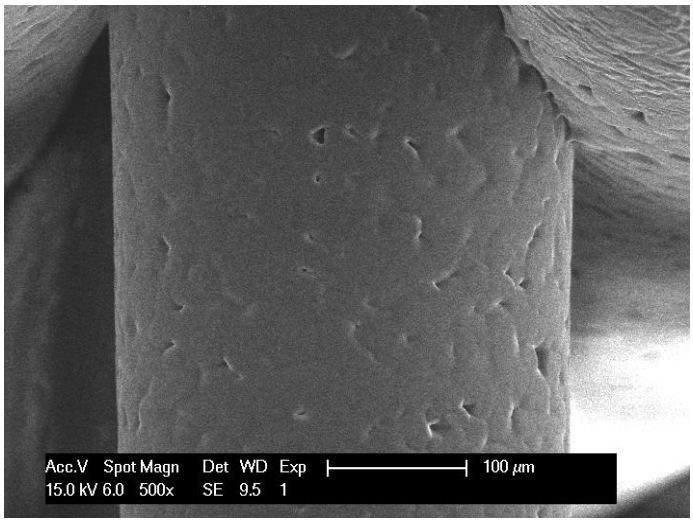

Fig.3.6. A typical SEM image of a single strut of a PCL scaffold, where a very smooth surface containing some porosities can be appreciated.

3.2. Surface roughness modification

3.2.1. Porous Ti6Al4V TE scaffolds

In order to improve surface properties of the porous Ti6Al4V scaffolds, two surface roughness modification steps were followed in this master thesis: (i) chemical etching and (ii) electrochemical polishing. These surface roughness modification procedures will, apart from removing the inhomogeneities of the struts, allow obtaining a cell-friendly strut topology.

3.2.1.1. Chemical etching

The chemical etching procedure is used in order to remove the unmelted powder grains attached to the surfaces of the struts and other surface impurities. The procedure has the following steps: (i) putting each sample in a chemical solution of 0.5 ml of HF and 50 g of distilled H_2O during 10 minutes (hydrofluoric acid, HF, Riedel-de Haën, Germany, p.a. 48%), (ii) removing the sample and putting it into a beaker with ethanol for cleaning and (iii) flushing the porous scaffolds a few times with distilled water and drying them.

3.2.1.2. Electrochemical polishing

The unmelted powder grains attached to the surface of the struts are removed by the chemical etching. As a result, the surface contains micro-pits and grooves, even more where a higher concentration of impurities and unmelted powder grains was present. The aim of electrochemical polishing is to obtain a more controlled and homogeneous surface roughness.

The applied electrolyte was prepared according to the following procedure: a mixture of 30 ml of H_2SO_4 and 55 ml of CH_3COOH (sulfuric acid H_2SO_4, Fisher Scientific, United Kingdom, p.a. >95%; acetic acid CH_3COOH, Acros Organics, Belgium, p.a. glacial) was left until cooled after which 15 ml of HF (hydrofluoric acid HF, Riedel-de Haën, Germany, p.a. 48%) was added carefully (these quantities were referred to 100 ml of electrolyte). The experimental setup is shown in figure 3.7, where the sample (anode, +), placed in the middle of the cylindrical platinum basket, (cathode, –) (Ø 30mm, 40mm height), was suspended with a platinum wire (Ø 300µm) in the polyethylene

beaker filled with electrolyte. The anode and the cathode were connected with cables to the direct current source (TS3021S –30V/2A, Thurlby Thandar Instruments Ltd., UK) and a current of 1.2 A was applied. The electrolyte was stirred during polishing with a magnetic stirrer. 8 minutes of electrochemical polishing was chosen. Finally, the sample was removed from the chemical solution, cleaned with ethanol, flushed a few times with water for cleaning and dried. The application of the cylindrical platinum basket as a cathode allows obtaining more homogenous conditions for polishing and allows 3D porous structures with very complex architectures to be polished.

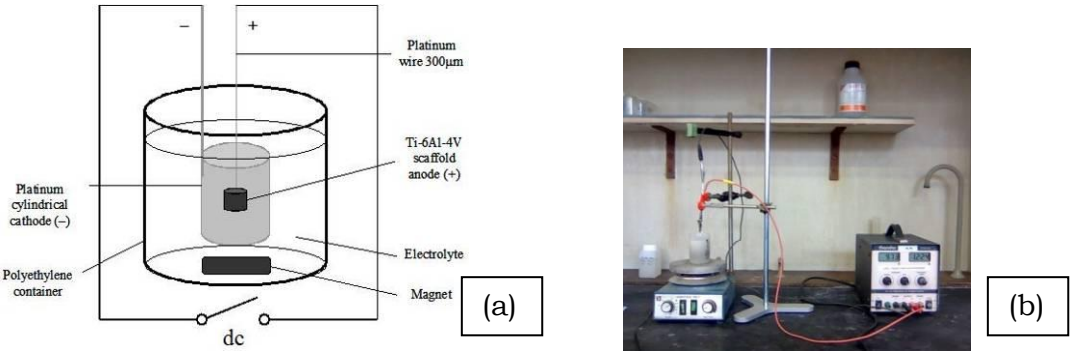

Fig.3.7. The experimental setup built for the electrolytic polishing of the Ti6Al4V bone scaffolds used for production of tested scaffolds

Fig.3.8 shows typical SEM images of a single strut after production with attached powder grains, of the same strut after chemical polishing where the unmelted powder grains are removed but micro-pits are still present, and after chemical and electrochemical polishing resulting in a smooth surface.

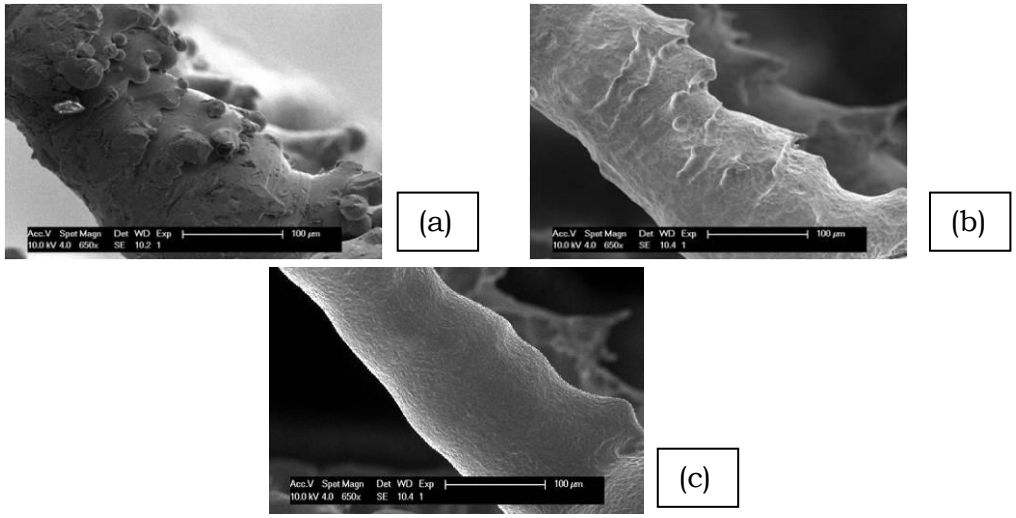

Fig.3.8. Typical SEM images of the: a) raw strut after production with attached powder grains, b) the same strut after chemical polishing, c) the same strut after chemical and electrochemical polishing.

3.2.2. Porous PCL TE scaffolds

For PCL scaffolds, surface roughness modification was performed applying an alkaline treatment according to Yeo et al. [2008]. The purpose was to obtain more controlled surface properties and better attachment and proliferation of the cells. According to Yeo et al. [2008], PCL scaffolds were immersed in phosphate buffered saline, PBS (137mM NaCl, 2.7 mM KCl, 10 mM Na_2HPO_4,

1.8 mM KH_2PO_4, pH 7.4) for 2 hours followed by immersion into 3M NaOH for 96 hours at 37ºC The same procedure was repeated using KOH instead of NaOH for another group of PCL porous scaffolds. Fig.3.9 illustrates the changes in the surface morphology that appeared because of the two different treatments carried out.

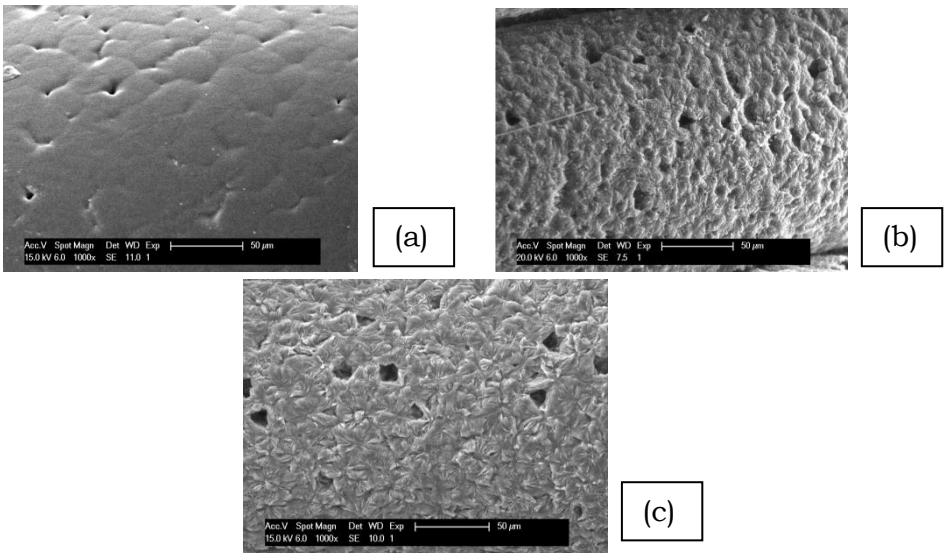

Fig.3.9. Typical SEM images of the: a) raw strut after production, b) strut after KOH 96h treatment, c) strut after NaOH 96h treatment.

3.3. Characterization techniques

3.3.1. Archimedes principle

In order to determine the density and the porosity of all the porous scaffolds, Archimedes tests were carried. The device used was a Sartorius YDK 01, YDK 01-0D Density Determination Kit. The density of a porous scaffold can be easily obtained if the density of the liquid it is immersed in is known. Ethanol was the liquid used and in order to calculate its density, a glass plummet of a known volume was introduced in that liquid. Measuring the buoyancy of that plummet, in other words, the mass of the liquid displaced by it, the liquid density is found with the help of eq. (3.1).

$$\rho(fl) = \frac{G}{V} = \frac{7.8583}{10} = 0.78583 \ {}^{g}/_{cm^3} \tag{3.1}$$

By measuring the mass of each porous scaffold outside (mass in the air W(a)) and inside the liquid (buoyancy, G), and by subtracting both values, the mass of each sample in ethanol (W(fl)) is obtain. Using eq. (3.2) the density of the porous scaffolds is calculated.

$$\rho = \frac{W(a)\cdot\rho(fl)}{W(a)-W(fl)} \tag{3.2}$$

Using the density of the porous scaffold material, the porosity can be obtained using eq. (3.3), (3.4) and (3.5). Fig.3.10 illustrates the Archimedes test device used for the calculation of density and porosity.

$$Vsample = Vcilinder = (\pi \cdot r^2) \cdot height \quad (3.3)$$

$$Vmaterial = \frac{W(a)}{\rho} \quad (3.4)$$

$$Porosity = \frac{(Vsample - Vmaterial)}{Vsample} \quad (3.5)$$

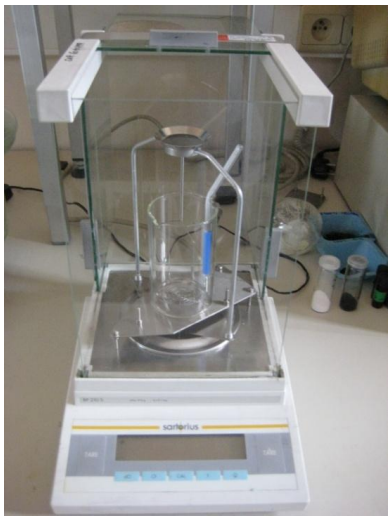

Fig.3.10. The Archimedes testing device.

3.3.2. Micro-CT

Microfocus X-ray Computed Tomography (micro-CT) is a non-destructive technique which allows making a precise study of external and internal properties of a material. The sample is located in between the microfocus X-ray source and the detector, and is radiated by the X-rays resulting in a series of 2D radiographic slices (Saey et al. [2006]). Because of the different absorption coefficients of different materials in the sample, the X-rays, which are travelling through it, are attenuated differently and the emergent rays with reduced intensities are captured by the detector. Finally the data acquisition system reads the signal from each individual detector element and converts it into numeric values, transferring the data to a computer to be processed. The results are 2D maps showing the material phases within the specimen (radiographs). Using a reconstruction algorithm, those images can be converted to 2D images of the section of the sample to be then stacked together to form a 3D image of the full sample in a non-destructive manner. Figure 3.11 clarifies this process. Fig.3.12 shows a typical radiographic image of a porous Ti6Al4V scaffold. In this master thesis the 'NRecon' software of SkyScan NV [Kontich, Belgium] was used for the reconstruction of the micro-CT images.Fig.3.13 represent typical cross-sectional micro-CT images of a porous Ti6Al4V scaffold after production, after chemical etching and after chemical etching and electrochemical polishing.

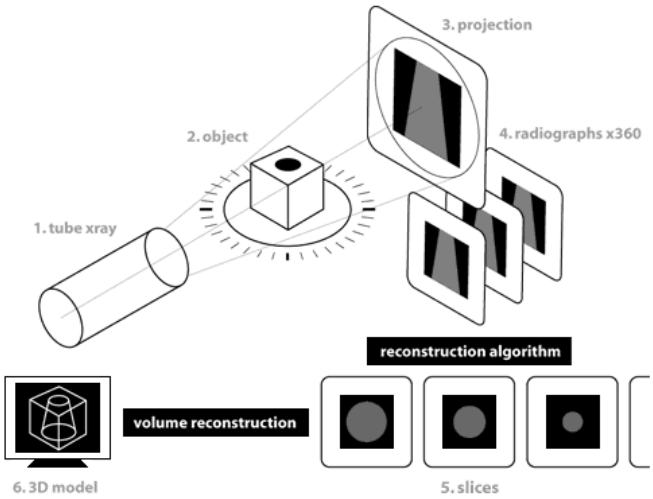

Fig.3.11. Schematic image showing the micro-CT process analysis (http://www.digitalscanservice.com).

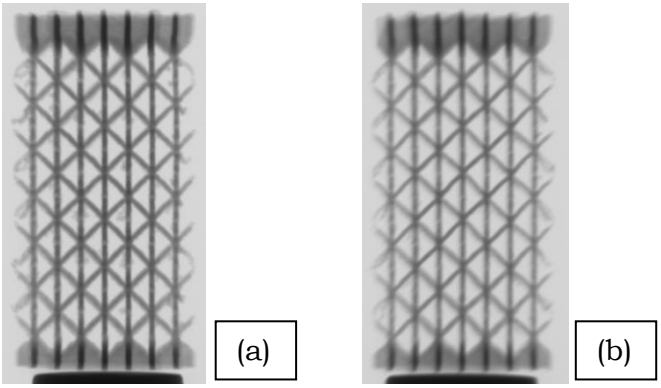

Fig.3.12. Typical radiographic images of a porous Ti6Al4V scaffold *(a)* prior to and *(b)* after chemical etching.

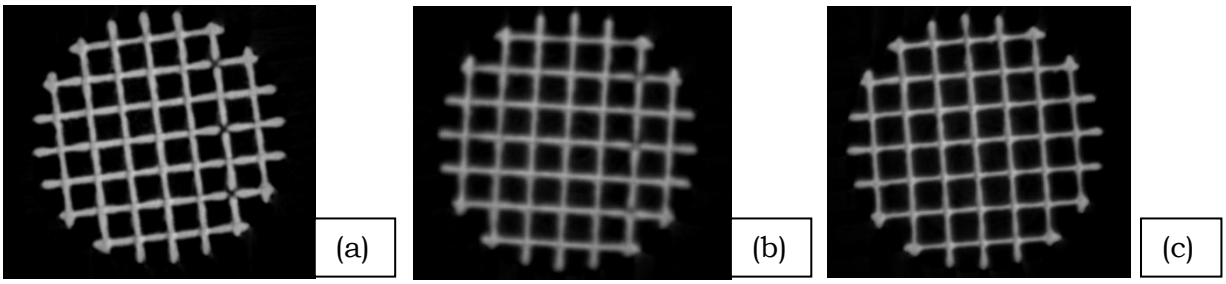

Fig.3.13. Typical cross-sectional micro-CT images of a porous Ti6Al4V scaffold (a) after production, (b) after chemical etching and (c) after chemical etching and electrochemical polishing.

Micro-CT scanning was applied on all porous scaffolds in order to characterize the samples morphologically before and after surface roughness modification and to determine the surface roughness of the porous scaffolds. The aim was to investigate the effect of the surface roughness modification on the most important morphological parameters of the samples such as percent object volume, object surface, object surface/volume ratio, structure thickness, structure separation and total porosity percentage. Additionally, high resolution micro-CT can be used to determine the surface roughness of the internal struts.

For the morphological analysis of the porous scaffolds the Philips HOMX 161 X-ray system [Philips X-ray – Hamburg, Germany] was used for micro-CT image acquisition. This micro-CT device is upgraded with the AEA Tomohawk [AEA Technology – Oxon, UK] computer tomography upgrade. A tube voltage of 90 kV and a current of 0.39 mA were applied. The angular increment was 0.3 degrees and a frame averaging of 32 was chosen. An isotropic voxel size of 12.6 μm was obtained for all the porous scaffold types. Table 3.8 summarizes the main characteristics of the Philips HOMX 161 X-ray system and Fig.3.14 illustrates the micro-CT machine used. For the image analysis of the cross-sectional micro-CT images, the 'CTAn' software program [SkyScan NV - Kontich, Belgium] was applied.

Table 3.8. Characteristics of the Philips HOMX 161 X-ray micro-CT device.

	Philips HOMX 161 X-ray system
Source type	Reflection
Voltage range (kV)	15-160
Maximum power (W)	32
Microfocal spot (μm)	from 5 to 200
Min. voxel size (μm)	± 5
Detector system	Image intensifier (TH 9428HX) and CCD camera - 1024 x 1024 pixels - 12 bit dynamic range
Max.sample diameter (mm)	110

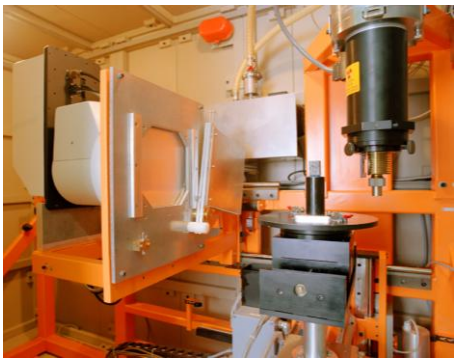

Fig.3.14. The Philips HOMX 161 X-ray system with AEA Tomhawk CT upgrade.

For the determination of the surface roughness, high resolution micro-CT was the technique chosen, since it allows generating images with better precision and image quality, and with higher spatial resolution. The high resolution micro-CT device used in this master thesis, namely the SkyScan 1172 system [SkyScan NV - Kontich, Belgium] gives a high spatial resolution without compromising sample size thanks to a new large format cooled X-ray digital camera. Another improvement of high resolution micro-CT comparing with the standard one is that has a more sensitive detector at low photon energies. The SkyScan 1172 scanner has a 100 kV tungsten X-ray source from Hamamatsu Photonics K.K. [Shizuoka, Japan]. The main specifications of this micro-CT device are given in Table 3.9 and an image of the SkyScan 1172 system is shown in Fig. 3.15. Fig. 3.16 shows typical high resolution micro-CT images of a porous Ti6Al4V scaffold prior to and after chemical etching. A description of the surface roughness calculation protocol based on the high resolution micro-CT images is provided in section 3.3.4.

Table 3.9. Characteristics of SkyScan 1172 scanner.

	SkyScan 1172
Source type	Reflection
Voltage range (kV)	20-100
Maximum power (W)	10
Microfocal spot (μm)	<5
Min. voxel size (μm)	±1
Detector system	Phosphor screen and high resolution cooled CCD camera - up to 4000 x 2300 pixels - 12 bit dynamic range
Max.sample diameter (mm)	35 mm for normal scan and 68 mm for scan with camera offset

Fig.3.15. The SkyScan 1172 micro-CT system.

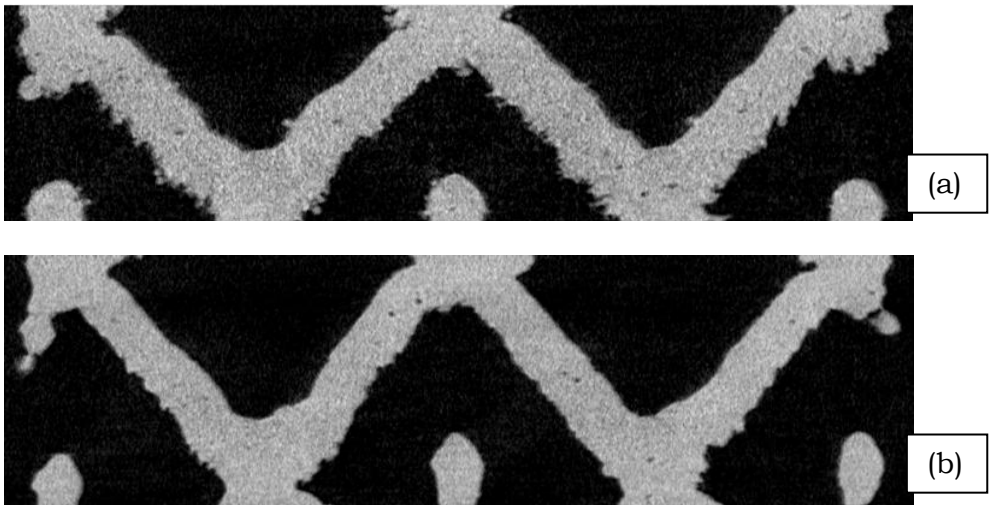

Fig.3.16. Typical high resolution micro-CT images of a porous Ti6Al4V scaffold (a) prior to and (b) after chemical etching.

3.3.3. SEM

To determine the surface roughness of the struts and to make a qualitative and quantitative analysis of the effect of surface roughness modification procedures on the surface roughness, Scanning Electron Microscopy (SEM) was used. A SEM device reproduces surface images of a material with high precision and definition, bombarding the sample with an accelerated electron

beam. The energy produced because of the electron-sample collision is dissipated in some ways of signals; one of them is the emission of secondary electrons which are collected by some specific detectors in order to produce the SEM images of the sample. Unlike micro-CT, SEM can only study the material outside, but it is very useful to quantify its surface morphology and to calculate the roughness of the scaffold struts which are localized at the edges of the scaffold. Fig.3.17 shows the mechanism of a SEM device.

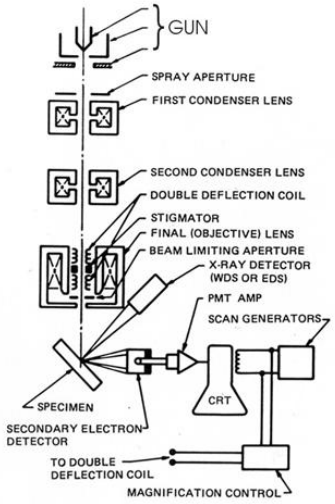

Fig.3.17. Schematic drawing of the electron and X-ray optics of a combined SEM-EPMA (http://serc.carleton.edu**).**

SEM images of porous Ti6Al4V scaffolds were taken before chemical etching, after chemical etching and after electrochemical polishing for two opposite sides of each sample and for 3 struts localized in different areas (top, middle and bottom of the scaffold). For this purpose, an acceleration voltage of 15.0 kV, a spot size of 6.0 μm and a working distance (WD) of 10.0 μm were used. Fig.3.18 shows the XL40 (Philips XL40 Series), the SEM machine used in this master thesis. Fig.3.19 indicates in the three SEM images of the same strut of a porous Ti6Al4V scaffold but after different steps in the surface modification procedure, the surface changes due to chemical etching and then electrochemical polishing.

Fig.3.18. The XL40 SEM device.

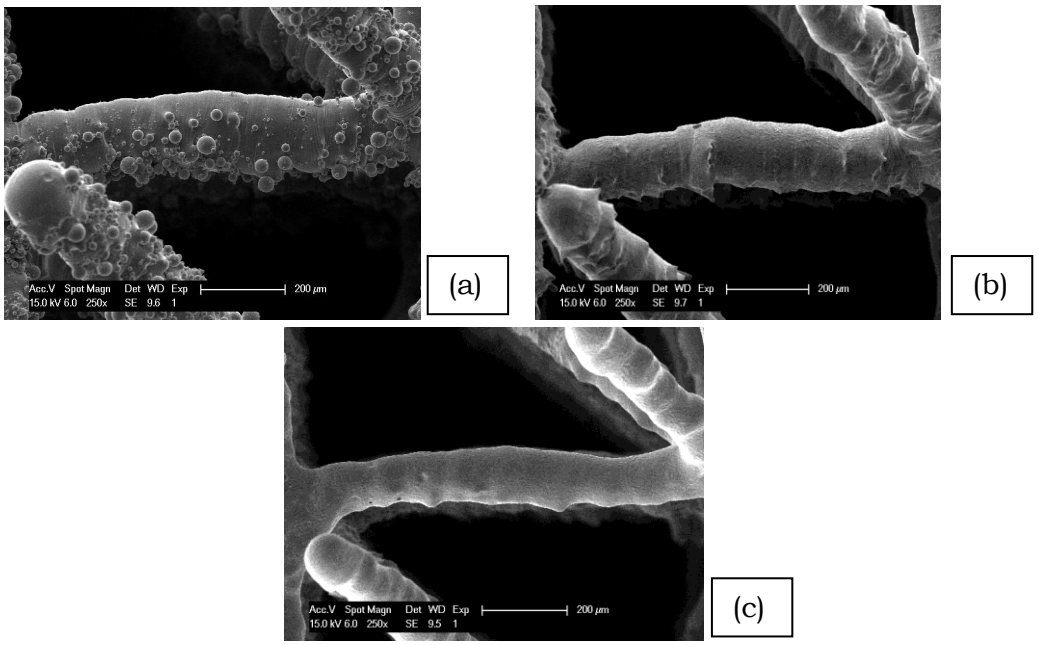

Fig.3.19. Typical SEM images of a single strut of a porous Ti6Al4V scaffold (a) after production showing the unmelted powder grains on the surface, (b) after chemical etching showing the removal of the unmelted powder grains but a remain of micro-pits and (c) after electrochemical polishing showing a smooth surface.

3.3.4. Surface roughness calculation

The surface roughness determines the surface morphology of a substrate in quantitative way. Therefore an appropriate analysis of the surface topology of the 3D porous structures is needed. Since commercially available profile measuring systems fail when determining the strut surface roughness of the complex, 3D porous structures, and because a high surface roughness of the strut compared to its dimension causes difficulties for the quantitative determination of the surface morphology, two new protocols for the quantitative analysis of the surface morphology are used in this master thesis using SEM and high resolution µCT cross-sectional 2D images. In these protocols, the roughness is calculated on the basis of the profile line of the strut surface in the 2D images.

- *SEM image based protocol* – no sample preparation is needed. 2D images of the struts were taken with the SEM (Philips XL40 Series) (Fig. 3.20a), which allows performing the measurements in a non-destructive way.
- *µCT image based protocol* - no sample preparation is needed. The high resolution SkyScan 1172 µCT system (SkyScan NV, Kontich, Belgium) has been applied in order to obtain 2D images of the longitudinal section of the struts (Fig. 3.20b and 3.20c).

An in-house developed MatLab routine (in cooperation with Dr. ir. Maarten Moesen) has been used to determine the following roughness parameters:

- the arithmetic average deviation $R_a = \frac{1}{n}\sum_{i=1}^{n}|y_i|$
- the root mean square deviation of the roughness profile from the mean line $R_q = \sqrt{\frac{1}{n}\sum_{i=1}^{n}y_i^2}$

- difference between highest peak and deepest valley $R_T = R_P - R_V$

where n = the number of data points in X direction, y = the surface height relative to the mean plane, R_P = the highest point and R_V = the lowest points in the evaluated length.

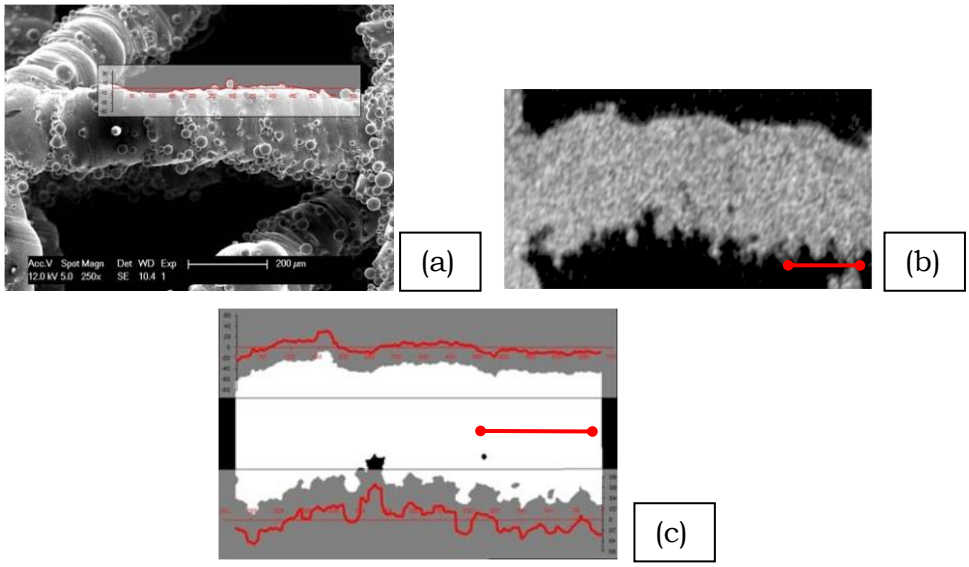

Fig.3.20. 2D images of a typical strut of a porous Ti6Al4V scaffold taken with (a) SEM where the profile line can be seen of the top of the strut, (b) high resolution µCT and (c) a binarized high resolution µCT slice where the profile line can be seen of the top and the bottom of the strut. Scale bars = 200 µm.

3.3.5. Mechanical testing

For mechanical testing of all the porous scaffolds, the in-situ loading stage for the micro-CT, as shown in Fig.3.21, has been used. Characteristics of the loading stage are summarized in Table 3.10. The porous scaffolds of different material types and different designs were continuously compressed until failure using the in-situ loading stage, obtaining the main mechanical properties using an in-house developed MatLab routine (in cooperation with Dr. ir. Maarten Moesen): E-modulus, ultimate compressive strength and ultimate compressive strain. Also, compression tests were performed on the surface roughness modified porous Ti6al4V scaffolds to evaluate the effect of the surface roughness modification on the mechanical properties. For PCL scaffolds, compression tests were only carried out prior to surface roughness modification. A compression speed of 0.2 mm/min and a preload of 0.01 kN were applied. A load cell of 3 kN was used. The tests were load controlled.

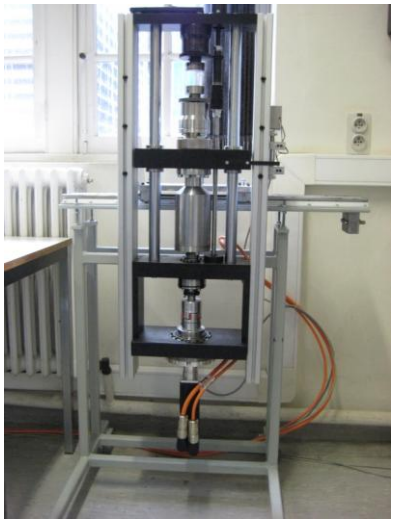

Fig.3.21. In situ loading stage for the micro-CT.

Table 3.10. Technical details of the in situ loading stage.

Crosshead speed (mm/min): 0.0014 - 12.5
Exchangeable “Sensy” load cells (30kN ± 30 N, 3 kN ± 1N , 100 N ± 0.02 N)
Max sample size: cylinder of 5 cm diameter and 5 cm height
Deformation rate between 0.005 en 5 mm/min
Load or displacement control
Control of relaxation

4. Initial experiment and problem statement

This master thesis was initiated with the characterization and comparison of two batches of porous Ti6Al4V scaffolds with a designed strut thickness of 100 μm in order to evaluate the effect of the surface roughness reduction on the biological cell behavior: one of them was named "as produced", and the other was named "surface modified". All the scaffolds where characterized morphologically and mechanically prior to surface roughness modification. For the "surface modified" scaffolds, three surface roughness modification steps were performed and again the morphological and mechanical properties were determined in order to evaluate the effect of surface roughness reduction. Three scaffolds per batch ("as produced" and "surface modified" after surface modification) were cut in half and were applied for *in vitro* cell behavior experiments.

4.1. Method

The three surface roughness modification steps that were done on the "surface modified" scaffolds were the following:

1) Chemical etching: elimination of undesirable unmeldted powder grains on the surface resulting from the production process.
2) Electrochemical polishing: obtaining a more homogeneous and smoother surface.
3) Chemical etching: extra step for introducing micro- or nano-pits and -holes to improve cell behavior. For this purpose, the porous Ti6Al4V scaffolds were immersed in ethanol after electrochemical polishing getting this additional chemical etching stage. This is not included in the standard process, but it could be interesting to study the effect of this third surface roughness modification in order to obtain better cell attachment and proliferation.

For both the as-produced and the surface roughness modified samples, morphological characterization, continuous mechanical testing, surface roughness measurements and biological experiments were performed. For the evaluation of the effect of the surface roughness reduction on the morphological properties, micro-CT scanning and image analysis were performed both prior to and after surface modification. Percent object volume, object surface, structure thickness and total porosity percent were the morphological properties obtained and compared. Additionally, the current density was determined since, as was found in the literature, it plays an important role on the scaffold properties after surface roughness modification. Also, SEM images were taken for the qualitative evaluation of the surface roughness. Finally, biological experiments were performed in order to obtain a direct feedback between the cell behaviour and the surface modification procedure. In these experiments, samples after surface roughness reduction were used for human periosteum derived (osteogenic) cells (hPDCs) seeding. After surface modification, 100,000 hPDCs were seeded on the scaffolds and were left for 7 days in an incubator in order to obtain static cells proliferation. After 7 days, live/dead staining, fluorescence imaging, SEM analysis and DNA

measurements have been performed in order to analyze the cell behaviour on the different surface morphologies.

4.2. Experimental results and discussion

- *Morphological characterization*

Table 4.1 summarizes the micro-CT derived morphological properties both prior to and after surface roughness modification. As can be seen in Table 4.1, the structure thickness of both batches at the raw stage was almost the same, also the total porosity percent. Percent object volume for "surface modified" batch diminish when surface roughness modifications were done. That is logical because the goal of them is the elimination of material making the pieces smoother and more homogeneous in their strut surfaces. Thus, object surface and structure thickness also diminished for this batch, whereas total porosity percent increased.

Table 4.1. Micro-CT derived morphological properties obtained for the "as produced" Ti6Al4V scaffolds and for the "surface modified" Ti6Al4V scaffolds prior to and after electrochemical polishing (EP).

Group name	Percent object volume (%)	Object surface (cm^2)	Structure thickness (μm)	Total porosity percent (%)
As produced	15,03 ± 0,49	9,41 ± 0,21	218,93 ± 3,23	84,96 ± 0,49
Surface modified	10,05 ± 0,47	7,63 ± 0,45	180,14 ± 11,65	89,95 ± 0,47

Figure 4.1 shows the reduction in structure thickness due to the surface roughness modification for one typical scaffold. A significant reduction of 38.79 μm after surface roughness modifications was obtained.

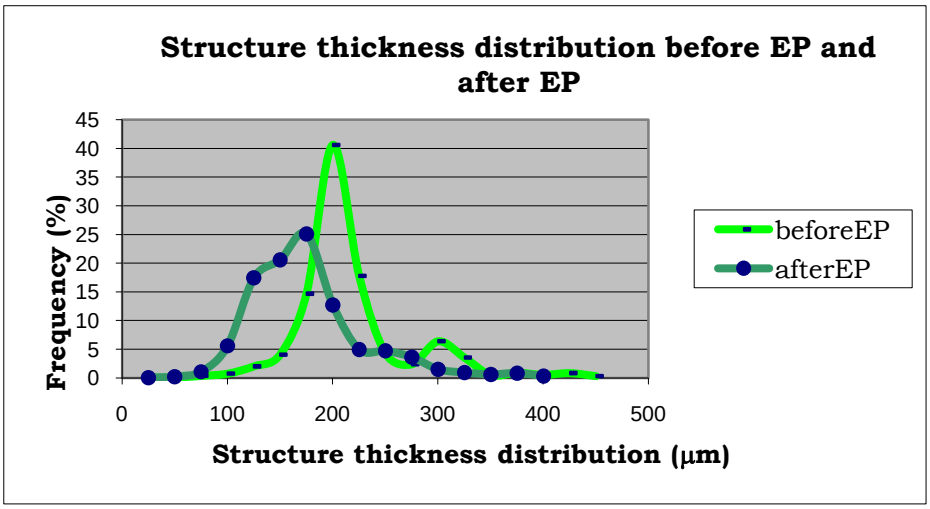

Fig.4.1. The micro-CT based structure thickness distribution for a typical porous Ti6Al4V scaffold prior to and after surface roughness modification.

The current density applied during electrochemical polishing will play an important role on the morphological properties of the surface modified Ti6Al4V scaffolds. It is defined as the current divided by the object surface. For the electrochemical polishing, a constant current of 1,2 A was used for all the scaffolds. According to the definition of the current density, the smaller the structure thickness of the sample is, the smaller is the object surface and hence the larger will the current density be. Figure 4.2 shows the current density values in function of the structure thickness. A decreasing trend can be appreciated, as was expected.

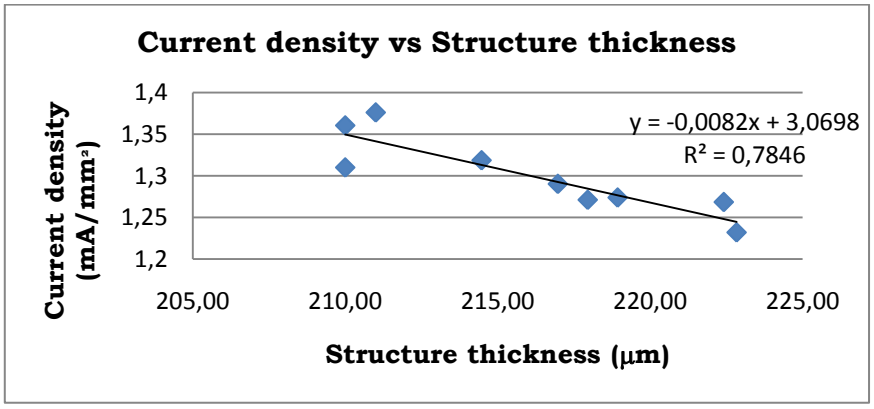

Fig.4.2. Current density in function of the structure thickness.

Even with differences of less than 15 μm in structure thickness, a small decrease in current density can be noticed. Therefore, it seems interesting for further experiments to study in depth the relation between current density and structure thickness.

To evaluate the surface roughness of the porous Ti6Al4V scaffolds both prior to and after surface roughness modification, SEM images were obtained and also prior to biological cell behavior experiments looking for significant differences in roughness after surface roughness modifications. Qualitative differences on the strut surface roughness of the Ti6Al4V scaffolds were observed.

- *In vitro cell behavior experiments*

Live/dead staining is an investigation that allows visualizing the living and dead cells on the substrate that with a fluorescent stereomicroscope. For this purpose, fluorescent markers should be added to the solution containing the cell seeded samples. In our experiments calcein has been used to visualize the living cells (cells are visualized with a green colour under the fluorescence microscope) and ethidium homodimer-1 for visualization of the dead cells (red colour). Figure 4.3 shows images of the living cells taken from the side (figure 4.3a-d) of scaffolds prior to and after surface roughness modification. The live-dead images did not show a significant amount of the dead cells, which implies a good biocompatibility of the Ti6Al4V scaffolds.

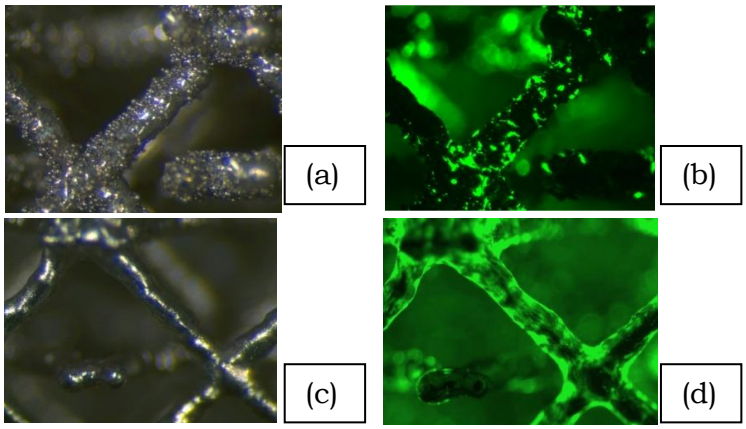

Fig.4.3. Live-dead stained images of the living cells on the Ti6Al4V scaffolds: view of the simple strut: prior to surface roughness modification– (a) without and (b) with seeded hPDCs after 14 days and after chemical etching and electrochemical polishing: (c) without and (d) with seeded hPDCs after 14 days.

In order to investigate the cell morphology on the modified surfaces with different roughness, SEM images of the scaffolds were taken with a SEM Philips XL30 Series device. For this purpose, the cells were fixed on the scaffolds with 2.5% glutaraldehyde compound. Before SEM investigation, the scaffolds were coated with gold and the SEM images were taken similarly like in the live/dead imaging, namely from the side (Fig. 4.4a-d) of the scaffolds with different surface roughness. Different cell behaviour was found, which is strongly related to the surface morphology. As can be seen in figure 4.4a,b, cells have the tendency to bridge places with high roughness and to build a 3D matrix-like structure close to the nodes. In case of struts with a smooth surface, a form of cell coating was formed (fig. 4.4c,d).

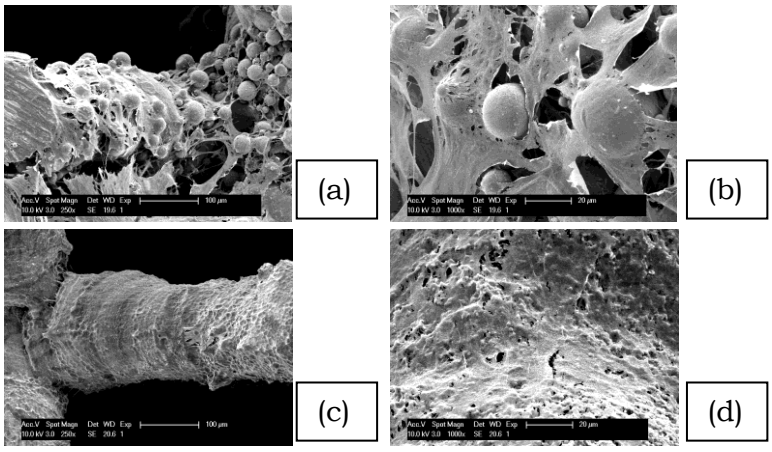

Fig.4.4. SEM pictures of the fixed cells on the scaffolds: view of the Ti6Al4V strut: (a,b) prior to and (c,d) after chemical and electrochemical polishing.

DNA measurements have been performed to determine the total cells amount on the scaffolds with different surface roughness. To quantify the cell DNA, the Qubit™ fluorometer protocol has been used, where the fluorescent signal from the cells DNA can be registered and quantified with the fluorometer. Figure 4.5 shows the results, indicating first a drop in the DNA-content for both the scaffolds prior to and after surface modification. However, for the surface modified scaffolds after 14 days an increase in the DNA-content was found, which can suggests better proliferation of the cells in this case.

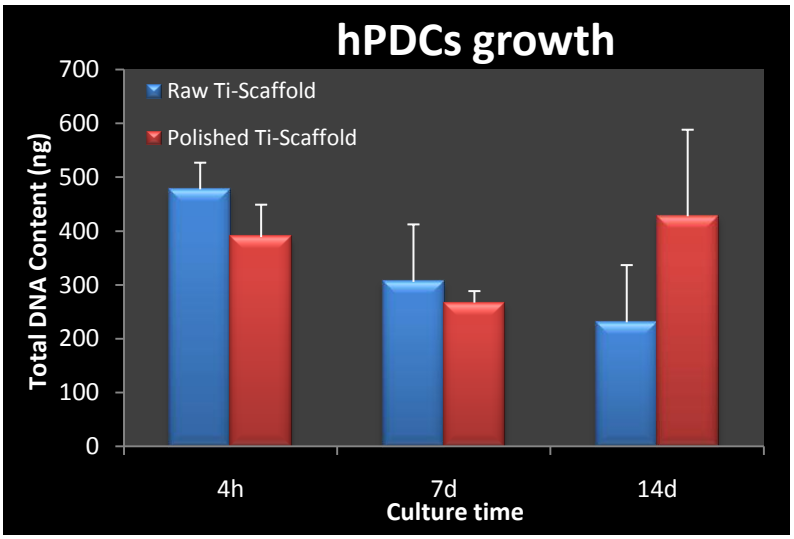

Fig.4.5. Results of the DNA measurements of the hPDCs cells after seeding on the scaffolds prior to and after surface roughness modification after 4h, 7 and 14 days of incubation.

Performed experiments revealed the differences in osteogenic cell response seeded on Ti6Al4V scaffolds with different surface roughness. Live/dead staining investigation and analysis of the DNA content indicate a better proliferation of the cells along the struts with modified surface, even diminishing the surface available due to mass reduction. This implies to assume that changes of the struts surface roughness can be used for controlling the cells behaviour. For these reasons further experiments with surface modification of the scaffolds with different design need to be performed.

4.3. Conclusion and problem statement

Important morphological properties changes for the porous Ti6Al4V scaffolds due to surface roughness modification were found. For instance, a significant structure thickness reduction due to surface roughness modifications was found. The current density decreased even with a small difference in structure thickness. Roughness values were also qualitatively different prior to and after surface roughness modification. Finally, biological experiments showed clearly different cell behavior for the Ti6Al4V scaffolds prior to and after surface roughness reduction. However, the available surface for the as-produced and the surface modified scaffolds also differed. Hence, the cell behaviour, and more specific the DNA-content measured, cannot be only contributed to the roughness of the scaffolds. Thus, a better control of the surface roughness modification procedure should be obtained and a thorough characterization of the effect of the surface roughness modification on the morphological, mechanical and surface properties needs to be performed

In order to study the role of the current density for the electrochemical polishing process, and in that way to fine-tune and to better control the electrochemical polishing step, in further experiments porous Ti6Al4V scaffolds with different designed strut thicknesses (100 μm, 140 μm and 180 μm) will be used.

5. Problem statement & Aims

The surface topology of porous scaffolds in tissue engineering (TE) plays an important role when it comes to controlling biological properties such as cell attachment and proliferation. One of the main goals of TE is to optimize the design of porous scaffold in order to obtain better biological properties without losing the mechanical ones. After analyzing the results from the first part of this master thesis (chapter 4), it became clear that the surface roughness modification procedures were not optimized and thus need to be optimized.

It is therefore the aim of this master thesis, to perform an in depth characterization of the effect of surface roughness modification on the morphological and mechanical properties, and on the surface roughness, so that in this way, the surface roughness modification procedure can be optimized and be made more controlled and robust to obtain a scaffold with the required properties.

Therefore, in the following parts of this master thesis, porous Ti6Al4V scaffolds with three different designed strut sizes were proposed for characterization of the effect of surface roughness modification: 100, 140 and 180 μm, prior to surface roughness modification, after chemical etching and after electrochemical polishing, Archimedes measurements, micro-CT image analysis, mechanical testing and roughness measurements using both SEM images and high resolution micro-CT images will be used. For the electrochemical polishing, the applied current will be kept fixed in order to study the role of this parameter on the properties of the surface roughness modified scaffolds. The electrochemical polishing time will be maintained constant. Changes in morphological and mechanical properties and in the surface roughness will have to be related to the applied surface roughness modification parameters, in this master thesis more specific to the current density.

If an optimization of both the morphological and mechanical properties, and the surface roughness will be reached, fine-tuning of the surface roughness modification protocol for specific morphological, mechanical or roughness requirements of the porous Ti6Al4V scaffolds will be feasible. Indeed, the end-goal is to be able to design scaffolds, which after production and surface roughness modification have the required morphological, mechanical and/or roughness properties.

6. Morphological and mechanical characterization

In order to optimize the surface roughness modification procedures, the effect of the surface roughness modification on the morphological and mechanical properties of the porous Ti6Al4V scaffolds with different designed strut thickness was determined. Based on these characterizations, in combination with the effect of the surface roughness modification on the roughness reduction (chapter 7), conclusions can be drawn concerning the surface roughness modification parameters such as current density. In this chapter, density and porosity, mass, percent object volume, object surface, average structure thickness and structure thickness distribution, average structure separation and structure separation distribution, E-modulus, maximum stress and strain at maximum stress were determined for the three scaffold designs (beam 100, 140 and 180) and were related to the current density.

6.1. Density and porosity

As explained in chapter 3, the density and porosity of the porous Ti6Al4V scaffolds was calculated using the Archimedes test device for the three scaffold designs (beam 100, 140 and 180) prior to any surface roughness modification. Table 6.1 shows the obtained results.

Table 6.1. Density and porosity for beam 100, 140 and 180 prior to surface roughness modification

Material	Group name	Density (g/cm³)	Porosity (%)
Ti6Al4V	Beam 100	4,42 ± 0,03	85,13 ± 0,37
	Beam 140	4,41 ± 0,02	81,34 ± 0,74
	Beam 180	4,40 ± 0,01	78,83 ± 0,44

Table 6.1 shows that the density for the three scaffold designs was similar, as expected since the material is the same. As was also expected, the porosity decreased from beam 100 to beam 140 and beam 180 successively, because of the increasing strut thickness. The values of the porosity obtained using Archimedes test were used as comparative data to the micro-CT derived porosity.

6.2. Mass measurements

The mass of five porous Ti6Al4V scaffolds of each scaffold design was measured prior to surface roughness modification, after chemical etching, and after electrochemical polishing. Table 6.2 and Fig. 6.1 show the results.

Table 6.2. Mass of the porous Ti6Al4V scaffolds prior to surface roughness modification, after chemical etching (CH) and after electrochemical polishing (EP).

Ti6Al4V						
Group name	**Mass raw samples (g)**	**Mass after CH (g)**	**Mass after EP (g)**	**Reduction in mass Raw-CH (g)**	**Reduction in mass CH-EP (g)**	**Reduction in mass Raw-EP (g)**
Beam 100	0,2165 ± 0,0048	0,1650 ± 0,0054	0,1356 ± 0,0071	0,0515 ± 0,0017	0,0294 ± 0,0062	0,0809 ± 0,0059
Beam 140	0,2857 ± 0,0087	0,2315 ± 0,0079	0,2052 ± 0,0092	0,0542 ± 0,0017	0,0263 ± 0,0085	0,0805 ± 0,0089
Beam 180	0,3540 ± 0,0030	0,2988 ± 0,0053	0,2726 ± 0,0154	0,0551 ± 0,0024	0,0262 ± 0,010	0,0814 ± 0,0092

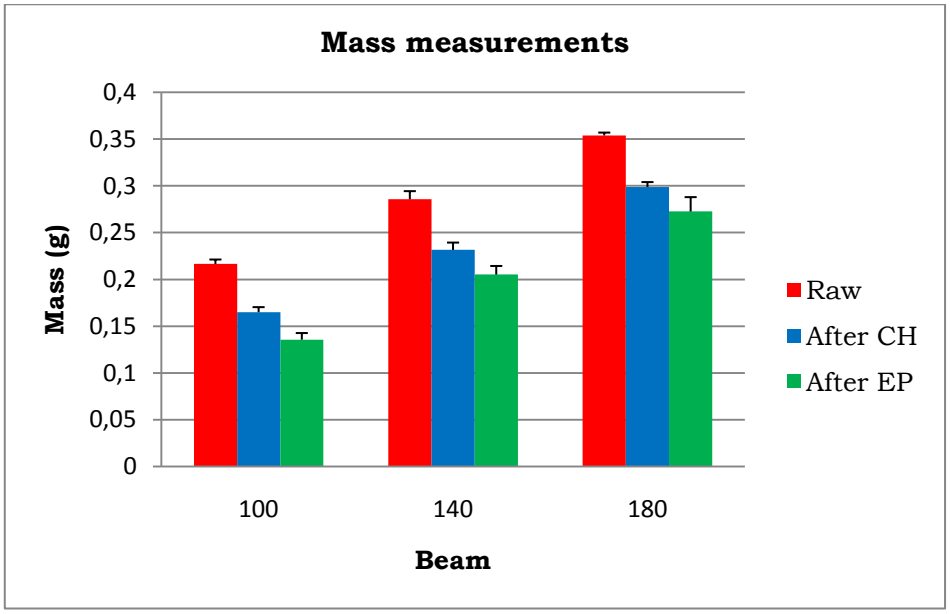

Fig.6.1. Mass measurements of all beams after each stages.

Table 6.2 indicates that there was always a reduction in mass because of both the chemical etching and the electrochemical polishing processes. It can be seen that the chemical etching step causes a higher mass reduction, mainly since in this step an elimination of the unmelted powder grains and other impurities on the surface was occurring. Minor differences in mass reduction between the three scaffold designs were also noticed. The percentages of mass reduction were also calculated for the different scaffold designs and the different surface roughness modification steps, but these will be shown later on in this chapter when related to the applied current density during electrochemical polishing.

6.3. Micro-CT based morphological characterization

One of the most important morphological parameters that have to be evaluated in function of the surface roughness modification for optimization of the surface roughness modification procedure for future biological experiments was the structure thickness for the three scaffold design after each surface roughness modification step. Indeed, it could give quantitative information about the efficiency of each surface roughness modification step.

Apart from the structure thickness calculation, the structure separation (= pore thickness), the percent object volume and the object surface were also determined using micro-CT based image analysis. Since the current for electrochemical polishing was kept constant, namely at 1.2 A, the current density could be determined based on the available surface of the porous Ti6Al4V scaffolds after chemical etching. This current density was then related to the changes in mass and strut thickness in order to determine the best value for the current density for future experiments.

6.3.1. Percent object volume and object surface

Table 6.3 represents the values of the micro-CT based percent object volume, the object surface, the average structure thickness and the average structure separation for the three scaffold designs prior to surface roughness modification, after chemical etching and after electrochemical polishing, respectively.

Table 6.3. Micro-CT based percent object volume, object surface, average structure thickness and average structure separation for the three scaffold designs prior to surface roughness modification, after chemical etching and after electrochemical polishing.

Ti6Al4V_Beam100								
Stage	**Percent object volume (%)**		**Object surface (cm²)**		**Average structure thickness (μm)**		**Average structure separation (μm)**	
	Av.	**Stdv.**	**Av.**	**Stdv.**	**Av.**	**Stdv.**	**Av.**	**Stdv.**
Raw	14,49	0,32	8,37	0,16	220,19	6,56	653,61	2,69
After CH	9,16	0,92	6,26	0,42	191,37	2,91	709,10	18,56
After EP	7,87	0,42	6,16	0,22	170,45	3,72	724,32	4,88
Ti6Al4V_Beam140								
Stage	**Percent object volume (%)**		**Object surface (cm²)**		**Average structure thickness (μm)**		**Average structure separation (μm)**	
	Av.	**Stdv.**	**Av.**	**Stdv.**	**Av.**	**Stdv.**	**Av.**	**Stdv.**
Raw	16,57	0,65	9,96	0,18	227,61	6,86	640,10	7,19
After CH	15,92	0,57	8,47	0,19	232,47	4,09	646,10	5,59
After EP	13,71	0,73	7,95	0,23	214,82	4,90	666,82	10,63
Ti6Al4V_Beam180								
Stage	**Percent object volume (%)**		**Object surface (cm²)**		**Average structure thickness (μm)**		**Average structure separation (μm)**	
	Av.	**Stdv.**	**Av.**	**Stdv.**	**Av.**	**Stdv.**	**Av.**	**Stdv.**
Raw	25,43	0,64	10,62	0,11	312,78	3,46	596,59	5,90
After CH	21,67	0,92	9,72	0,13	285,77	6,45	626,85	8,97
After EP	19,06	1,13	9,80	0,28	261,08	7,35	648,89	4,88

Table 6.3 shows a reduction in percent object volume and object surface after chemical etching and after electrochemical polishing. That was in accordance with the observed mass reductions mentioned earlier.

Using the micro-CT based percent object volume values the porosity can be easy calculated. For the three scaffold designs prior to surface roughness

modification, a porosity of 85.51% for beam 100, 83.43% for beam 140 and 74.57% for beam 180 respectively were found. Comparing these values witch those obtained with Archimedes tests, minor insignificant differences can be noticed. These results proved that micro-CT also is a good method to obtain the morphological properties of a porous Ti6Al4V scaffold.

6.3.2. Reduction in average structure thickness and changes in structure thickness distribution

Fig. 6.2, Fig. 6.3 and 6.4 represent the structure thickness distributions for each scaffold design prior to surface roughness modification, after chemical etching and after electrochemical polishing. Table 6.4 shows the reduction in average structure thickness for each scaffold design prior to surface roughness modification, after chemical etching and after electrochemical polishing, except for beam 140, where there was an increasing in that value, comparing prior to and after chemical etching. However, paying attention to the standard deviation values, both data stay in the range, so this increasing in average structure thickness could be understood insignificant.

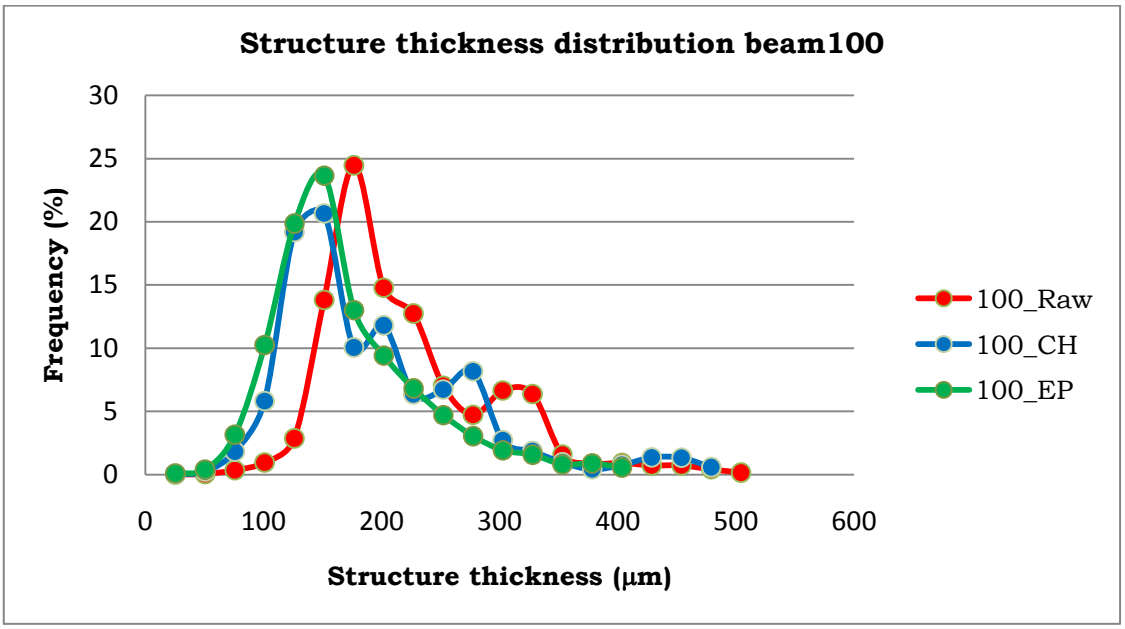

Fig.6.2. Structure thickness distribution for scaffold design beam 100 prior to surface roughness modification, after chemical etching and after electrochemical polishing.

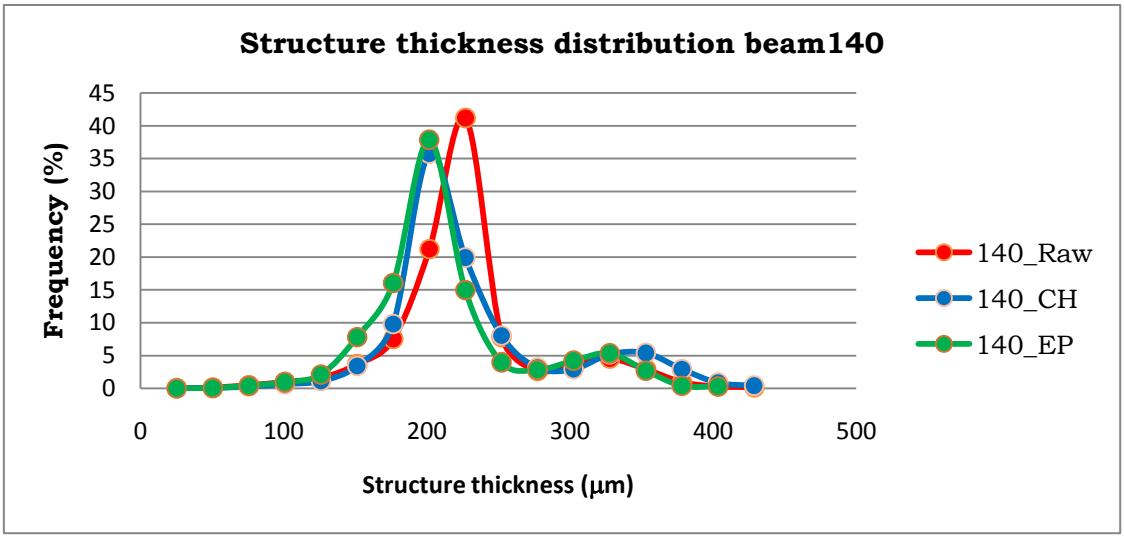

Fig.6.3. Structure thickness distribution for scaffold design beam 140 prior to surface roughness modification, after chemical etching and after electrochemical polishing.

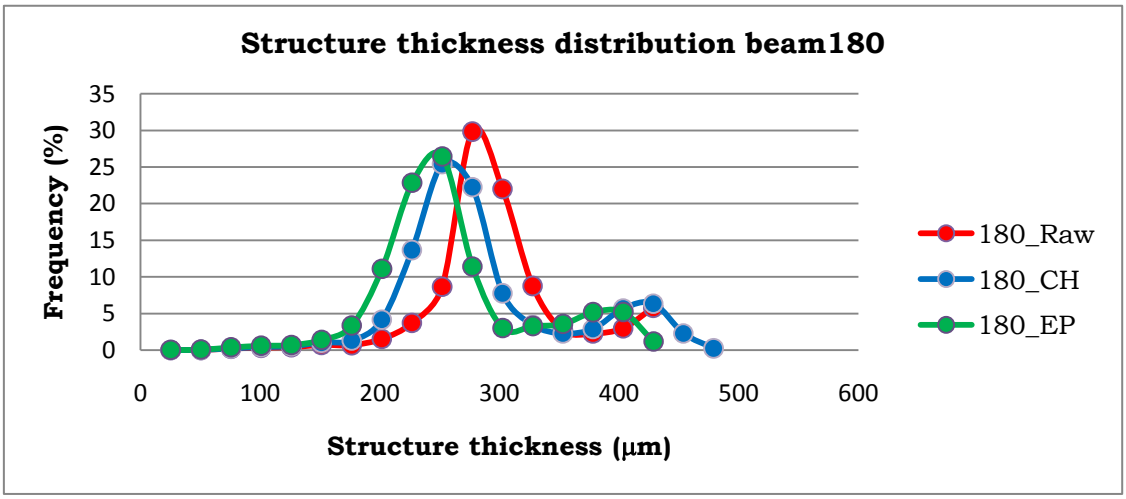

Fig.6.4. Structure thickness distribution for scaffold design beam 180 prior to surface roughness modification, after chemical etching and after electrochemical polishing.

Table 6.4. Reduction in average structure thickness for each scaffold design prior to surface roughness modification, after chemical etching and after electrochemical polishing.

Ti6Al4V			
Group name	**Reduction str. Th_Raw-CH (µm)**	**Reduction str. Th_CH-EP (µm)**	**Reduction str. Th_Raw-EP (µm)**
Beam 100	28,82	20,92	49,74
Beam 140	-4,86	17,65	12,79
Beam 180	27,01	24,69	51,70

Table 6.4 shows that there was a significant reduction in the average structure thickness, after chemical etching and after electrochemical polishing. Similar to the mass reduction, the chemical etching process introduces larger reductions in the structure thickness. Indeed, the chemical etching removes a significant amount of unmelted powder grains from the surface, whereas with the electrochemical polishing the goal was to make a smoother and more uniform strut surface roughness, so less amount of material was removed. As was discuss when table 6.3 was introduced, there was an increasing in the average structure thickness in beam 140 comparing prior to and after chemical etching, but looking at the standard deviation values of those data, it can be understood insignificant. The reduction in average structure thickness after chemical etching and after electrochemical polishing can be also appreciated in fig. 6.2, fig. 6.3 and fig. 6.4. The peaks of the curves, representing the main strut thickness of the scaffolds, do not shift anymore after electrochemical polishing, indicating that the global thickness of the struts does not reduce significantly because of the electrochemical polishing. The curve after electrochemical polishing shows however a reduction in the other peaks or a shift of these peaks to lower thickness values, indicating that the roughness of the struts reduces due to the electrochemical polishing.

The percentage of reduction in average strut thickness after chemical etching was calculated for all scaffold designs in order to correlate them with the current density. The results are mentioned later on.

6.3.3. Change in average structure separation and structure separation distribution

Similar conclusion as for the average structure thickness and structure thickness distribution could be made for the average structure separation (= pore thickness) values and the structure separation distribution for the different scaffold designs after each surface modification step. Fig. 6.5, Fig.6.6 and Fig.6.7 show the structure separation distributions for the different scaffold designs after each surface modification step.

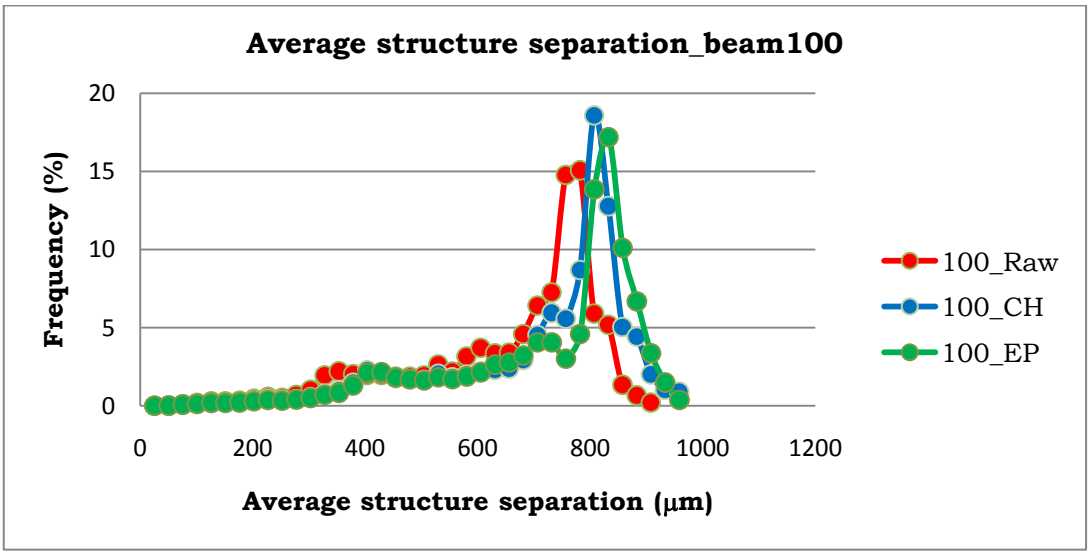

Fig.6.5. Structure separation distribution for scaffold design beam 100 prior to surface roughness modification, after chemical etching and after electrochemical polishing.

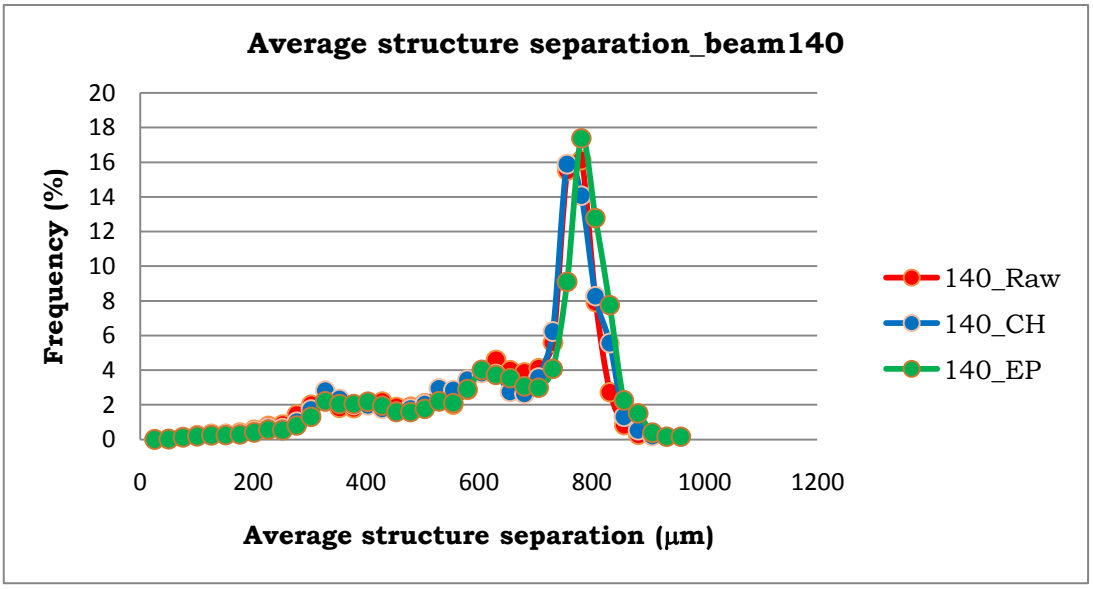

Fig.6.6. Structure separation distribution for scaffold design beam 140 prior to surface roughness modification, after chemical etching and after electrochemical polishing.

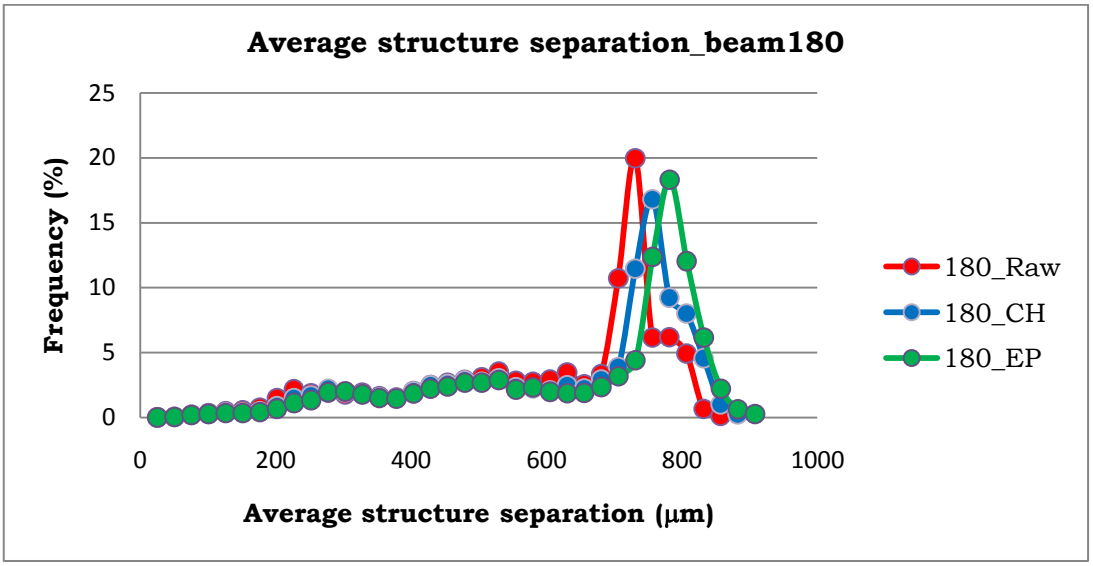

Fig.6.7. Structure separation distribution for scaffold design beam 180 prior to surface roughness modification, after chemical etching and after electrochemical polishing.

Fig. 6.5, Fig.6.6 and Fig.6.7 show that the main pore thickness value, which corresponds to the largest peak, increases after each surface roughness modification step. Similar to the structure thickness reduction, the chemical etching process introduces larger increases in the pore thickness. Again, these results were logical since, when the structure thickness reduces, the distances between the struts will increase.

6.4. Correlation with the current density

For the three scaffold designs, a different effect on the morphological properties was noticed after electrochemical polishing. As was found in the first part of the master thesis work, the initial experiments (chapter 4), the current density changes even with minor differences in strut thickness, and this could lead to structure thickness related differences in the effect of the electrochemical polishing. Since the current density plays an important role in electrochemical polishing, the variation of this parameter was studied for all the scaffold designs and was related to the reduction in mass and structure thickness. The current density values for the different scaffold designs after chemical etching are shown in Table 6.5 and Fig.6.8, where the difference of this parameter with the different designed strut thicknesses is demonstrated.

Table 6.5. Current density values for the different scaffold designs after chemical etching.

Group name	Current density (mA/mm²)_CH
Beam 100	1,92 ± 0,132
Beam 140	1,42 ± 0,032
Beam 180	1,24 ± 0,016

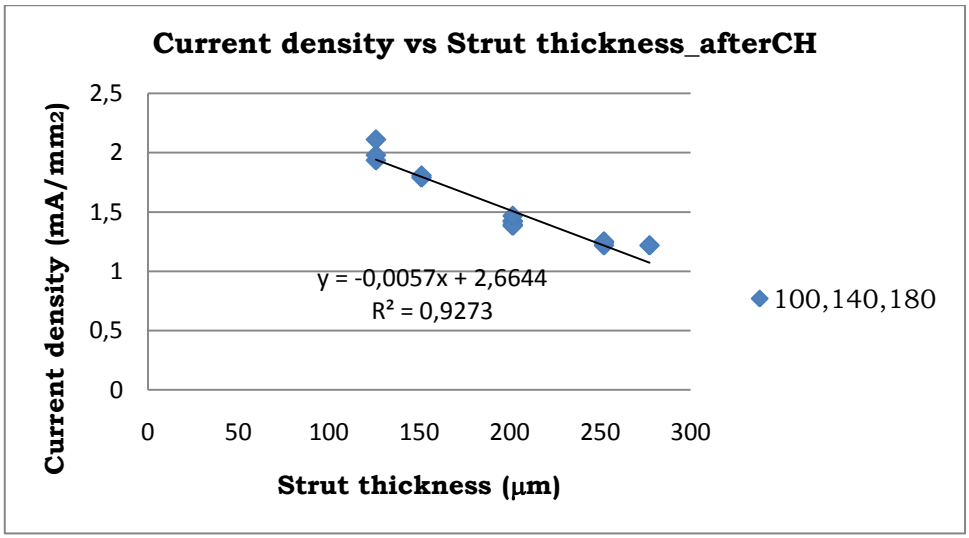

Fig.6.8. Current density in function of the structure thickness for the different scaffold designs after chemical etching (CH).

As can be seen in fig. 6.8, a negative value for the slope of the trend line was obtained. Since current density is defined as the current (in this master thesis, it was kept constant for all the scaffold designs at 1.2 A) divided by the object surface, when the strut thickness increases, and hence also the available surface, the current density will decrease. Thus, a different current density occurs for different strut thicknesses, and hence a different reduction in mass and strut thickness after electrochemical polishing is expected for the different scaffold designs.

6.4.1. Relation between the reduction in mass percentage and the current density

As was said when reduction mass was calculated, a relation between this parameter and the current density was expected. Table 6.6 and Fig. 6.9 show the relationship between the mass reduction after electrochemical polishing and the current density.

Table 6.6. Percentage of mass reduction after electrochemical polishing and the related current density for the different scaffold designs.

Group name	Mass reduction CH-EP (%)	Current density_CH (mA/m²)
Beam 100	17,82	1,92 ± 0,1322
Beam 140	11,36	1,42 ± 0,032
Beam 180	8,77	1,23 ± 0,016

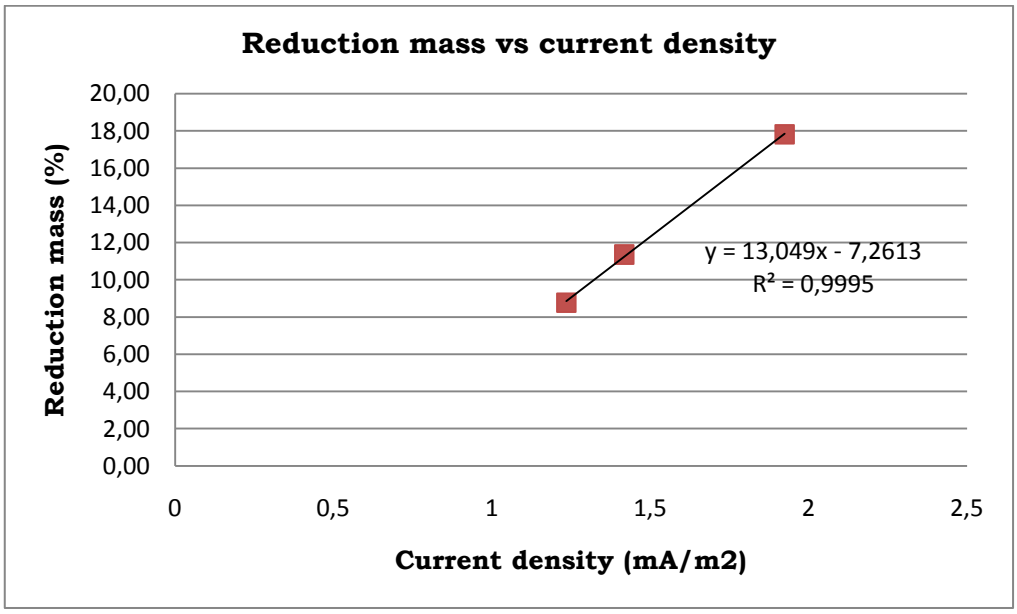

Fig.6.9. Percentage of mass reduction in function of the current density for the three scaffold designs.

Fig.6.9 shows the linear relation between the percentage of mass reduction and the current density. Indeed, as was expected, higher values of current density cause a larger reduction in mass. The equation of the linear trend line can be used to optimize the surface roughness modification procedures.

6.4.2. Relation between the percentage of average structure thickness reduction and the current density

Table 6.7 and Fig. 6.10 show the relation between the average structure thickness reduction and the current density.

Table 6.7. Percentage of average structure thickness reduction for the three scaffold designs.

Ti6Al4V		
Group name	**Reduction str. th_CH-EP (%)**	**Current density (mA/mm²)_CH**
Beam 100	10,93	1,92 ± 0,132
Beam 140	7,59	1,42 ± 0,032
Beam 180	8,64	1,23 ± 0,016

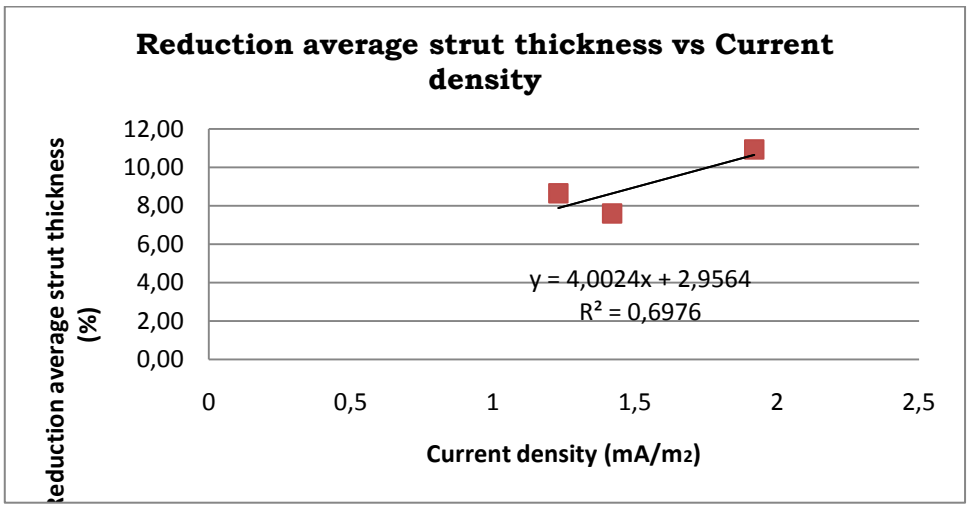

Fig.6.10. Percentage of average structure thickness reduction in function of the current density for the three scaffold designs.

Fig. 6.10 shows that the higher the current density is, the larger the reduction in average structure thickness is. Thus, a larger percentage of structure thickness reduction was expected for the scaffold designs with the thinnest designed strut thickness. Again, the equation of the linear trend line can be used to optimize the surface roughness modification procedures.

6.5. E-modulus, maximum stress and strain at maximum stress

The mechanical properties of the three scaffold designs were calculated prior to surface roughness modification and after electrochemical polishing in order to quantify the effect of the surface roughness modification on the mechanical behaviour. Table 6.8 and Table 6.9 and Fig.6.11, Fig.6.12, and Fig.6.13 show the obtained results.

Table 6.8. E-modulus, maximum stress and strain at maximum stress for the three scaffold designs prior to surface roughness modification.

Material	Group name	E-modulus (Mpa)	Max. Stress (Mpa)	Strain at max. Stress (%)
Ti6Al4V (prior to)	Beam 100	266,32 ± 17,23	8,15 ± 0,53	6,68 ± 0,58
	Beam 140	655,76 ± 40,88	20,10 ± 0,63	6,10 ± 0,23
	Beam 180	1051,36 ± 56,90	32,61 ± 0,50	6,24 ± 0,16

Table 6.9. E-modulus, maximum stress and strain at maximum stress for the three scaffold designs after electrochemical polishing.

Material	Group name	E-modulus (Mpa)	Max. Stress (Mpa)	Strain at max. Stress (%)
Ti6Al4V (after EP)	Beam 100	140,75 ± 11,66	3,99 ± 0,44	5,95 ± 0,97
	Beam 140	430,85 ± 30,92	13,01 ± 1,23	6,56 ± 0,21
	Beam 180	862,92 ± 97,45	25,93 ± 2,19	6,63 ± 0,08

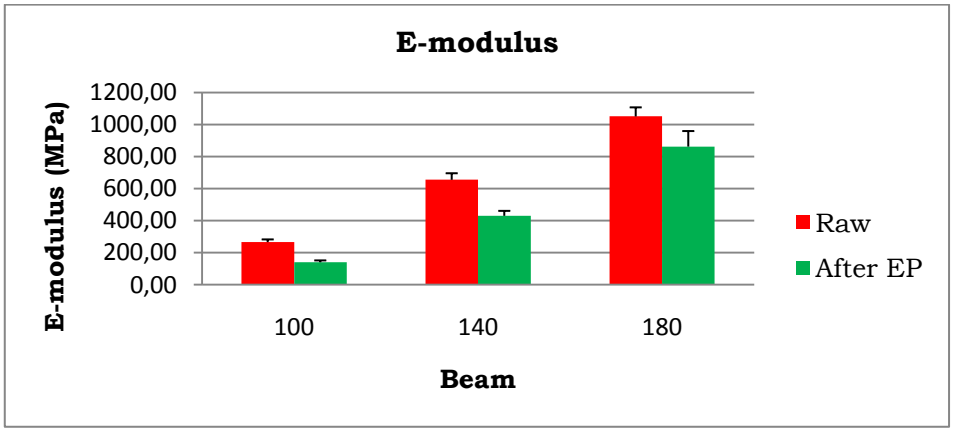

Fig.6.11. E-modulus for the three scaffold designs prior to surface modification and after electrochemical polishing.

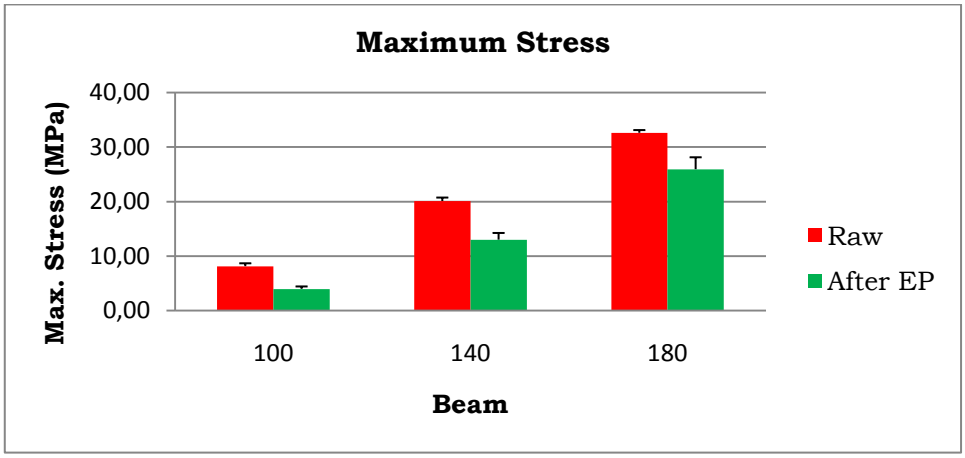

Fig.6.12. Maximum stress for the three scaffold designs prior to surface modification and after electrochemical polishing.

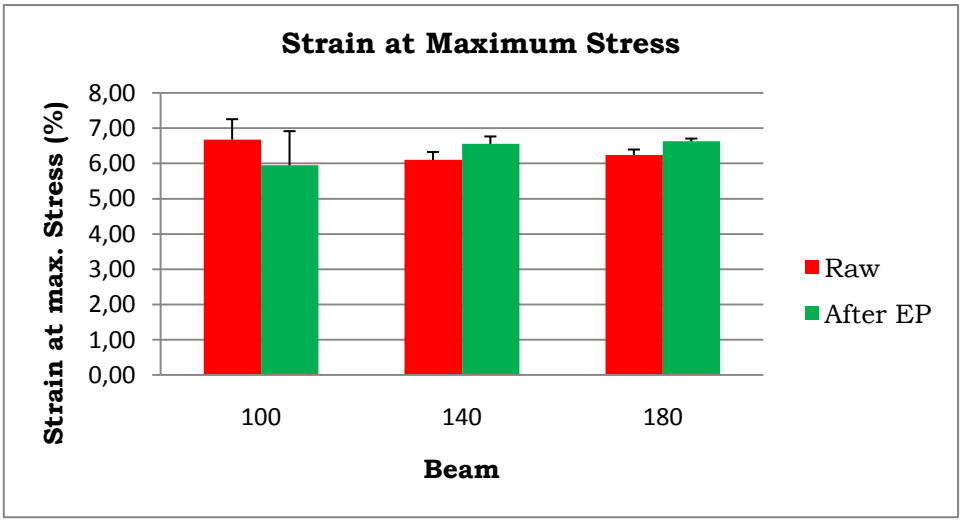

Fig.6.13. Strain at maximum stress for the three scaffold designs prior to surface modification and after electrochemical polishing.

Fig.6.11, Fig.6.12, and Fig.6.13 show a decrease of both the E-modules and the strength after surface roughness modification. Indeed, after electrochemical polishing, the structure thickness diminishes as was shown previously, thus a lower cross sectional area of the struts will be able to withstand the compression load and this will entail in a decreasing E-modulus and maximum stress. However, the surface roughness modification only has a limited effect on the strain at maximum stress. Table 6.10 and fig. 6.14 show the relation between the reduction in mechanical properties and structure thickness.

Table 6.10. Percentage of reduction in E-modulus and maximum stress percentages for the different scaffold designs after electrochemical polishing (EP).

Group name	E-modulus reduction_Raw-EP (%)	Max. Stress reduction_Raw-EP (%)
Beam 100	47,15	51,04
Beam 140	34,30	35,27
Beam 180	17,92	20,48

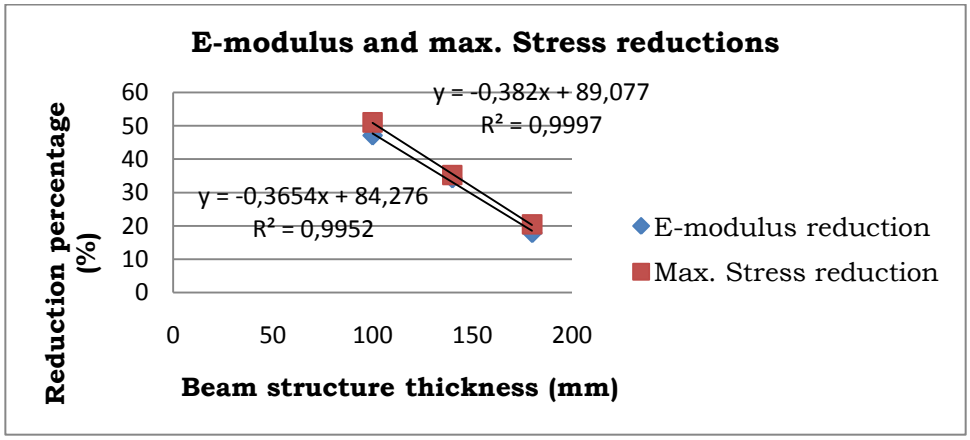

Fig.6.14. Percentage of reduction in E-modulus and maximum stress percentages for the different scaffold designs after electrochemical polishing (EP) in function of the structure thickness.

Both for percentage reduction of the E-modulus and the maximum stress, a decreasing linear relation with the structure thickness was found. Therefore, the larger the structure thickness of the scaffolds is, the smaller the reduction of the mechanical properties is. Connecting these results with current density values obtained previously, lower values of the current density indeed correspond to a smaller strut thickness reduction and hence also a smaller reduction of the mechanical properties. The equation of the linear trend line can be used to optimize the surface roughness modification procedures in function of the mechanical properties.

6.6 Conclusions

The equations of the linear relations between the mass reduction, the reduction in structure thickness, and the mechanical properties with the current density will allow predicting the morphological and mechanical properties that will be obtained on porous Ti6Al4V TE scaffolds when controlling the current density parameter. The aim for future work will be to find the suitable value of current density for the required morphological and mechanical properties.

7. Roughness measurement techniques

7.1. Introduction

Since roughness has a crucial role in the cell behavior on porous Ti6Al4V scaffolds, one of the main goals of this master thesis was to be able to quantify the surface roughness as precise as possible. For this purpose, two different techniques have been used and compared, namely (i) SEM-based measurements and (ii) high-resolution micro-CT based measurements.

For the SEM-based roughness measurements, SEM images were taken of the three scaffold designs prior to surface modification and after each surface modification step in order to analyze and quantify the strut surface roughness. However, using SEM images to obtain the surface roughness parameters means that only external measurements could be obtained.

High resolution micro-CT based roughness measurements go beyond the SEM-based roughness measurements. As a non-destructive technique, it allows to quantify the surface roughness parameters even of the inside of the porous scaffold without having to cut it. Thus, roughness calculations can be carried out both on the centre and on the sides of the scaffolds, obtaining a more complete characterization of the surface roughness of the porous Ti6Al4V scaffolds. Roughness results prior to surface roughness modification, after chemical etching and after electrochemical polishing for the three scaffold designs are presented below, both using the SEM-based roughness measurement technique as the high-resolution micro-CT based roughness measurement technique. Additionally, a comparison between both techniques is provided.

7.2. SEM-based roughness measurements

7.2.1. Roughness measurements

Together with the effect of the surface roughness modification on the morphological and the mechanical properties (chapter 6), accurate roughness measurement is also important in order to quantify the effect of the surface roughness modification. For the SEM-based roughness measurements SEM images of 6 top and 6 bottom struts were taken in total in three different zones of the scaffold (top, middle and bottom), in two opposite faces for 5 per scaffold design prior to surface roughness modification, after chemical etching and after electrochemical polishing. The following roughness parameters were studied: Rt, Ra, Rq, and Rz. Rt is known as the maximum height, and Ra is the roughness average; Rq is obtained as the root mean square (RMS) average; and finally, Rz is obtained as the average separation between 10 peaks and 10 valleys.

Ra, Rq, Rz and Rt, values are shown in Table 7.1 for scaffold design beam 100, differentiating between top, middle and bottom zones of the scaffolds, and between top and bottom surfaces of the strut. Notable differences were observed between the three steps of surface roughness modification.

Table 7.1. SEM based roughness parameters for scaffold design beam 100 prior to surface roughness modification, after chemical etching (CH) and after electrochemical polishing (EP).

Ti6Al4V_beam100									
Raw									
		Ra		**Rq**		**Rz**		**Rt**	
		Av.	Stdv.	Av.	Stdv.	Av.	Stdv.	Av.	Stdv.
TOP	Tops	5,93	2,03	7,42	2,51	20,69	6,14	35,70	11,41
	Bottoms	9,02	2,55	11,31	3,71	31,95	8,38	52,03	17,02
	Total	7,47	2,18	9,36	2,75	26,32	7,96	43,86	11,55
MIDDLE	Tops	6,33	2,07	8,39	2,58	21,72	8,02	41,12	11,98
	Bottoms	12,89	4,73	15,33	5,56	41,48	14,32	62,89	21,55
	Total	9,61	4,64	11,86	4,91	31,60	13,97	52,01	15,40
BOTTOM	Tops	6,22	2,28	7,38	2,68	20,57	6,68	30,80	10,53
	Bottoms	9,45	2,12	11,60	2,41	34,63	6,90	54,34	12,33
	Total	7,83	2,28	9,49	2,98	27,60	9,94	42,57	16,65
	Total Tops	6,16	0,21	7,73	0,57	20,99	0,63	35,87	5,16
	Total Bottoms	10,45	2,12	12,75	2,24	36,02	4,92	56,42	5,73
	GLOBAL	8,30	3,03	10,24	3,55	28,51	10,63	46,14	14,53
AfterCH									
		Ra		**Rq**		**Rz**		**Rt**	
		Av.	Stdv.	Av.	Stdv.	Av.	Stdv.	Av.	Stdv.
TOP	Tops	5,02	1,75	5,98	1,99	16,68	5,27	25,34	8,20
	Bottoms	6,71	1,48	8,17	1,77	23,47	5,01	36,79	9,53
	Total	5,87	1,20	7,08	1,55	20,07	4,81	31,07	8,09
MIDDLE	Tops	5,11	2,52	6,10	2,96	16,11	6,80	24,90	9,74
	Bottoms	10,85	5,10	13,01	5,87	33,50	10,16	53,71	19,33
	Total	7,98	4,06	9,56	4,89	24,81	12,30	39,30	20,37
BOTTOM	Tops	5,77	2,41	6,86	2,61	16,20	6,32	27,21	8,08
	Bottoms	7,74	1,46	9,64	1,96	27,05	5,56	46,32	14,07
	Total	6,75	1,40	8,25	1,96	21,63	7,67	36,76	13,51
	Total Tops	5,30	0,41	6,32	0,48	16,33	0,30	25,82	1,23
	Total Bottoms	8,44	2,15	10,28	2,48	28,01	5,08	45,60	8,48
	GLOBAL	6,87	2,22	8,30	2,80	22,17	8,26	35,71	13,99

AfterEP									
		Ra		**Rq**		**Rz**		**Rt**	
		Av.	Stdv.	Av.	Stdv.	Av.	Stdv.	Av.	Stdv.
TOP	Tops	4,68	1,70	5,59	2,00	14,89	4,99	22,63	7,47
	Bottoms	4,45	1,21	5,49	1,44	14,87	4,14	23,10	5,97
	Total	4,56	0,16	5,54	0,06	14,88	0,02	22,86	0,33
MIDDLE	Tops	4,65	2,84	5,57	3,29	14,70	7,22	22,57	10,51
	Bottoms	6,10	2,28	7,54	2,85	18,62	6,85	32,46	11,49
	Total	5,37	1,02	6,56	1,39	16,66	2,77	27,51	7,00
BOTTOM	Tops	5,51	2,66	6,45	2,89	19,06	7,90	26,08	9,72
	Bottoms	5,39	1,35	6,69	1,45	18,90	5,55	31,51	8,29
	Total	5,45	0,08	6,57	0,17	18,98	0,11	28,80	3,84
	Total Tops	4,94	0,49	5,87	0,51	16,22	2,46	23,76	2,01
	Total Bottoms	5,31	0,83	6,58	1,03	17,46	2,25	29,03	5,15
	GLOBAL	5,13	0,26	6,22	0,50	16,84	0,88	26,39	3,72

Decreasing tendencies for all the roughness parameters were obtained for scaffold design beam 100 when these porous Ti6Al4V scaffolds were subjected to the different surface roughness modification steps. The roughness parameters for the whole scaffolds are presented in Fig. 7.1. It confirms that the surface roughness modification steps introduce a removal of the unmelted powder grains on the surface and a smoother and more homogeneous surface roughness.

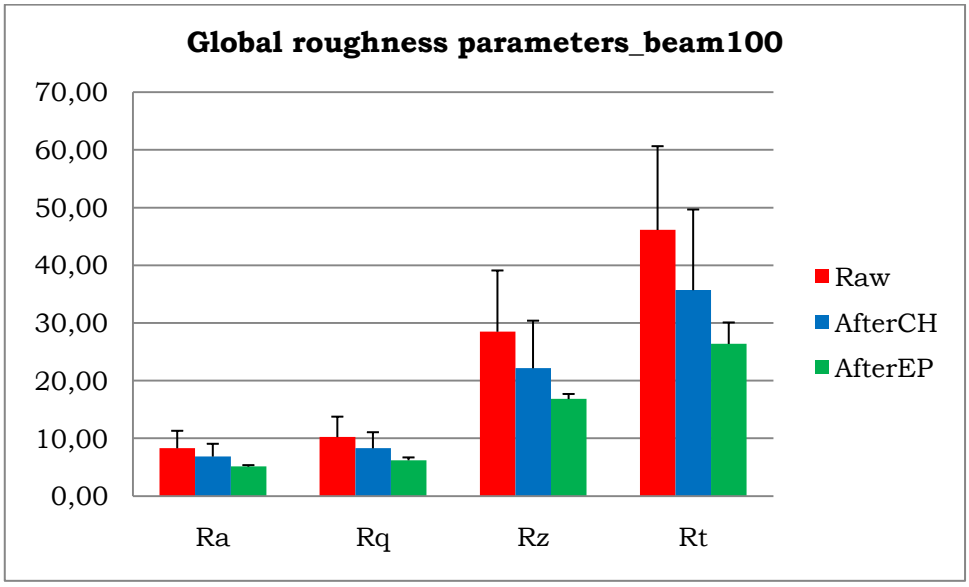

Fig.7.1. SEM based roughness parameters for scaffold design beam 100 prior to surface roughness modification, after chemical etching (CH) and after electrochemical polishing (EP).

When differentiating between roughness at the top, middle and bottom of the scaffold, minor differences were found as shown in Fig. 7.2.

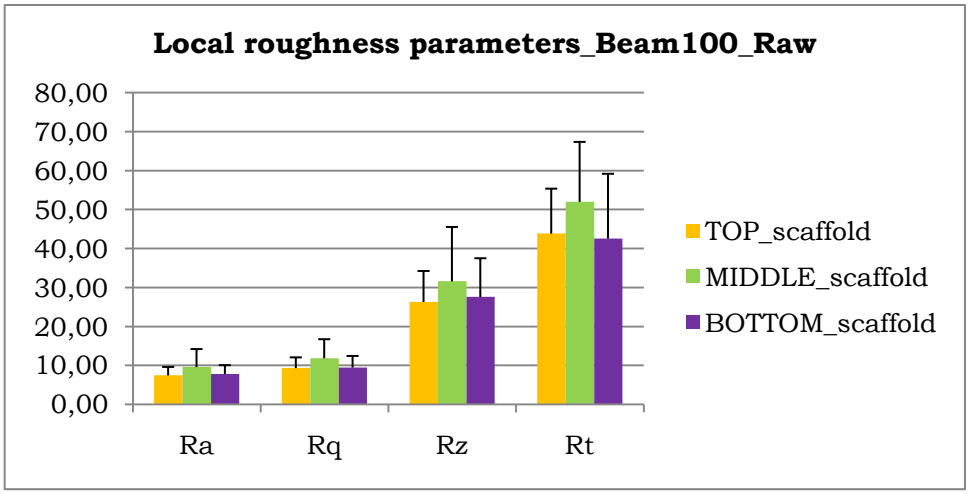

(a)

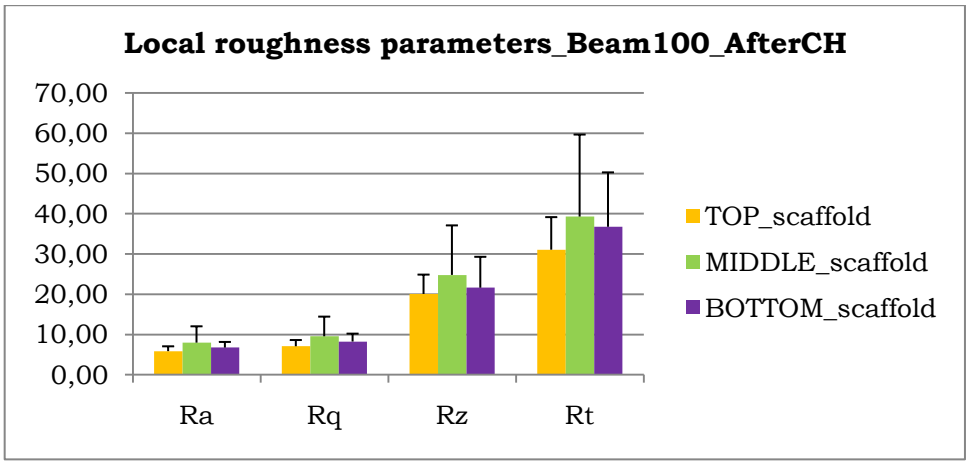

(b)

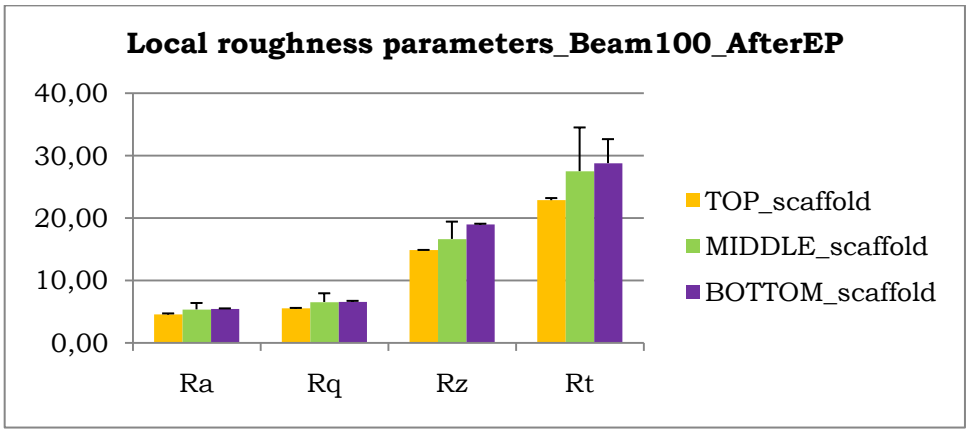

(c)

Fig.7.2. SEM based roughness parameters for the top, middle and bottom zones of the scaffolds of scaffold design beam 100, for the three surface roughness modification steps: (a) prior to surface roughness modification, (b) after chemical etching (CH) and (c) after electrochemical polishing (EP).

For the porous Ti6Al4V scaffolds prior to surface roughness modification of scaffold design beam 100, the highest values of the four roughness parameters were observed in the middle part of the scaffold, whereas in the top and bottom zones these were similar. However, these differences are not significant. Hence, a minor non-homogeneous roughness distribution was found in the Ti6Al4V scaffolds after production.

After chemical etching, the same trend was observed for lower roughness values. Therefore, homogeneous chemical etching can be deduced.

However, this trend changed when electrochemical polishing was applied. The highest values of Ra, Rq, Rz and Rt were found for the bottom of the scaffolds, while the lowest ones corresponded to the top zones. Heterogeneous electrochemical polishing process could be assumed since roughness reduction was higher in top and middle areas of the scaffolds than in the bottom zone.

Fig. 7.3 shows the difference in roughness parameters when tops and bottoms of the strut were assessed.

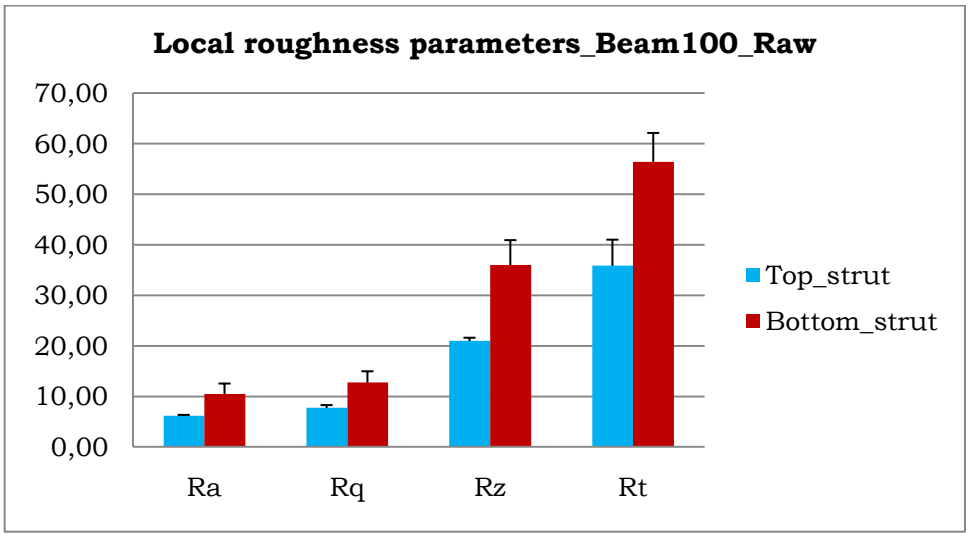

(a)

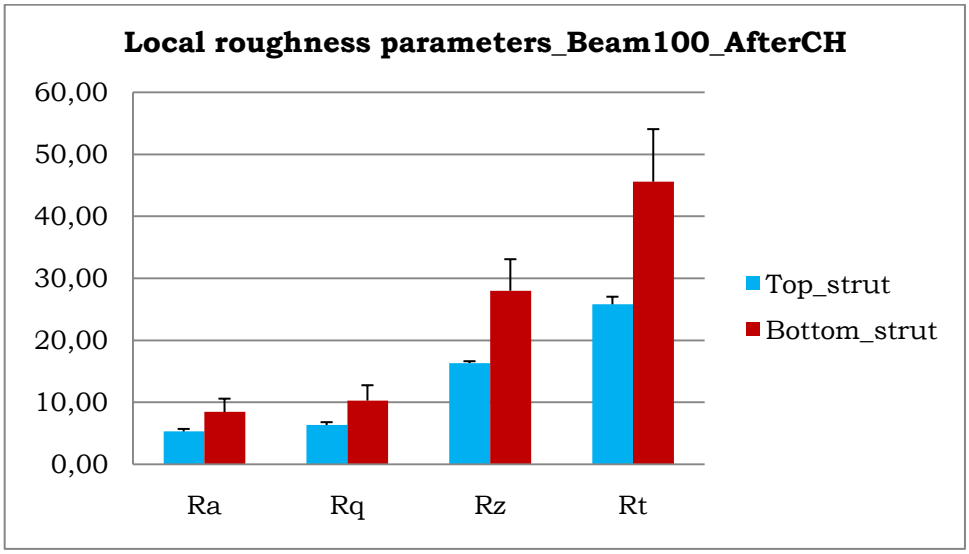

(b)

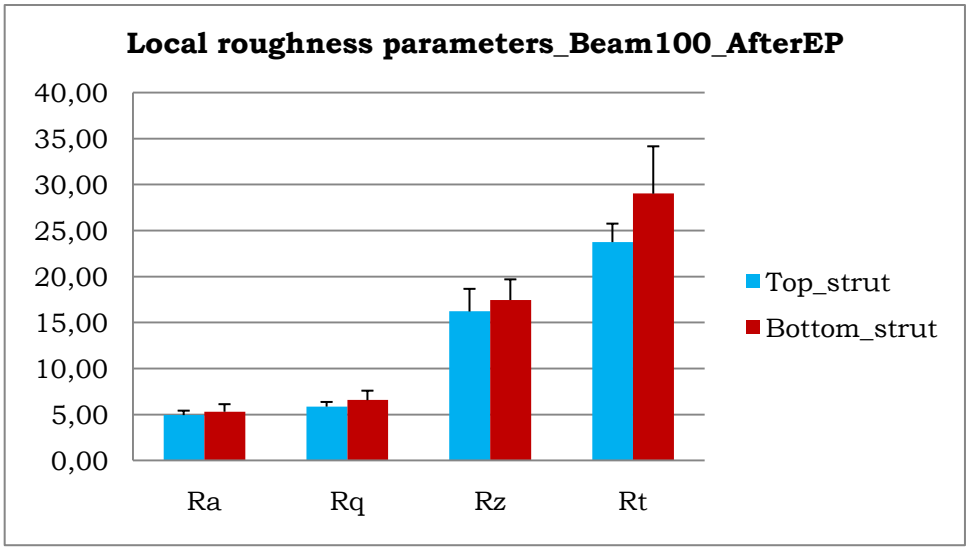

(c)

Fig.7.3. SEM based roughness parameters for the top and bottom of the struts for scaffold design beam 100, for the three surface roughness modification steps: (a) prior to surface roughness modification, (b) after chemical etching (CH) and (c) after electrochemical polishing (EP).

Bottom roughness values of the 6 parameters analyzed were higher for all the stages comparing with the top ones. While for raw and after CH samplers the differences were considerable, after EP these differences reduced.

Similar study was carried out for Ti6Al4V scaffolds of beam 140. Table 7.2 shows the roughness values obtained.

Table 7.2. SEM based roughness parameters for scaffold design beam 100 prior to surface roughness modification, after chemical etching (CH) and after electrochemical polishing (EP).

Ti6Al4V_beam140									
Raw									
		Ra		Rq		Rz		Rt	
		Av.	Stdv.	Av.	Stdv.	Av.	Stdv.	Av.	Stdv.
TOP	Tops	6,58	1,61	8,22	1,85	19,74	4,18	36,95	7,31
	Bottoms	14,69	5,46	17,30	5,99	45,45	14,71	72,24	16,24
	Total	10,64	5,74	12,76	6,42	32,59	18,18	54,60	24,95
MIDDLE	Tops	6,27	1,68	7,84	2,11	19,33	5,81	34,11	9,13
	Bottoms	13,18	4,22	14,94	4,61	40,95	11,18	64,85	18,58
	Total	9,72	4,89	11,39	5,02	30,14	15,29	49,48	21,73
BOTTOM	Tops	6,24	2,37	8,00	2,57	18,18	5,26	35,79	7,89
	Bottoms	12,36	4,10	14,62	4,46	39,89	10,62	62,71	11,65
	Total	9,30	4,33	11,31	4,68	29,03	15,35	49,25	19,04
	Total Tops	6,36	0,19	8,02	0,19	19,08	0,81	35,62	1,43
	Total Bottoms	13,41	1,18	15,62	1,46	42,10	2,95	66,60	5,00
	GLOBAL	9,89	4,98	11,82	5,37	30,59	16,27	51,11	21,91

AfterCH									
		Ra		Rq		Rz		Rt	
		Av.	Stdv.	Av.	Stdv.	Av.	Stdv.	Av.	Stdv.
TOP	Tops	6,29	2,24	7,72	2,39	19,10	5,64	35,51	10,38
	Bottoms	12,72	5,10	15,66	5,80	42,55	13,77	65,45	18,35
	Total	9,50	4,55	11,69	5,61	30,82	16,58	50,48	21,17
MIDDLE	Tops	4,33	1,51	5,32	1,87	14,03	6,11	24,97	10,59
	Bottoms	10,81	3,56	12,97	3,95	36,08	9,86	57,25	13,98
	Total	7,57	4,58	9,15	5,41	25,05	15,59	41,11	22,82
BOTTOM	Tops	5,20	1,80	6,55	2,06	17,20	5,26	30,61	7,95
	Bottoms	10,55	3,85	12,49	4,14	34,96	9,12	52,57	10,81
	Total	7,87	3,78	9,52	4,19	26,08	12,55	41,59	15,53
	Total Tops	5,27	0,98	6,53	1,20	16,78	2,56	30,36	5,27
	Total Bottoms	11,36	1,19	13,71	1,71	37,86	4,10	58,42	6,52
	GLOBAL	8,31	4,31	10,12	5,07	27,32	14,91	44,39	19,84

AfterEP									
		Ra		Rq		Rz		Rt	
		Av.	Stdv.	Av.	Stdv.	Av.	Stdv.	Av.	Stdv.
TOP	Tops	5,98	1,40	7,11	1,43	18,25	3,16	29,20	5,28
	Bottoms	10,65	2,01	12,91	2,17	34,52	8,07	57,55	9,44
	Total	8,32	3,30	10,01	4,10	26,39	11,50	43,37	20,05
MIDDLE	Tops	5,36	2,81	6,32	3,35	17,81	10,19	25,87	13,90
	Bottoms	10,81	4,17	13,02	4,57	36,02	12,45	55,49	15,77
	Total	8,08	3,86	9,67	4,73	26,91	12,88	40,68	20,94
BOTTOM	Tops	3,92	2,49	4,79	3,03	13,05	8,16	21,33	12,62
	Bottoms	8,81	5,28	10,39	6,04	25,86	15,42	41,66	23,36
	Total	6,36	3,46	7,59	3,96	19,45	9,06	31,49	14,38
	Total Tops	5,09	1,06	6,08	1,18	16,37	2,88	25,46	3,95
	Total Bottoms	10,09	1,11	12,10	1,49	32,13	5,48	51,57	8,64
	GLOBAL	7,59	3,54	9,09	4,26	24,25	11,15	38,52	18,46

Fig. 7.4 presents the decrease of the roughness parameters in function of the surface roughness modification step. A similar trend as for the scaffold design beam 100 were found, but for lower roughness values.

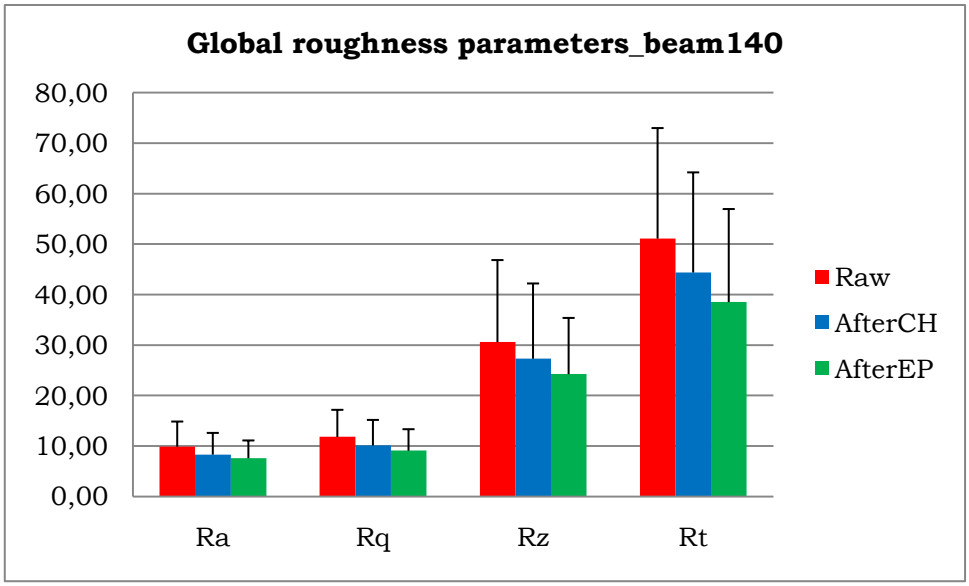

Fig.7.4. SEM based roughness parameters for scaffold design beam 140 prior to surface roughness modification, after chemical etching (CH) and after electrochemical polishing (EP).

Fig. 7.5 shows minor differences when differentiating between roughness at the top, middle and bottom of the scaffold.

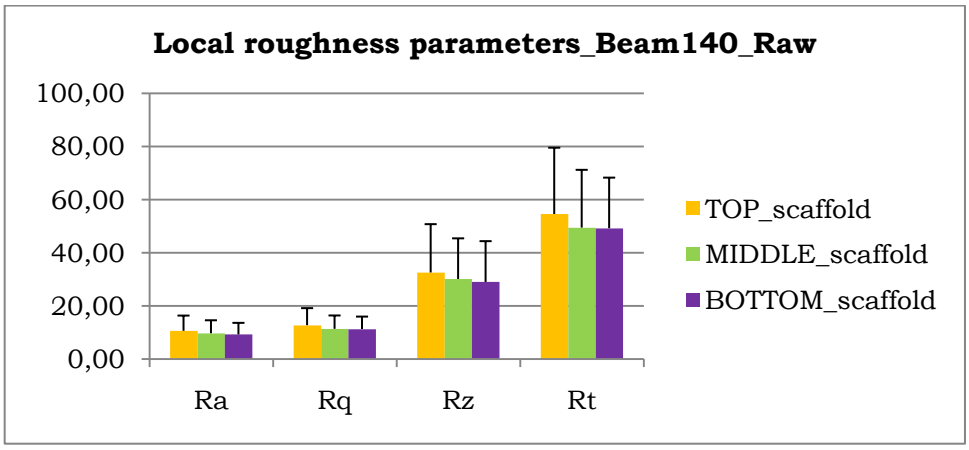

(a)

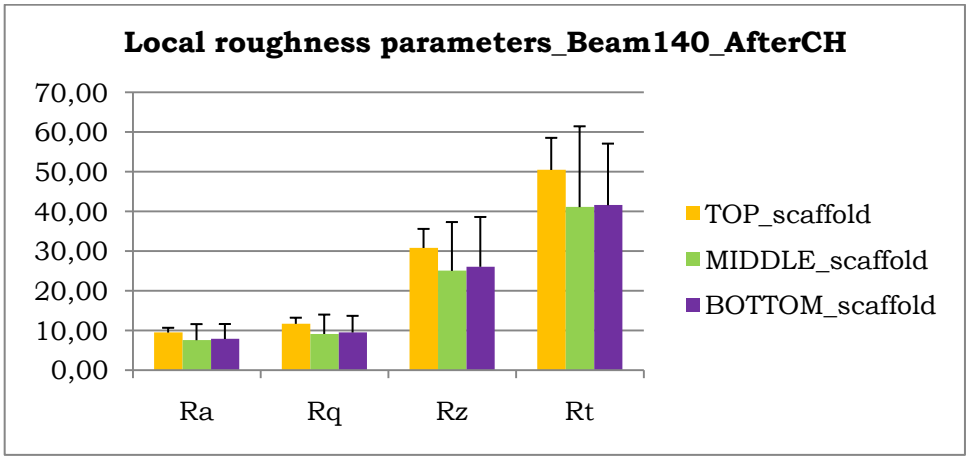

(b)

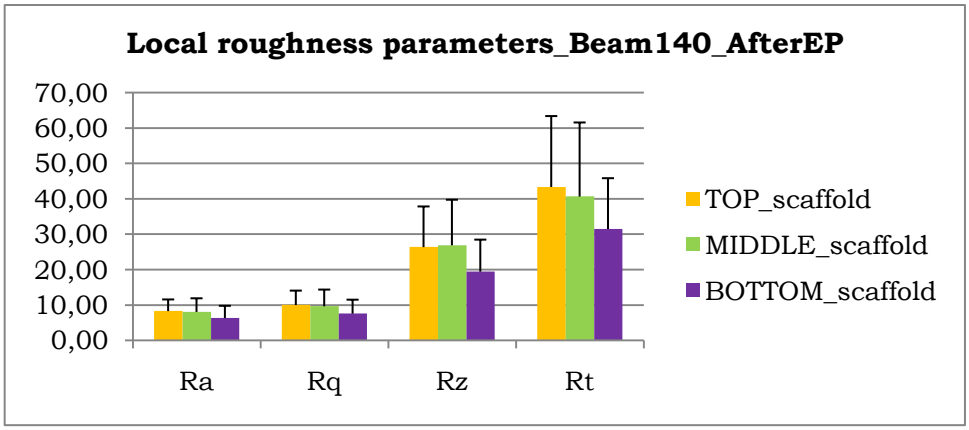

(c)

Fig.7.5. SEM based roughness parameters for the top, middle and bottom zones of the scaffolds of scaffold design beam 140, for the three surface roughness modification steps: (a) prior to surface roughness modification, (b) after chemical etching (CH) and (c) after electrochemical polishing (EP).

For scaffold design beam 140, the roughness measurements were the highest for the top of the Ti6Al4V scaffolds for the three steps of the surface roughness modification, while the lowest ones corresponded to the bottom area. However, the differences were only minor; The same conclusions as for scaffold design beam 100 could be made, namely that a homogeneous chemical etching process was supposed because differences between top, middle and bottom measurements were maintained after this first surface treatment, and that, since the differences in roughness parameters values reduced after electrochemical polishing, this surface modification step was considered to be less homogeneous.

Fig. 7.6 presents the roughness measurements after each surface roughness modification step and prior to surface roughness modification analyzing top and bottom of the strut separately. Significant differences were observed.

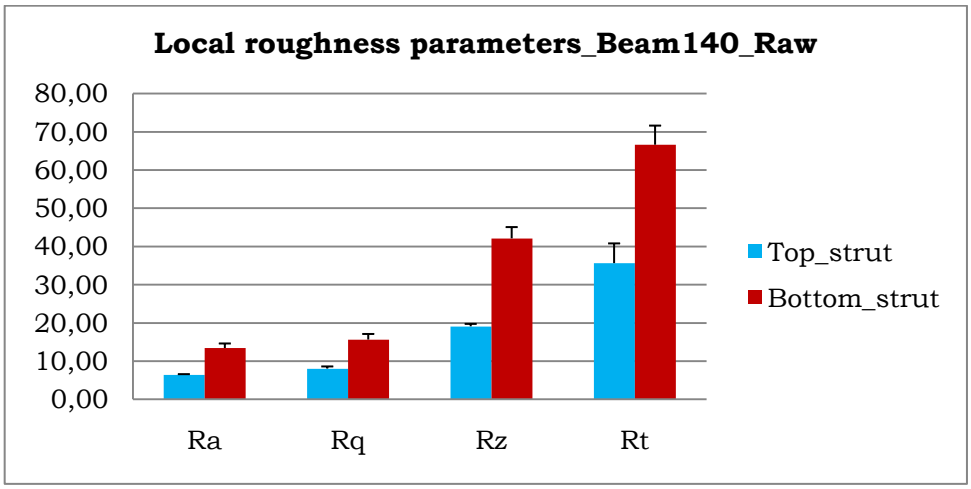

(a)

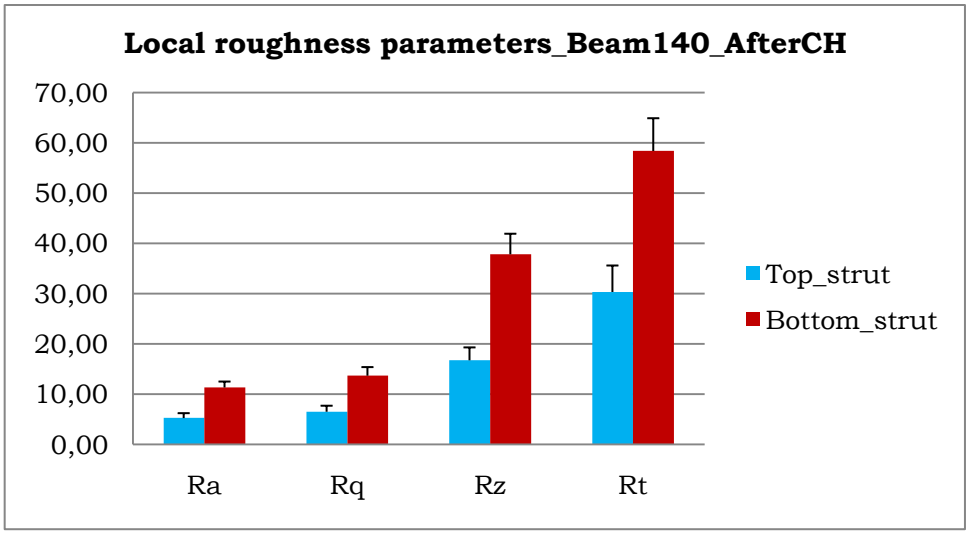

(b)

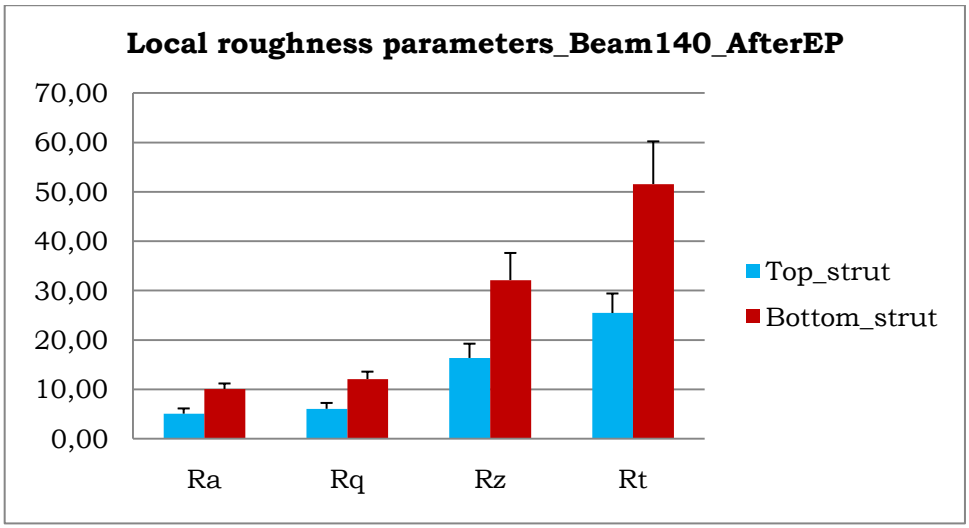

(c)

Fig.7.6. SEM based roughness parameters for the top and bottom of the struts for scaffold design beam 140, for the three surface roughness modification steps: (a) prior to surface roughness modification, (b) after chemical etching (CH) and (c) after electrochemical polishing (EP).

Similar to what was found for scaffold design beam 100, the roughness parameters differed significantly between top and bottom of the struts. Higher values for the bottom region were obtained for the three surface roughness modification steps.

Finally, the roughness parameters of scaffold design beam 180 were calculated, as summarized in Table 7.3 for scaffolds prior to surface roughness modification, after chemical etching and after electrochemical polishing.

Table 7.3. SEM based roughness parameters for scaffold design beam 180 prior to surface roughness modification, after chemical etching (CH) and after electrochemical polishing (EP).

Ti6Al4V_beam180									
Raw									
		Ra		**Rq**		**Rz**		**Rt**	
		Av.	Stdv.	Av.	Stdv.	Av.	Stdv.	Av.	Stdv.
TOP	Tops	8,89	2,96	10,98	3,56	25,52	9,06	47,44	17,64
	Bottoms	12,30	2,28	14,87	2,63	37,96	6,30	63,09	10,10
	Total	10,59	2,41	12,93	2,75	31,74	8,80	55,27	11,07
MIDDLE	Tops	8,95	1,62	10,94	1,89	28,53	5,47	48,27	8,80
	Bottoms	12,12	4,27	14,32	5,06	37,33	11,43	62,27	16,86
	Total	10,53	2,25	12,63	2,39	32,93	6,22	55,27	9,90
BOTTOM	Tops	8,48	2,22	10,69	2,79	25,85	6,40	49,70	16,09
	Bottoms	10,71	1,92	12,83	2,34	35,73	6,75	54,55	7,81
	Total	9,59	1,58	11,76	1,51	30,79	6,98	52,13	3,43
	Total Tops	8,77	0,26	10,87	0,16	26,63	1,65	48,47	1,15
	Total Bottoms	11,71	0,87	14,01	1,06	37,01	1,15	59,97	4,71
	GLOBAL	10,24	2,08	12,44	2,22	31,82	7,33	54,22	8,13
AfterCH									
		Ra		**Rq**		**Rz**		**Rt**	
		Av.	Stdv.	Av.	Stdv.	Av.	Stdv.	Av.	Stdv.
TOP	Tops	5,84	2,79	7,68	3,76	18,11	6,50	39,11	19,25
	Bottoms	10,83	2,31	12,44	2,15	36,93	6,09	55,07	10,10
	Total	8,33	3,53	10,06	3,37	27,52	13,30	47,09	11,29
MIDDLE	Tops	6,32	2,01	7,99	2,38	19,86	8,68	41,68	13,46
	Bottoms	9,96	3,13	11,95	3,18	33,51	9,48	55,29	12,86
	Total	8,14	2,57	9,97	2,80	26,69	9,65	48,48	9,63
BOTTOM	Tops	6,60	2,37	8,09	3,07	19,35	6,59	37,01	15,38
	Bottoms	9,32	1,50	11,36	1,87	30,59	6,28	50,18	8,61
	Total	7,96	1,92	9,73	2,32	24,97	7,95	43,59	9,31
	Total Tops	6,25	0,38	7,92	0,21	19,11	0,90	39,26	2,34
	Total Bottoms	10,04	0,76	11,92	0,54	33,68	3,17	53,51	2,89
	GLOBAL	8,14	2,68	9,92	2,83	26,39	10,30	46,39	10,08

AfterEP									
		Ra		Rq		Rz		Rt	
		Av.	Stdv.	Av.	Stdv.	Av.	Stdv.	Av.	Stdv.
TOP	Tops	5,37	2,25	6,91	3,26	18,34	9,02	32,62	16,50
	Bottoms	10,24	3,24	12,11	3,53	33,13	11,46	49,41	11,13
	Total	7,80	3,45	9,51	3,68	25,73	10,45	41,02	11,87
MIDDLE	Tops	5,48	1,65	6,82	1,92	16,99	4,56	32,04	10,77
	Bottoms	9,87	2,48	11,87	2,51	31,79	7,88	52,42	9,17
	Total	7,67	3,10	9,34	3,57	24,39	10,47	42,23	14,41
BOTTOM	Tops	5,55	2,05	6,80	2,49	16,68	4,82	32,69	11,94
	Bottoms	8,05	2,48	9,70	2,80	25,31	9,88	41,39	10,51
	Total	6,80	1,77	8,25	2,05	21,00	6,10	37,04	6,16
	Total Tops	5,46	0,09	6,84	0,06	17,34	0,88	32,45	0,36
	Total Bottoms	9,39	1,17	11,23	1,32	30,08	4,18	47,74	5,70
	GLOBAL	7,42	2,78	9,03	3,10	23,71	9,01	40,10	10,81

Similar to scaffold designs beam 100 and beam 140, for scaffold design beam 180 a decrease in the roughness parameters was observed for the different surface roughness modification steps. Fig. 7.7 shows the results.

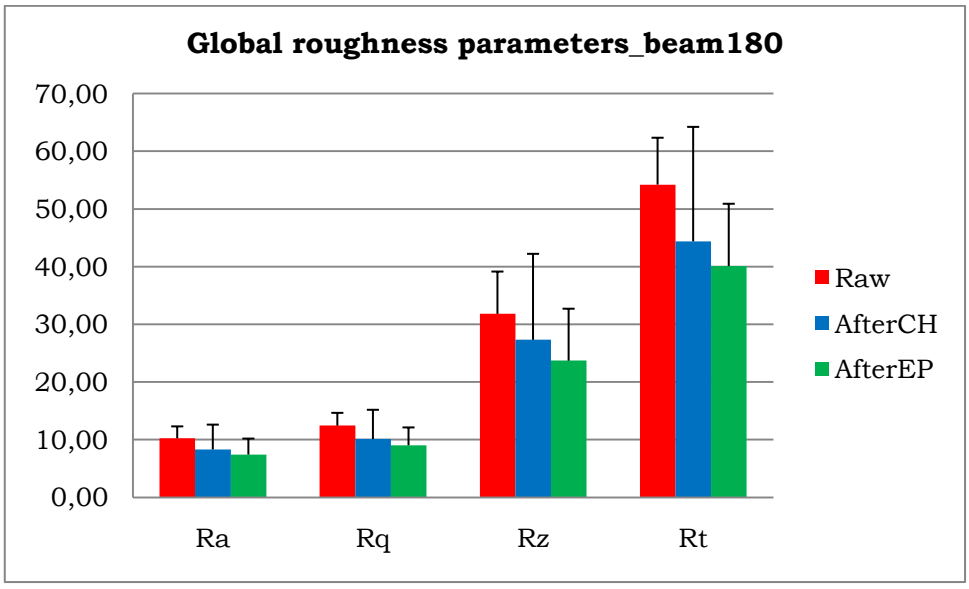

Fig.7.7. SEM based roughness parameters for scaffold design beam 180 prior to surface roughness modification, after chemical etching (CH) and after electrochemical polishing (EP).

Similar to scaffold designs beam 100 and beam 140, Fig. 7.8 shows for scaffold design beam 180 minor differences when differentiating between roughness at the top, middle and bottom of the scaffold.

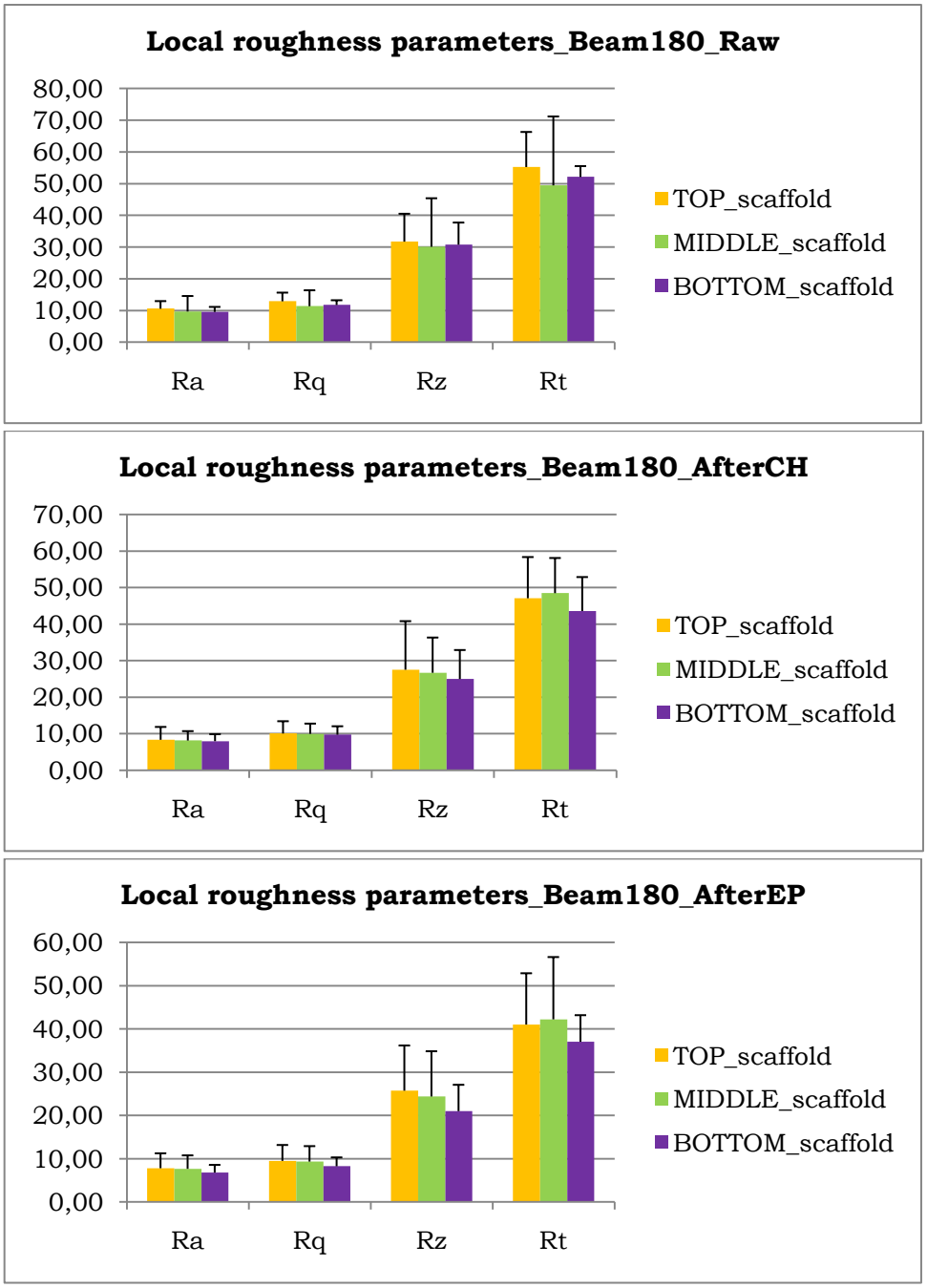

Fig.7.8. SEM based roughness parameters for the top, middle and bottom zones of the scaffolds of scaffold design beam 180, for the three surface roughness modification steps: (a) prior to surface roughness modification, (b) after chemical etching (CH) and (c) after electrochemical polishing (EP).

Except for Rt, roughness parameters were the highest in the top region of the Ti6Al4V scaffolds, for the three stages. The lowest ones corresponded to the bottom zones. That is what was obtained for beam 140, although the differences for beam 180 were no so significant. More homogeneous surface treatments were supposed because of the close differences in roughness parameters maintenance, comparing with previous beams 100 and 140.

Fig. 7.9 shows the roughness measurements after each surface roughness modification step and prior to surface roughness modification analyzing top and bottom of the strut separately for scaffold design beam 180.

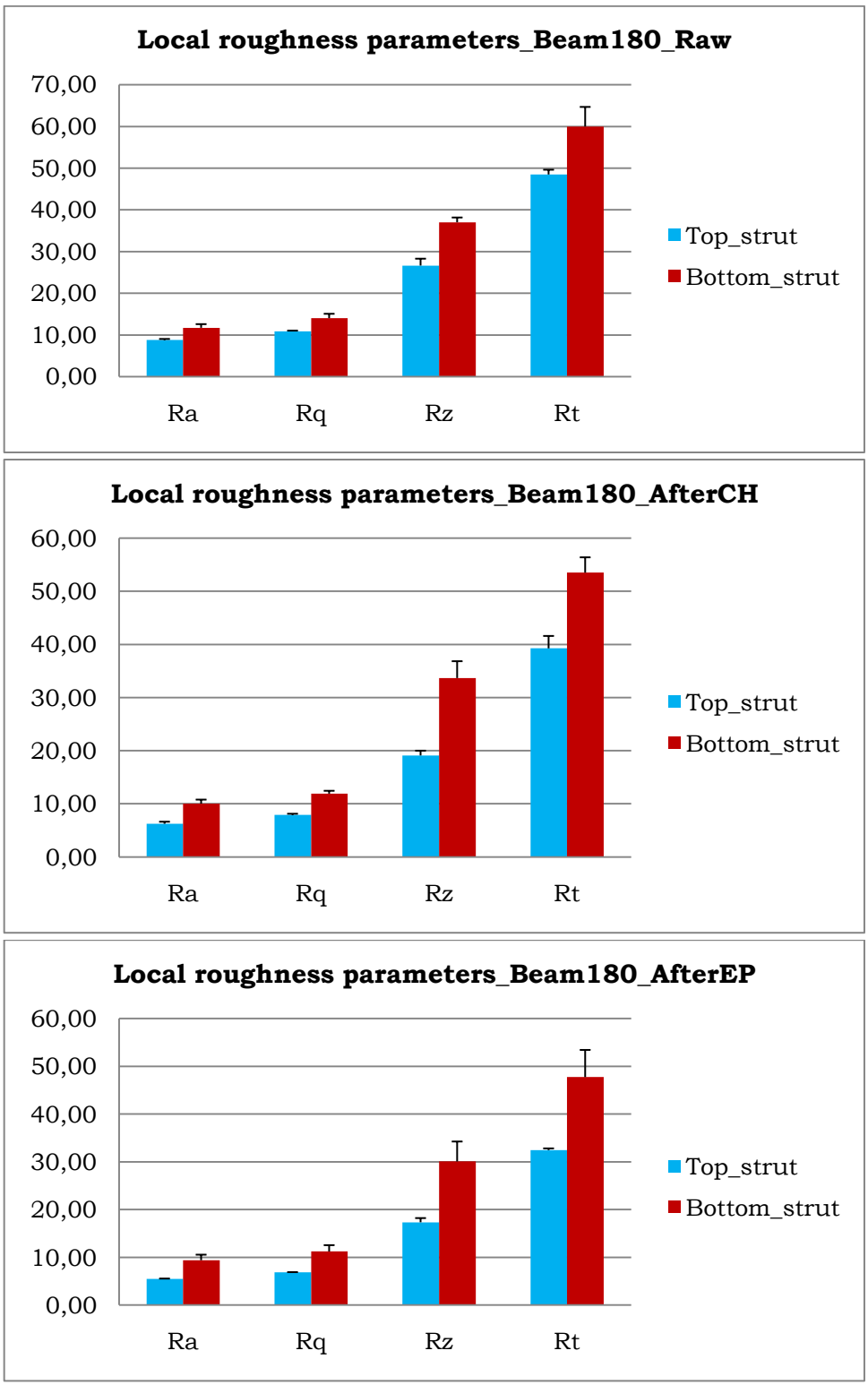

Fig.7.9. SEM based roughness parameters for the top and bottom of the struts for scaffold design beam 180, for the three surface roughness modification steps: (a) prior to surface roughness modification, (b) after chemical etching (CH) and (c) after electrochemical polishing (EP).

Also for scaffold design beam 180, similar to scaffold designs beam 100 and beam 140, the roughness measurements for the bottom of the struts were significantly higher comparing than of the top of the struts for all steps of the surface roughness modification.

Next, as can be observed in Fig. 7.10, a comparison of the full Ti6Al4V scaffolds roughness measurements shows the differences between each surface roughness modification per each strut design.

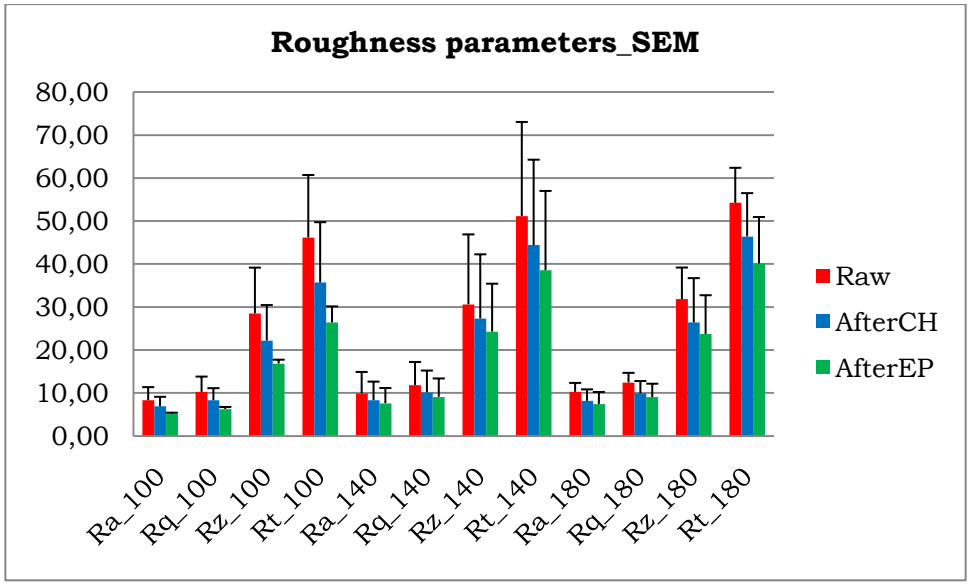

Fig.7.10. SEM based roughness parameters for the full scaffolds of the three strut designs, prior to surface roughness modifications, after chemical etching and after electrochemical polishing.

As it is reflected in Fig. 7.10, the roughness measurements of the full scaffolds showed a decreasing trend in function of the applied surface roughness modification steps. Nevertheless, when roughness analyses were carried out more locally, differences in roughness measurements were discovered, even after production, when comparing different regions of the Ti6Al4V scaffolds. The two consecutive surface roughness modification steps were not able to fully homogenize the roughness along the samples. Also, significant differences were also observed, comparing top and bottom of the struts. Therefore, optimization of the surface treatment procedures is required. We tried to correlate these heterogeneities in roughness values with the current density values for each scaffold design.

7.2.2. Relation between the reduction of the roughness parameters and the current density

The percentage of reduction in Ra, Rq, Rz and Rt was calculated and is shown in Table 7.4, in order to find the relation with the current density. Table 7.4 shows for the chemical etching step a higher roughness reduction for the scaffold design beam 180 compared to the other scaffold designs. With the knowledge that the roughness after production was already the highest for scaffold design beam 180, it can be concluded that the chemical etching process is relatively well controlled and will remove the unmelted powder grains on the surface as much as possible. More grains, thus a higher roughness, will result in a removal of a larger amount of grains and hence a larger percentage of roughness reduction. Concerning the electrochemical

polishing, Fig. 7.11 shows the roughness reduction in function of the applied current density.

Table 7.4. SEM based percentage of reduction in the roughness parameters for the different steps of the surface roughness modification procedure for the different scaffold designs.

Ti6Al4V			
Beam 100	**Raw-CH reduction (%)**	**CH-EP reduction (%)**	**Raw-EP reduction (%)**
Ra	17,32	25,31	38,25
Rq	18,99	24,99	39,23
Rz	22,23	24,04	40,93
Rt	22,61	26,09	42,81
Beam 140	**Raw-CH reduction (%)**	**CH-EP reduction (%)**	**Raw-EP reduction (%)**
Ra	15,90	8,75	23,26
Rq	14,38	10,18	23,09
Rz	10,70	11,23	20,72
Rt	13,14	13,24	24,64
Beam 180	**Raw-CH reduction (%)**	**CH-EP reduction (%)**	**Raw-EP reduction (%)**
Ra	20,46	8,83	27,49
Rq	20,27	8,93	27,39
Rz	17,05	10,18	25,50
Rt	14,44	13,56	26,05

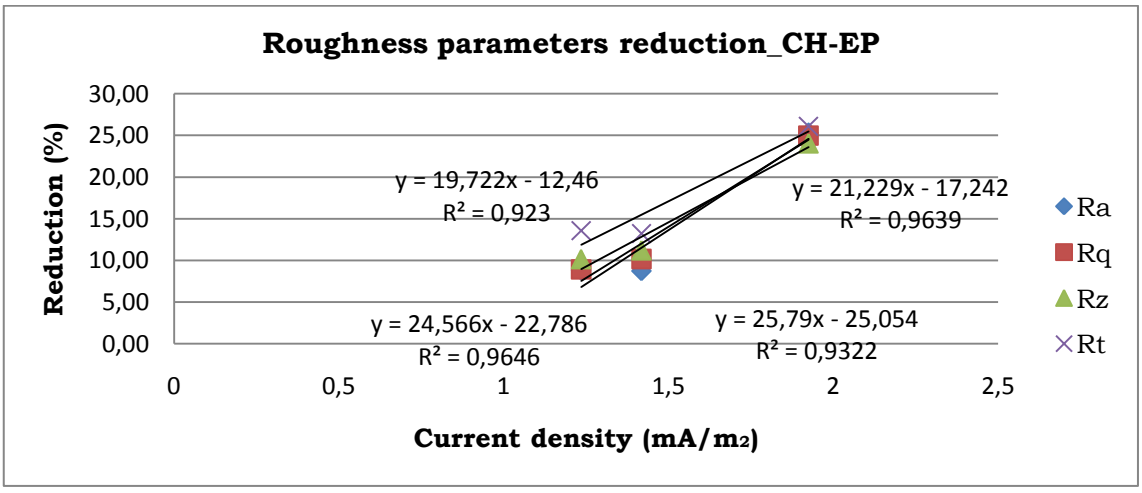

Fig.7.11. SEM based percentage of reduction in the roughness parameters in function of the current density.

As can be seen in Fig.7.11, an increasing linear relation between the percentage of reduction in the roughness parameters and the current density was found. That means that for higher values of current density, a higher reduction in roughness is obtained. Therefore, higher values of current density will be desirable for future experiments, although, as was concluded in previous chapter, mechanical properties and the structure thickness decrease significantly. The most suitable balance between these two types of properties should be found, and the linear equation from this graph, combined with the

linear equations obtained in the previous chapter should be combined in order to find the best settings for the current density for a specific design and required morphological, mechanical and roughness properties. Indeed, after analyzing all these relations, the significant role of the current density on the effect of the surface roughness modification was determined. Therefore, depending on current density during electrochemical polishing, different morphologies, mechanical properties and surface roughnesses could be obtained by controlling the surface roughness modification procedure.

7.3. Micro-CT based roughness measurements

For the high-resolution micro-CT based roughness measurements, due to time restrictions, only one region of one Ti6Al4V scaffold per scaffold design of the three stages was selected, namely the top zone, and the roughness was determined in the centre and on the sides of this zone in two directions. Additionally, the roughness parameters of top and bottom surfaces of the struts were obtained for two struts of both the centre and the side of the top zone. Table 7.5 shows the results obtained for Ra, Rq, Rz and Rt, for scaffold design beam 100 prior to surface roughness modification, after chemical etching and after electrochemical polishing.

Table 7.5. High-resolution micro-CT based roughness parameters for scaffold design beam 100 prior to surface roughness modification, after chemical etching (CH) and after electrochemical polishing (EP).

Ti6Al4V_beam100									
Raw									
		Ra		**Rq**		**Rz**		**Rt**	
		Av.	Stdv.	Av.	Stdv.	Av.	Stdv.	Av.	Stdv.
Centre	Tops	10,88	3,86	13,50	4,22	27,05	6,97	58,60	19,48
	Bottoms	10,85	4,12	13,94	5,94	31,14	8,83	69,03	32,83
	Total	10,86	0,02	13,72	0,31	29,09	2,89	63,82	7,38
Side	Tops	5,18	1,58	6,63	1,70	15,48	3,84	30,50	6,80
	Bottoms	9,71	2,10	12,11	2,52	31,43	8,34	54,78	10,64
	Total	7,44	3,21	9,37	3,88	23,46	11,28	42,64	17,17
	GLOBAL	9,15	2,42	11,55	3,08	26,28	3,99	53,23	14,98
After CH									
		Ra		**Rq**		**Rz**		**Rt**	
		Av.	Stdv.	Av.	Stdv.	Av.	Stdv.	Av.	Stdv.
Centre	Tops	8,37	3,93	9,30	3,73	23,59	8,25	31,02	6,00
	Bottoms	8,30	3,16	10,21	3,86	23,89	7,40	43,56	16,97
	Total	8,34	0,05	9,75	0,65	23,74	0,21	37,29	8,86
Side	Tops	6,00	2,04	7,27	2,43	18,38	5,56	30,75	11,20
	Bottoms	7,35	1,77	9,33	2,33	22,74	6,32	44,67	10,09
	Total	6,68	0,95	8,30	1,46	20,56	3,09	37,71	9,84
	GLOBAL	7,51	1,17	9,03	1,03	22,15	2,25	37,50	0,29

After EP									
		Ra		Rq		Rz		Rt	
		Av.	Stdv.	Av.	Stdv.	Av.	Stdv.	Av.	Stdv.
Centre	Tops	8,09	3,10	9,29	2,90	24,31	7,02	33,82	5,97
	Bottoms	8,51	3,08	10,34	3,81	23,99	6,39	42,16	17,31
	Total	8,30	0,30	9,82	0,74	24,15	0,23	37,99	5,90
Side	Tops	4,34	0,94	5,43	1,44	13,02	1,94	23,30	4,34
	Bottoms	5,72	1,89	7,16	2,53	17,18	5,32	32,29	11,81
	Total	5,03	0,98	6,30	1,23	15,10	2,94	27,79	6,36
	GLOBAL	6,66	2,31	8,06	2,49	19,63	6,40	32,89	7,21

Similar as for the SEM-based roughness measurements, the roughness parameters for the full scaffold decreased after each surface roughness modification step, as shown in Fig. 712, which is logical because the goal of the successive surface roughness modification steps was to get a smoother and more homogeneous surface roughness.

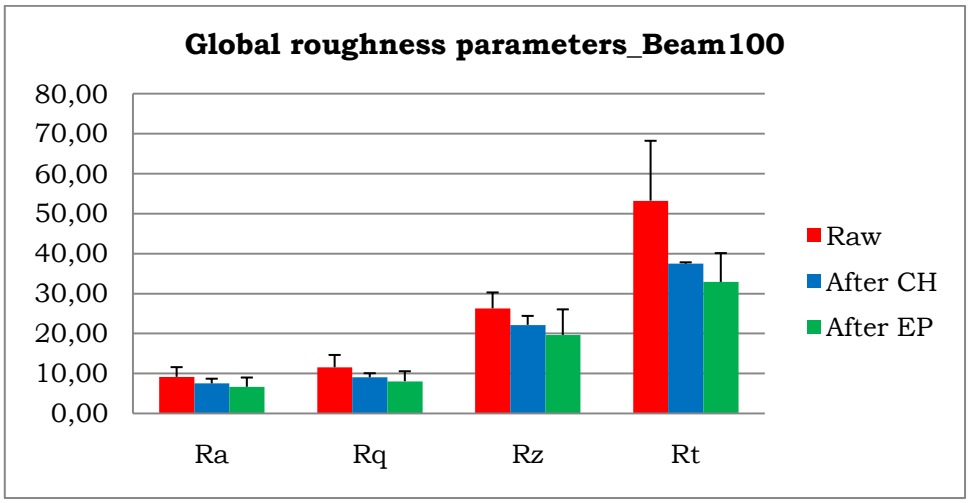

Fig.7.12. High-resolution micro-CT based roughness parameters for scaffold design beam 100 prior to surface roughness modification, after chemical etching (CH) and after electrochemical polishing (EP).

As shown in Fig. 7.13, significant differences were found when comparing the roughness parameters of the centre and the side of each Ti6Al4V scaffold prior to surface roughness modification, after chemical etching and after electrochemical polishing.

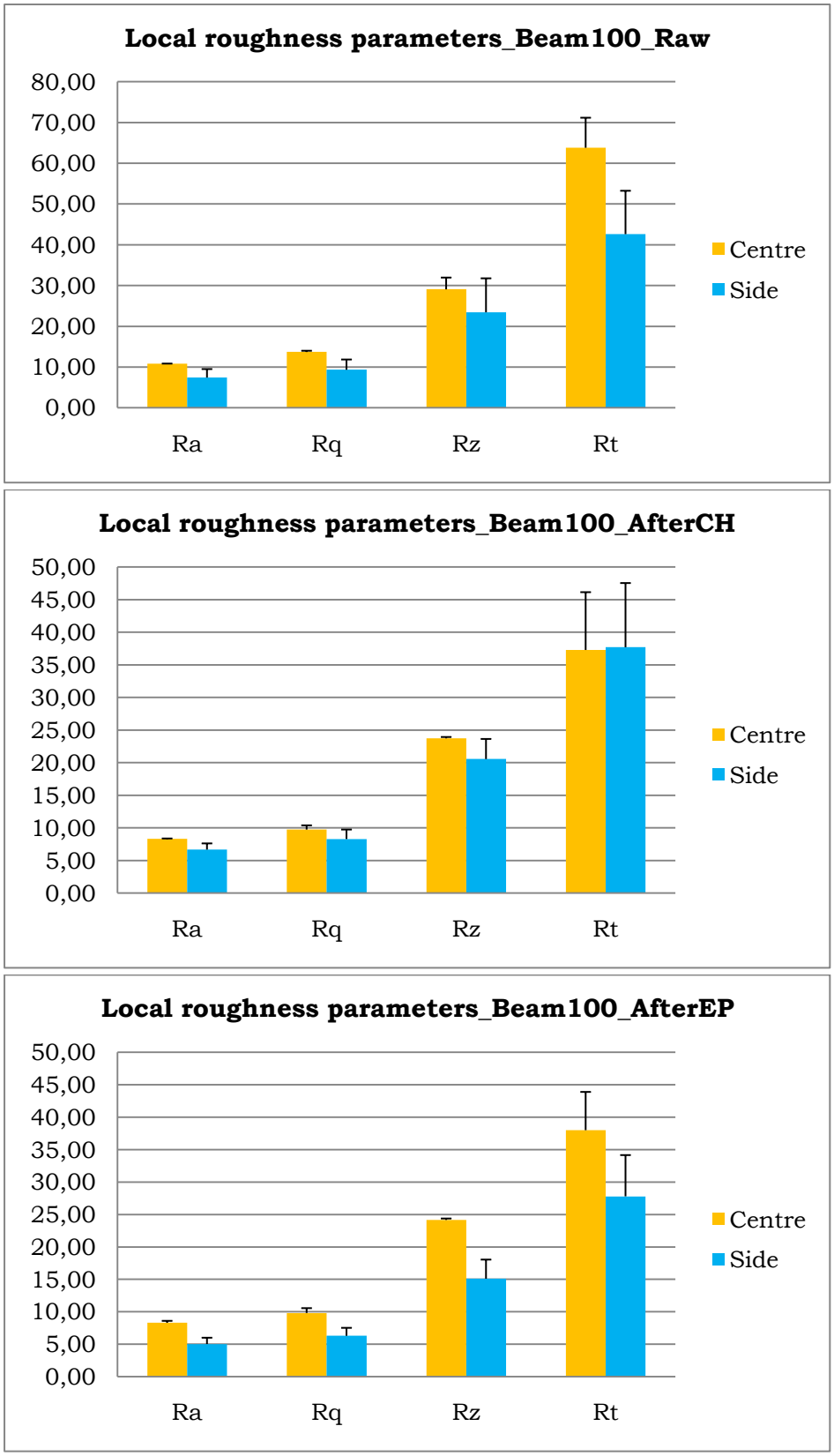

Fig. 7.13. High-resolution micro-CT based roughness parameters for the centre and the sides of the top zone of the scaffolds of scaffold design beam 100, for the three surface roughness modification steps: (a) prior to surface roughness modification, (b) after chemical etching (CH) and (c) after electrochemical polishing (EP).

Significant differences in roughness parameters between the centre and the sides of the Ti6Al4V scaffolds were observed. For all the surface roughness modification steps, the roughness was higher in the centre compared to the sides, even after production. Hence, a heterogeneous fabrication process was assumed. After chemical etching, the differences between the centre and the sides diminished. Thus, the efficiency of the chemical etching step is high, since it removes all the unmelted powder grains on the surfaces, also when the concentration is higher compared to other locations. Finally, the differences in roughness parameters after electrochemical polishing increased again, thus concluding that the electrochemical polishing step is not homogeneous and has more effect on the edges of the scaffolds than on the centre.

Similar to what was observed using the SEM-based roughness measurements, the roughness values of the top of the struts were lower than for the bottom of the struts, for all the surface roughness modification steps.

Table 7.6 presents the high-resolution micro-CT based roughness parameters for scaffold design beam 140.

Table 7.6. High-resolution micro-CT based roughness parameters for scaffold design beam 140 prior to surface roughness modification, after chemical etching (CH) and after electrochemical polishing (EP).

Ti6Al4V_beam140									
Raw									
		Ra		**Rq**		**Rz**		**Rt**	
		Av.	Stdv.	Av.	Stdv.	Av.	Stdv.	Av.	Stdv.
Centre	Tops	8,72	1,42	11,11	1,51	29,40	7,49	57,12	12,92
	Bottoms	15,41	3,08	19,08	3,44	52,30	7,45	87,28	12,30
	Total	12,07	4,73	15,09	5,63	40,85	16,19	72,20	21,32
Side	Tops	8,10	2,03	10,74	2,96	25,97	7,83	55,54	13,45
	Bottoms	12,93	1,17	16,17	1,44	44,92	5,27	70,02	9,06
	Total	10,51	3,41	13,45	3,84	35,44	13,40	62,78	10,24
	GLOBAL	11,29	1,10	14,27	1,16	38,15	3,83	67,49	6,66
After CH									
		Ra		**Rq**		**Rz**		**Rt**	
		Av.	Stdv.	Av.	Stdv.	Av.	Stdv.	Av.	Stdv.
Centre	Tops	6,94	0,99	8,53	1,64	22,37	2,24	41,48	7,62
	Bottoms	15,33	1,77	19,32	2,83	51,06	8,56	90,38	14,18
	Total	11,14	5,93	13,93	7,63	36,71	20,29	65,93	34,58
Side	Tops	6,07	2,03	7,41	2,45	19,92	5,83	32,39	8,74
	Bottoms	9,69	2,96	12,40	3,79	32,42	6,49	55,73	15,93
	Total	7,88	2,56	9,90	3,53	26,17	8,84	44,06	16,50
	GLOBAL	9,51	2,30	11,92	2,84	31,44	7,45	55,00	15,46

After EP									
		Ra		Rq		Rz		Rt	
		Av.	Stdv.	Av.	Stdv.	Av.	Stdv.	Av.	Stdv.
Centre	Tops	8,35	1,46	10,71	1,54	25,05	4,43	52,74	5,46
	Bottoms	17,82	9,59	21,70	10,47	50,88	18,37	101,89	44,54
	Total	13,08	6,70	16,20	7,77	37,96	18,26	77,31	34,75
Side	Tops	5,36	1,72	6,71	1,92	16,92	3,35	32,10	6,06
	Bottoms	8,07	2,26	9,73	2,70	26,59	6,11	43,13	12,26
	Total	6,71	1,92	8,22	2,14	21,76	6,84	37,62	7,80
	GLOBAL	9,90	4,50	12,21	5,65	29,86	11,46	57,46	28,07

As can be seen in Fig.7.14, a decrease in roughness was observed, similar as for scaffold design beam 100 and for the SEM-based roughness measurements of scaffold design beam 140.

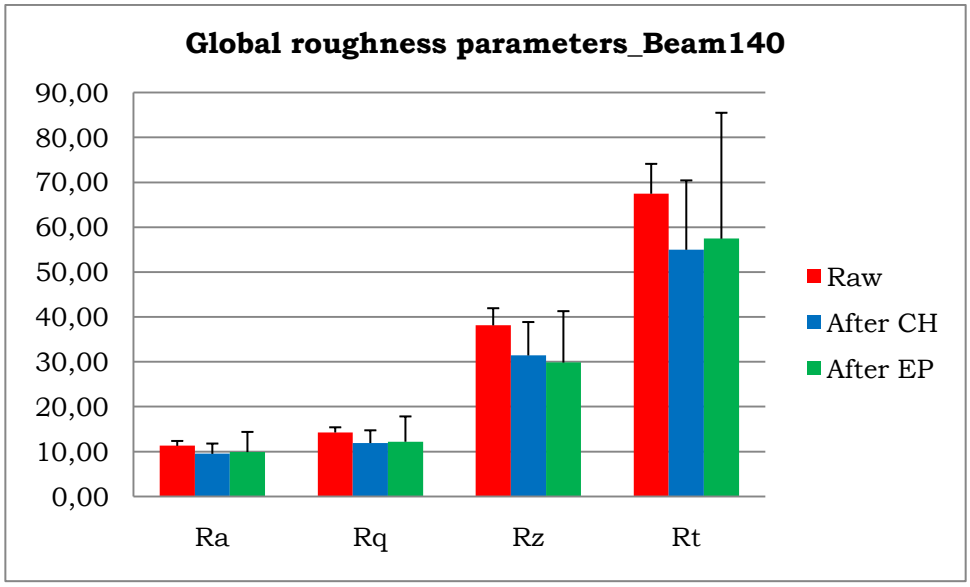

Fig.7.14. High-resolution micro-CT based roughness parameters for scaffold design beam 140 prior to surface roughness modification, after chemical etching (CH) and after electrochemical polishing (EP).

Fig. 7.15 shows the comparison between the roughness at the centre and the side of the scaffolds prior to surface roughness modification, after chemical etching and after electrochemical polishing.

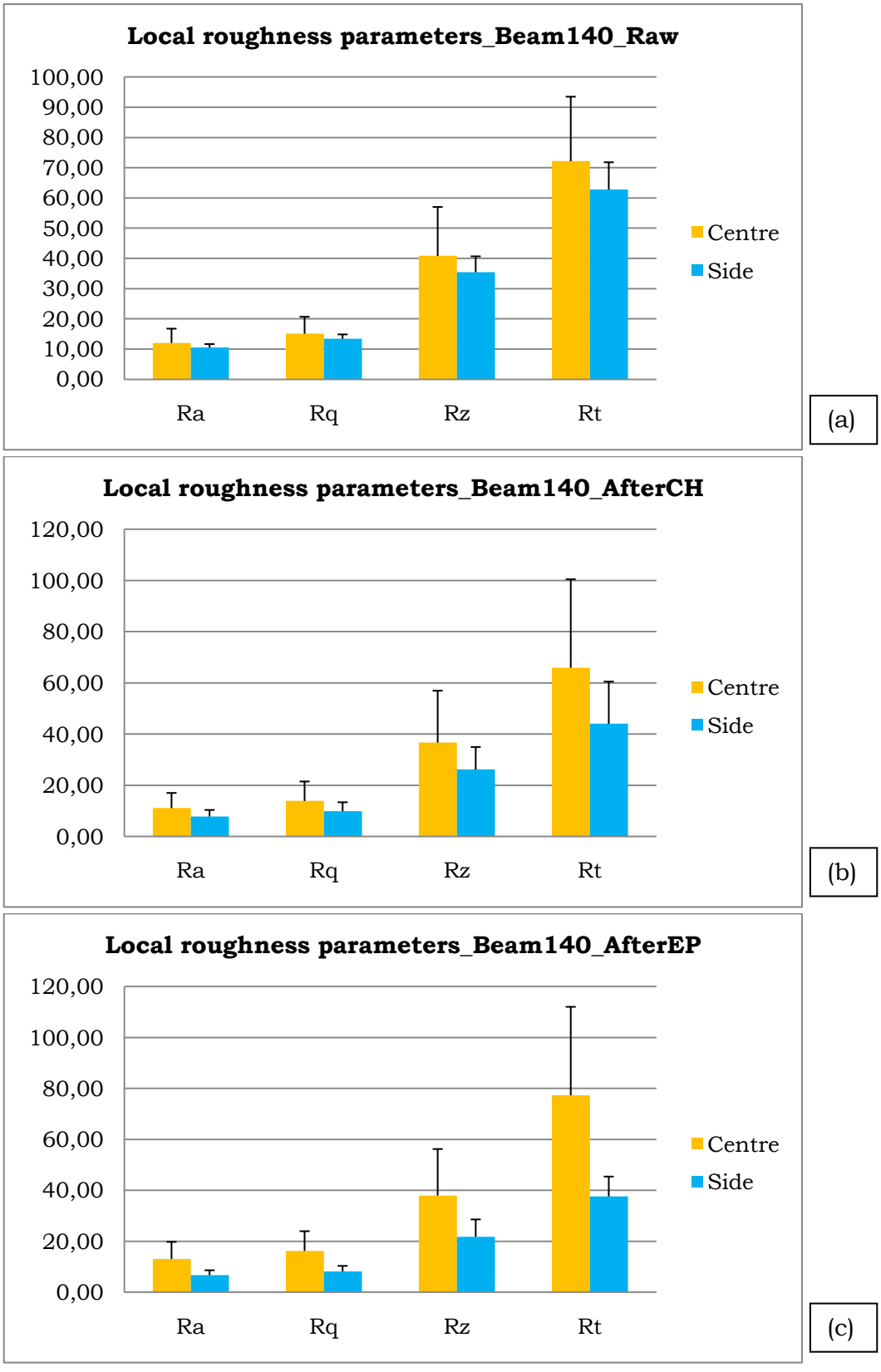

Fig. 7.15. High-resolution micro-CT based roughness parameters for the centre and the sides of the top zone of the scaffolds of scaffold design beam 140, for the three surface roughness modification steps: (a) prior to surface roughness modification, (b) after chemical etching (CH) and (c) after electrochemical polishing (EP).

For all the surface roughness modification steps, the roughness in the centre measurements was higher than at the side. Similar conclusions as for scaffold design beam 100 can be drawn. However, it has to be mentioned that for scaffold design 140 and beam 180 (see below), the obtained results were not always corresponding to the expectations. For example, as can be seen in Fig. 7.15, the high-resolution micro-CT based average roughness values increased after electrochemical polishing, which is not expected. No definite reason for this can be found, but it has to be mentioned that for the high-resolution micro-CT based average roughness measurements only one sample was assessed. Hence, definite conclusions can only be drawn when significantly more samples have been assessed.

Similar to scaffold design beam 100, and comparable to the SEM-based roughness measurements, the surface roughness of the tops and bottoms of the struts differed significantly, namely the bottom of the struts had a larger roughness. Table 7.7 reflects the results for scaffold design beam 180, for the as-produced scaffolds, after chemical etching and after electrochemical polishing.

Table 7.7. High-resolution micro-CT based roughness parameters for scaffold design beam 180 prior to surface roughness modification, after chemical etching (CH) and after electrochemical polishing (EP).

Ti6Al4V_beam180									
Raw									
		Ra		**Rq**		**Rz**		**Rt**	
		Av.	Stdv.	Av.	Stdv.	Av.	Stdv.	Av.	Stdv.
Centre	Tops	9,23	1,88	11,77	2,08	34,49	5,88	53,51	7,26
	Bottoms	16,57	3,32	19,95	3,92	57,13	10,69	84,02	16,70
	Total	12,90	5,18	15,86	5,79	45,81	16,01	68,76	21,58
Side	Tops	8,26	1,65	10,55	1,87	27,08	3,54	50,03	10,83
	Bottoms	16,78	5,13	19,97	5,20	55,51	13,50	86,26	18,17
	Total	12,52	6,03	15,26	6,66	41,29	20,10	68,14	25,62
	GLOBAL	12,71	0,27	15,56	0,42	43,55	3,19	68,45	0,44
After CH									
		Ra		**Rq**		**Rz**		**Rt**	
		Av.	Stdv.	Av.	Stdv.	Av.	Stdv.	Av.	Stdv.
Centre	Tops	7,34	2,39	8,85	2,65	25,08	6,84	41,25	8,82
	Bottoms	14,42	1,61	17,38	1,75	46,58	5,96	71,76	5,24
	Total	10,88	5,01	13,12	6,03	35,83	15,20	56,51	21,57
Side	Tops	6,07	3,13	7,54	3,54	20,98	8,23	35,51	12,97
	Bottoms	10,78	5,47	13,85	6,52	36,75	14,74	68,73	29,41
	Total	8,42	3,33	10,70	4,46	28,87	11,15	52,12	23,49
	GLOBAL	9,65	1,74	11,91	1,71	32,35	4,92	54,31	3,10

After EP									
		Ra		Rq		Rz		Rt	
		Av.	Stdv.	Av.	Stdv.	Av.	Stdv.	Av.	Stdv.
Centre	Tops	3,88	1,57	4,92	2,16	11,87	2,87	25,52	13,27
	Bottoms	13,96	4,55	16,77	5,04	41,63	16,57	74,28	25,22
	Total	8,92	7,13	10,84	8,37	26,75	21,04	49,90	34,48
Side	Tops	4,83	2,88	5,95	3,33	12,40	6,84	27,02	13,05
	Bottoms	11,62	2,45	14,49	3,39	33,90	8,18	66,56	21,13
	Total	8,22	4,80	10,22	6,04	23,15	15,21	46,79	27,96
	GLOBAL	8,57	0,49	10,53	0,44	24,95	2,55	48,35	2,20

Again, the average surface roughness of the full scaffold decreased after the different surface roughness modification steps. Fig. 7.16 shows that the chemical etching step introduces the highest roughness reduction.

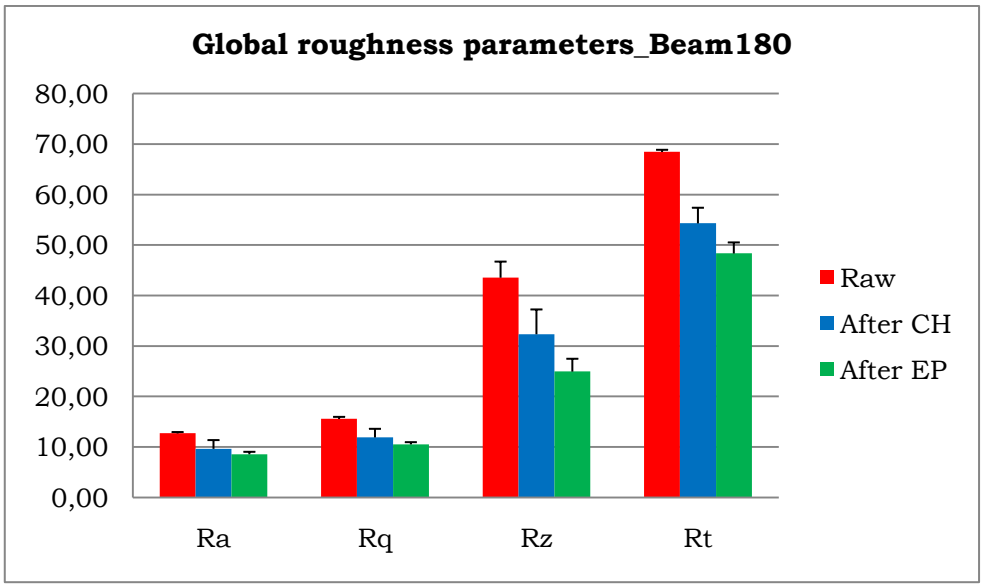

Fig.7.16. High-resolution micro-CT based roughness parameters for scaffold design beam 180 prior to surface roughness modification, after chemical etching (CH) and after electrochemical polishing (EP).

When focusing on the centre and the side regions of the scaffolds, difference in roughness were found, as can be seen in Fig. 7.17.

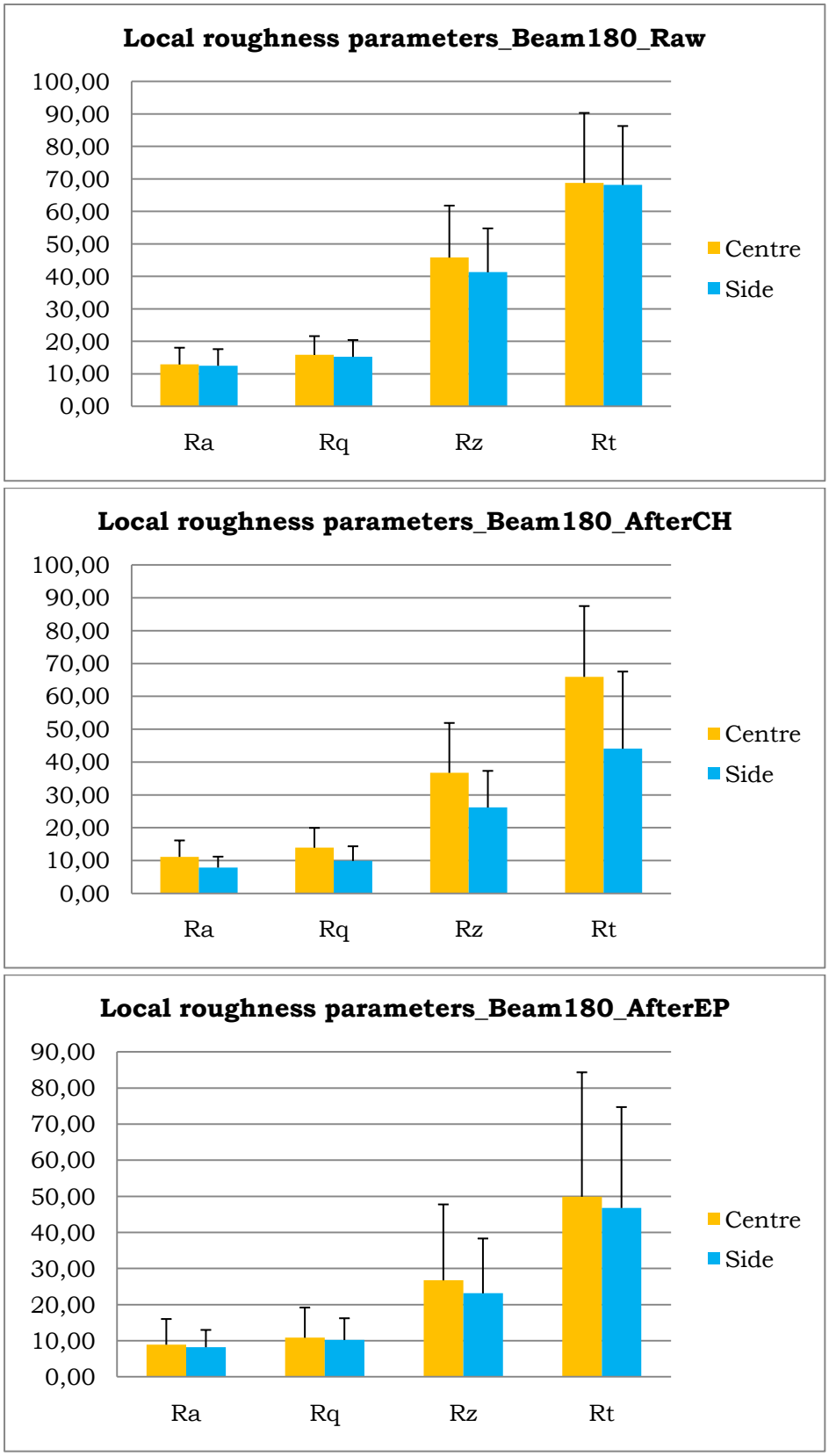

Fig. 7.17. High-resolution micro-CT based roughness parameters for the centre and the sides of the top zone of the scaffolds of scaffold design beam 180, for the three surface roughness modification steps: (a) prior to surface roughness modification, (b) after chemical etching (CH) and (c) after electrochemical polishing (EP).

Concerning the high-resolution micro-CT measured roughness difference between the centre and the sides of the scaffolds after chemical etching and after electrochemical polishing, the same conclusions as for scaffolds design beam 140 can be drawn.

Again, the roughness measurements, after each surface roughness modification step, of the bottom of the struts was significantly higher than of the top of the struts.

7.4. Comparison of both roughness measurement techniques

A comparison between SEM-based and high-resolution micro-CT based roughness measurements was made, as shown in Table 7.8 and Fig. 7.18.

Table 7.8. Average roughness parameters for the top zone of the scaffolds calculated both using the SEM-based and the high-resolution micro-CT based roughness measurement technique, for all scaffold designs and all surface roughness modification steps.

		Ra		**Rq**		**Rz**		**Rt**	
Beam 100		Av.	Stdv.	Av.	Stdv.	Av.	Stdv.	Av.	Stdv.
Raw	**SEM**	7,47	2,18	9,36	2,75	26,32	7,96	43,86	11,55
	HRm-CT	9,15	2,42	11,55	3,08	26,28	3,99	53,23	14,98
After CH	**SEM**	5,87	1,20	7,08	1,55	20,07	4,81	31,07	8,09
	HRm-CT	7,51	1,17	9,03	1,03	22,15	2,25	37,50	0,29
After EP	**SEM**	4,56	0,16	5,54	0,06	14,88	0,02	22,86	0,33
	HRm-CT	6,66	2,31	8,06	2,49	19,63	6,40	32,89	7,21
		Ra		Rq		Rz		Rt	
Beam 140		Av.	Stdv.	Av.	Stdv.	Av.	Stdv.	Av.	Stdv.
Raw	**SEM**	10,64	5,74	12,76	6,42	32,59	18,18	54,60	24,95
	HRm-CT	11,29	1,10	14,27	1,16	38,15	3,83	67,49	6,66
After CH	**SEM**	9,50	4,55	11,69	5,61	30,82	16,58	50,48	21,17
	HRm-CT	9,51	2,30	11,92	2,84	31,44	7,45	55,00	15,46
After EP	**SEM**	8,32	3,30	10,01	4,10	26,39	11,50	43,37	20,05
	HRm-CT	9,90	4,50	12,21	5,65	29,86	11,46	57,46	28,07
		Ra		Rq		Rz		Rt	
Beam 180		Av.	Stdv.	Av.	Stdv.	Av.	Stdv.	Av.	Stdv.
Raw	**SEM**	10,59	2,41	12,93	2,75	31,74	8,80	55,27	11,07
	HRm-CT	12,71	0,27	15,56	0,42	43,55	3,19	68,45	0,44
After CH	**SEM**	8,33	3,53	10,06	3,37	27,52	13,30	47,09	11,29
	HRm-CT	9,65	1,74	11,91	1,71	32,35	4,92	54,31	3,10
After EP	**SEM**	7,80	3,45	9,51	3,68	25,73	10,45	41,02	11,87
	HRm-CT	8,57	0,49	10,53	0,44	24,95	2,55	48,35	2,20

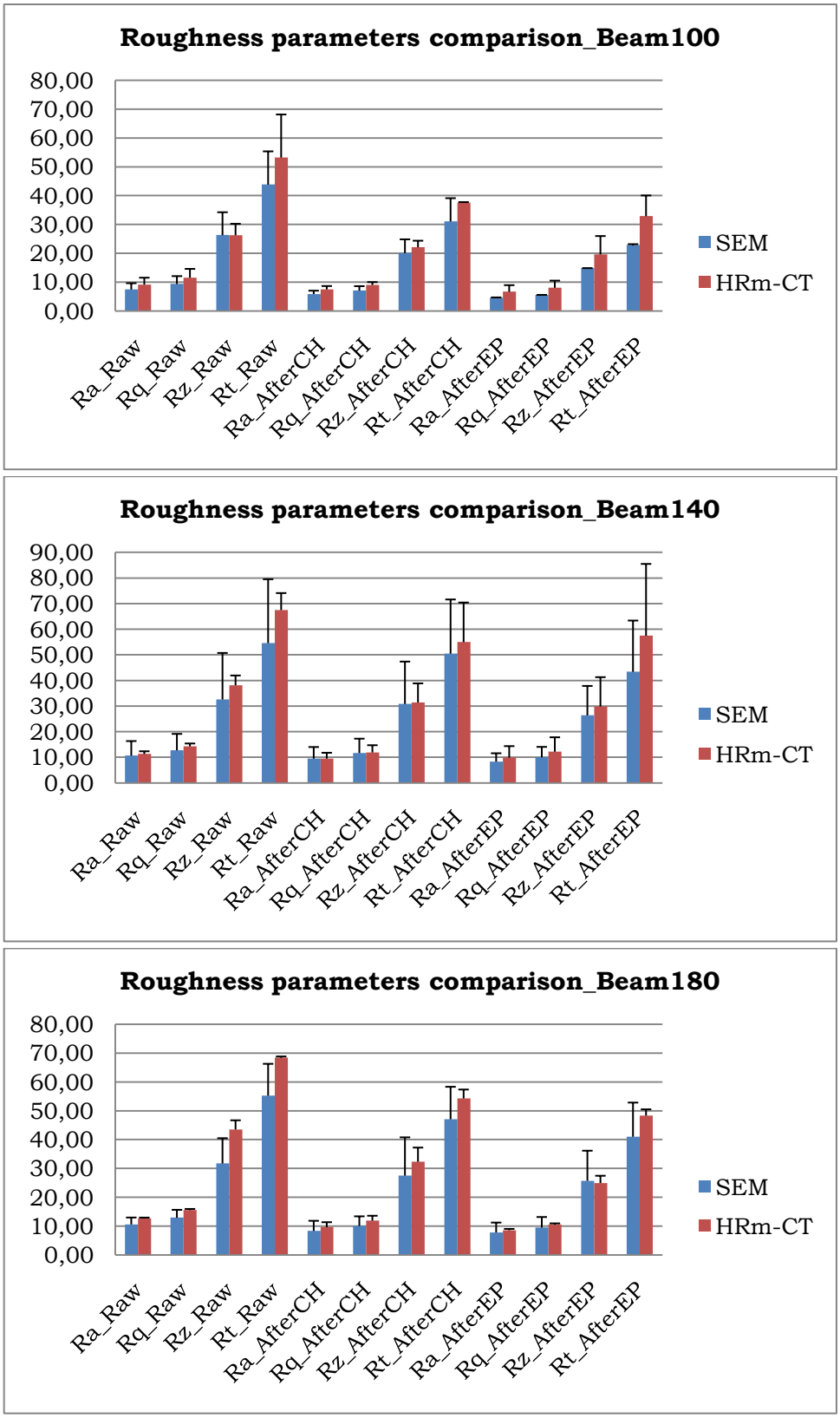

Fig.7.18. Average roughness parameters for Ti6Al4V scaffolds calculated both using the SEM-based and the high-resolution micro-CT based roughness measurement technique, for all surface roughness modification steps: (a) for beam 100, (b) for beam 140 and (c) for beam 180.

Table 7.8 and Fig. 7.18 show higher values for the roughness parameters when measured with high-resolution micro-CT, compared to the SEM-based

results, for all scaffold designs and for each surface roughness modification step. But, taking into account the standard deviations, no significant differences were found between both measurement techniques. Concerning the standard deviations, it also has to be mentioned that the standard deviations of SEM-based roughness measurements is larger, except for beam 100, compared to the high-resolution micro-CT based measurements, indicating that the high-resolution micro-CT based technique is more repeatable and hence more controlled. Indeed, when using SEM images for roughness measurements, the struts are visualized in 3D and hence grains on the surface that are not exactly oriented in the same plain as the image itself are also measured. Hence the height of these grains will be underestimated, resulting in a lower roughness measurement.

7.5. Conclusion

The average surface roughness for the full scaffolds, on the micro-scale, decreased for the three scaffold designs in function of the surface roughness modification. This was a desired effect of the surface roughness modifications, which had the aim to produce a more homogeneous surface. Within one scaffold, differences in roughness were found in function of the height. Additionally, the results showed significant differences in roughness between the top and bottom of the struts and also between the different regions of the scaffold (top, middle or bottom). Therefore, the surface roughness modification steps, and more specific the electrochemical polishing since the chemical etching is more controlled, need to be improved in order to obtain similar values of roughness parameters wherever they will be calculated in any scaffold. Indeed, more control on morphological and mechanical properties (ref. chapter 6), but also on the surface roughness will lead to further improvement in biological cell behaviour.

Comparing the two roughness measurement techniques used in this master thesis, high-resolution micro-CT gives more information. Indeed, since this technique is non-destructive, the roughness can be evaluated throughout the whole scaffold. Hence, not only the roughness at the sides of the scaffold needs to be analyzed, as is the case when the SEM-based measurement technique is used. Additionally, the standard deviation on the results normally is smaller when using high-resolution micro-CT, indicating that this technique is more accurate.

8. Characterization of the PCL scaffolds

8.1. Introduction

The third part of this master thesis consisted in morphological and mechanical characterization of polycaprolactone (PCL) scaffolds and in the preliminary and qualitatively evaluation of two surface roughness modification procedures. The PCL scaffolds were of interest because of their biocompatibility due to its non-toxic degradability.

As mentioned in chapter 3, two different scaffold designs were used: the 0-45-90-45´ lay-up design (beam A) and the 0-90 lay-up design (beam B). The dimensions of all the scaffolds were measured, as was shown in chapter 3. Additionally, density and porosity was calculated using Archimedes device and micro-CT image analysis was carried out on as-produced scaffolds in order to study their morphological properties. Mechanical parameters were then calculated performing compression tests. Finally, the PCL scaffolds were separated in two groups in order to apply two different surface roughness modification procedures, as described in chapter 3.

8.2. Density and porosity

Table 8.1 summarizes the density and porosity of the porous PCL TE scaffolds using the Archimedes tests.

Table 8.1. Archimedes-based density and porosity of the two PCL samples scaffold designs (beams A and beam B).

Material	Group name	Density (g/cm³)	Porosity (%)
PCL	Beam A	1,10 ± 0,05	44,88 ± 3,87
	Beam B	1,14 ± 0,01	50,43 ± 2,16

As expected, similar values of density were found. Porosity values differed depending on the design of the scaffold. These values can be compared with the micro-CT image analysis based results.

8.3. Micro-CT based morphological characterization

Micro-CT was used in order to determine the morphological properties of the PCL scaffolds. Percent object volume, object surface, average strut thickness and average strut separation were the parameters mentioned in Table 8.2, which shows the results for the two scaffold designs prior to surface roughness modification.

Table 8.2. Percent object volume, object surface, average strut thickness and average strut separation for the two PCL scaffold designs prior to surface modification.

PCL_Raw								
Group name	Percent object volume (%)		Object surface (cm²)		Strut thickness (μm)		Strut separation (μm)	
	Av.	Stdv.	Av.	Stdv.	Av.	Stdv.	Av.	Stdv.
Beam A	60,17	1,25	15,53	0,53	343,75	37,51	326,79	17,15
Beam B	62,53	2,19	15,63	0,31	346,28	25,31	316,46	7,11

As can be observed in Table 8.2, scaffold designs beam A and beam B have similar values for the 4 morphological properties. The porosity can be easily obtained from percent object volume data. 39.83% for scaffold design beam A and 37.47% for scaffold design beam B were the porosity values given by micro-CT. Comparing these results with those obtained with the Archimedes test, significant differences were appreciated. Since the threshold for binarization of the micro-CT images was selected manually, an overestimation can be made using micro-CT.

8.4. Mechanical properties

The mechanical properties were calculated using a compression test. The E-modulus, the maximum stress and the strain at maximum stress were determined for the two PCL scaffold designs prior to surface roughness modification, as shown in Table 8.3.

Table 8.3. E-modulus, maximum stress and strain at maximum stress for both PCL scaffold designs prior to surface roughness modification.

Material	Group name	E-modulus (Mpa)	Max. Stress (Mpa)	Strain at max. Stress (%)
PCL	Beam A	32,29 ± 6,58		
	Beam B	36,58 ± 3,57	4,22 ± 0,47	23,07 ± 3,16

Similar values for the E-modulus were obtained for both scaffold designs. However, due to experimental errors, the maximum stress and strain at maximum stress were not determined for scaffold design beam A, and hence cannot be compared to the other scaffold design.

8.5. Surface roughness modification

As mentioned in chapter 3, two different surface roughness modification procedures were carried out on the different PCL scaffold designs to be able to obtain controlled surface properties. First procedure consisted of immersion into 3M NaOH during 96 hours and the second one of immersion into 3M KOH during the same time, as was explained in detail in chapter 3. Qualitative, SEM-based evaluation and comparison of the surface roughness was done for both surface roughness modification procedures.

SEM images were taken for as-produced PCL scaffolds, after NaOH treatment and after KOH treatment, and the differences in surface roughness were studied qualitatively. Fig. 8.1 shows the differences in surface topology prior to surface roughness modification and after each surface roughness modification.

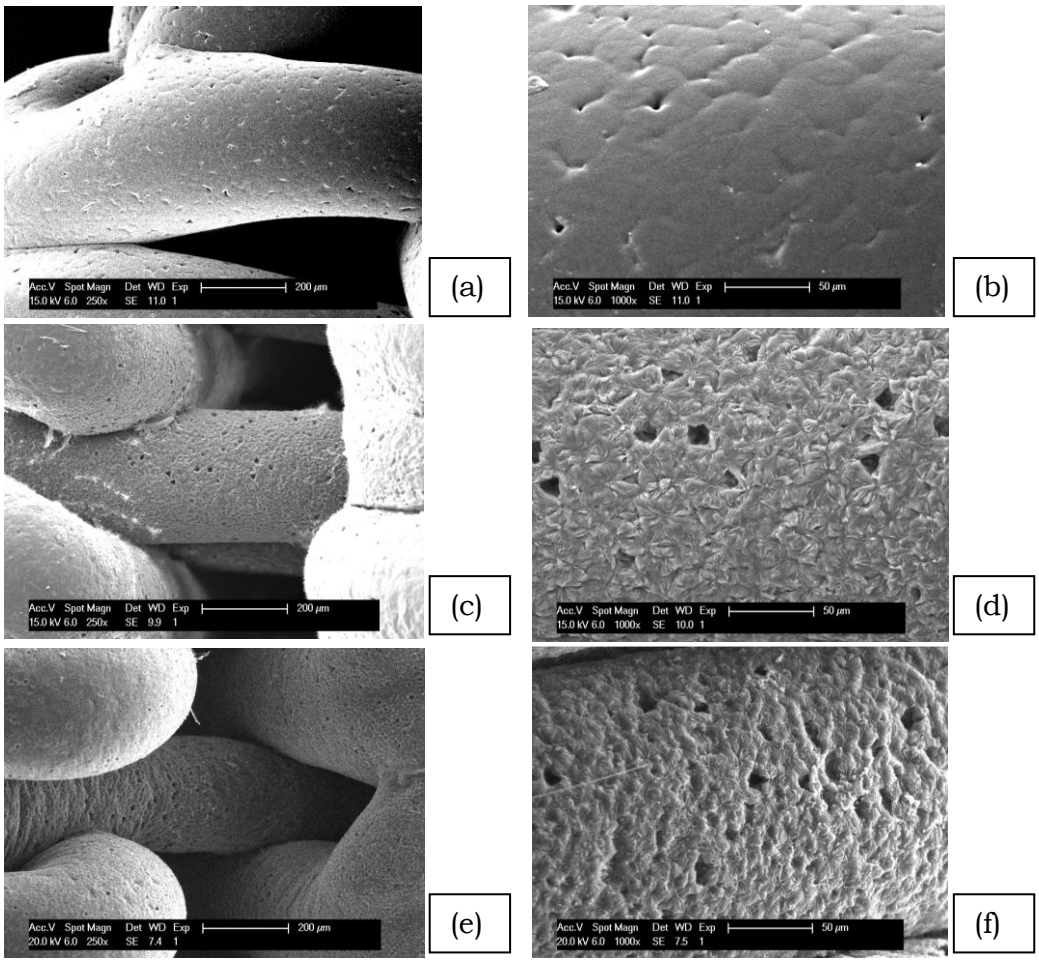

Fig.8.1. Typical SEM images of PCL scaffolds: (a) and (b) prior to surface roughness modification, (c) and (d) after 96 hours of NaOH treatment, and (e) and (f) after 96 hours of KOH treatment.

Larger micro-pits and -holes were observed for the surface roughness modified scaffold compared to the as-produced ones, which have a smooth surface with very small pits. Rounded holes and micro-pits can be observed on the surface of the PCL scaffolds after 96 hours of KOH treatment, while the scaffolds treated with NaOH have deeper holes and a less rough, but cauliflower-shaped surface.

8.6. Conclusion

This chapter shows a morphological and mechanical characterization of the different PCL scaffold designs prior to surface modification. Compared to the Ti6Al4V scaffolds, they have lower porosity, thicker struts, more available surface and much lower mechanical properties. Additionally, the roughness of the PCL scaffolds is much lower than that of the Ti6Al4V scaffolds. Concerning the surface roughness modification procedures, further biological cell behavior experiments have to be performed on the PCL scaffolds in order to evaluate which surface roughness modification procedure performs the best in relation to cell attachment and cell proliferation. Additionally, a thorough characterization of the effect of the surface roughness modification on the morphological and mechanical properties and on the roughness needs to be performed, as was done for the Ti6Al4V scaffolds.

9. Conclusions and suggestions for future work

9.1. Ti6Al4V scaffolds

Since the surface roughness is an important property of porous TE scaffolds that will determine and control cell attachment and proliferation, a control over the surface roughness becomes important. Since selective laser melting (SLM) cannot provide a robust control on surface roughness, two surface modifications were carried out on the porous Ti6Al4V TE scaffolds. First, chemical etching was performed to eliminate unmelted powder grains and impurities adhered to the strut surfaces after production. Once this goal was accomplished, electrochemical polishing was done, to obtain a smoother, more controlled and cell-friendly surface. Achieving more controlled and more homogeneous surface properties after surface roughness modification, without decreasing the mechanical properties too much, was one of the main aims of this master thesis. A characterization of three scaffold designs with varying designed strut thickness prior to surface roughness modification and after each surface roughness modification step was done in order to study not only changes in morphological but also in mechanical properties due to the surface roughness modification.

Concerning the chemical etching, a reduction in mass, object surface, strut thickness and roughness was found when Archimedes tests and micro-CT scanning and roughness measurements were done on the chemically etched scaffolds compared to the as-produced scaffolds. SEM images confirmed the elimination of unmelted powder grains on the surface of the struts. The chemical etching step was quite controlled and robust, since independent of the initial surface roughness of the scaffold, most of the unmelted powder grains were removed.

In order to get more homogeneity and a better smoother surface, electrochemical polishing was done. Mass calculations, micro-CT scanning and SEM images were carried out again. Reduction in mass, strut thickness and roughness were again found after characterization, but, as was present prior to surface roughness modification, heterogeneities in roughness within one scaffold were still present.

For the roughness measurements, two different techniques were used. Whereas SEM images only allow to determine the surface roughness parameters on the outside of the scaffolds, high-resolution micro-CT was able to detect heterogeneities in roughness even within the sample, which makes a comparison between the internal strut surfaces and the external ones possible. In that way, the efficiency of the surface roughness modification steps can be evaluated more locally. Thus, high-resolution micro-CT based roughness measurements were concluded to be more accurate, also because the standard deviation on the results was smaller compared to the SEM-based roughness measurements.

As was shown in chapter 7, different values of roughness between top and bottom of the struts, between the top, middle and bottom zones of the scaffolds and between the centre and the sides of the scaffolds were obtained, even prior to surface roughness modification. During the electrochemical polishing process, as was explained in depth in chapter 3, the porous Ti6Al4V TE scaffolds are localized in the middle of the cylindrical platinum basket

inside the polyethylene beaker filled with electrolyte. The porous scaffold functions as the anode while the cylindrical basket acts as the cathode. As both anode and cathode are cylindrical, the distances between them stayed the same, at least for the outer surface of the scaffold. Since the diameter of the cylindrical platinum basket is 30 mm and the diameter of the scaffolds is between 5.98 and 6.39 mm, the radius of the scaffolds might be significantly large compared to the distance from the centre of the scaffold to the cathode to introduce a different efficiency of polishing between the edges and the centre of the scaffolds. This might explain why the roughness values were not the same when comparing the side and the centre of the Ti6Al4V scaffolds after electrochemical polishing. Thus, as a possible solution, increasing the diameter of the cylindrical platinum basket could make the radius of the scaffolds neglectable compared to the distance between the centre of the scaffold and the cathode, and thus similar efficiency of electrochemical polishing would be expected. Indeed, higher values of current or longer polishing time will not avoid differences in roughness measurements within one scaffold, and will cause a higher reduction in structure thickness.

The role the current density plays during electrochemical polishing was studied and interesting results for future work were obtained. Due to the different designed strut thickness of the three scaffold designs and the constant current applied during electrochemical polishing, different values of current density were obtained for the different scaffold designs. The percentage of reduction of mass, strut thickness and roughness parameters were strongly dependent of current density. Also the mechanical properties, more specific the E-modulus and the maximum stress decreased with increasing current density.

Linear relations were found for all these properties in function of the current density, which can be used for fine-tuning the required properties after surface roughness modification. Additionally, they allow even to fine-tune the design in order to obtain scaffolds with the desired morphological and mechanical properties and the required roughness after surface roughness modification. Mechanical properties, which are strongly dependent on the structure thickness, should definitely be taken into account when designing the scaffolds, thus a balance between a homogeneous and more controlled surface roughness and a small decrease in mechanical properties should be aimed at. Additionally, knowing in advance the reduction in structure thickness caused by the surface modification, the designed strut thickness can be fine-tuned in function of the required strut thickness after surface roughness modification. Future work will firstly consist of changing the current value during electrochemical polishing in order to get the same current density for the three scaffold designs. The same reduction of mass, structure thickness and roughness would be expected. If this is true, scaffolds can be designed for biological cell behavior experiments where the surface-modified scaffolds have the same strut thickness as the as-produced scaffolds, and thus the effect of only the surface roughness difference on the cell behavior can be assessed.

9.2. PCL scaffolds

In this master thesis, characterization of porous PCL scaffolds was also initiated as it is an interesting material for TE applications. Since fused deposition modeling (FDM) provides very smooth surfaces for the PCL scaffolds, cells might not be able to attach to the surfaces properly. Thus, two

different surface modifications were proposed in this master thesis based on the literature review namely 96 hours of immersion in NaOH or in KOH. SEM images showed qualitatively differences in surface morphology comparing the as-produced scaffolds with the surface roughness modified ones. While porous PCL scaffolds treated with KOH showed more rounded holes and micro-pits, those ones treated with NaOH also had big holes but with a cauliflower shaped surface roughness.

Compared to the Ti6Al4V scaffolds, PCL scaffolds have a lower porosity, thicker struts, more available surface and much lower mechanical properties. Both the morphological and mechanical properties were similar for the two scaffold designs. Additionally, the roughness of the PCL scaffolds is much lower than that of the Ti6Al4V scaffolds. Concerning the surface roughness modification procedures, further biological cell behavior experiments have to be performed on the PCL scaffolds in order to evaluate which surface roughness modification procedure performs the best in relation to cell attachment and cell proliferation. Additionally, a thorough characterization of the effect of the surface roughness modification on the morphological and mechanical properties and on the roughness needs to be performed, as was done for the Ti6Al4V scaffolds.

10. Reference list

1. Gibson L.J. and Ashby M.F. (1988) Cellular solids: structure and properties. *Pergamon Press*.

2. Torquato S. (2001) Random Heterogeneous Materials, Microstructure and Macroscopic Properties. *Springer, New York*.

3. Greet Kerckhofs (2009) Morphological and Mechanical Quantification of Porous Structures by Means of Micro-CT. Katholieke Universiteit Leuven.

4. E. Sachlos and J. T. Czernuszka (2003) Making tissue engineering scaffolds work. Review on the application of solid freeform fabrication technology to the production of tissue engineering scaffolds. *European Cells and Materials* 32, 35, 36.

5. Wai-Yee Yeong, Chee-Kai Chua, Kah-Fai Leong and Margam Chandrasekaran (2004) Rapid prototyping in tissue engineering: challenges and potential. *Elsevier* 643.

6. T. M. Freyman, I. V. Yannas, L. J. Gibson (2001) Cellular materials as porous scaffolds for tissue engineering. *Pergamon* 274, 281.

7. Garrett Ryan, Patrick McGarry, Abhay Pandit, Dimitrios Apatsidis (2008) Analysis of the Mechanical Behaviour of a Titanium Scaffold With a Repeating Unit-Cell Substructure. *Journal of Biomedical Materials Research* 894, 895, 897.

8. Ying Wan, Hua Wu, Xiaoying Cao, Siqin Dalai (2008) Compressive mechanical properties and biodegradability of porous poly(caprolactone)/chitosan scaffolds. *Elsevier* 1736, 1741.

9. K. F. Leong, C. M. Cheah, C. K. Chua (2002) Solid freeform fabrication of three-dimensional scaffolds for engineering replacement tissues and organs. *Elsevier* 2363, 2367-2376.

10. Peter Heinl, Lenka Müller, Carolin Körner, Robert F. Singer, Frank A. Müller (2008) Cellular Ti-6AL-4V structures with interconnected macro porosity for bone implants fabricated by selective electron beam melting. *Elsevier* 1536, 1537, 1539.

11. Jianyu Xiong, Yuncang Li, Xiaojian Wang, Peter Hodgson, Cui'e Wen (2008) Mechanical properties and bioactive surface modification via alkali-heat treatment of a porous Ti-18Nb-4Sn alloy for biomedical applications. *Elsevier* 1963, 1964.

12. Y. Gao, B. Gao, R. Wang, J. Wu, L. J. Zhang, Y. L. Hao, X. J. Tao (2008) Improved biological performance of low modulus Ti-24Nb-4Zr-7.9Sn implants due to surface modification by anodic oxidation. *Elsevier* 5009.

13. Wei-Wen Hu, Yaseen Elkasabi, Hsien-Yeh Chen, Ying Zhang, Joerg Lahann, Scott J. Hollister, Paul H. Krebsbach (2009) The use of reactive polymer coatings to facilitate gene delivery from poly (ε-caprolactone) scaffolds. *Elsevier* 5785, 5786.

14. A. Yeo, W. J. Wong, H. H. Khoo, S. H. Teok (2008) Surface modification of PCL-TCP scaffolds improve interfacial mechanical interlock and enhance early bone formation: An in vitro and in vivo characterization. *Wiley Interscience* 311, 312.

15. Eric Maire, Arnaud Fazekas, Luc Salvo, Remy Dendievel, Souhail Youssef, Peter Cloetens, Jean Michel Letang (2003) X-ray tomography applied to the characterization of cellular materials. Related finite element modeling problems. *Elsevier* 2437, 2442.

16. E. Bayraktar, M. A. Gonzalez Garza, C. Bathias (2008) A comprehensive study of plastic deformation mechanism of the metallic materials by "X-ray" computed tomography ("X-ray" CT). *Elsevier* 134.

17. Saey Tuan Ho, Dietmar W. Hutmacher (2006) A comparison of micro CT with other techniques used in the characterization of scaffolds. *Elsevier* 1366, 1370.

18. T. Ohgaki, H. Toda, M. Kobayashi, K. Uesugi, M. Niinomi, T. Akahori, T. Kobayash, K. Makii and Y. Arugas (2006) *In situ* observations of compressive behaviour of aluminium foams by local tomography using high-resolution X-rays. *Philosophical Magazine* 4418, 4420.

19. A-F. Bastawros, H. Bart-Smith, A.G. Evans (2000) Experimental analysis of deformation mechanisms in a closed-cell aluminium alloy foam. *Pergamon* 302, 305, 316, 317, 319.